NONDESTRUCTIVE EVALUATION TECHNOLOGY INITIATIVES II
Delivery Order 0002: Whole Field Turbine Disk Inspection

Donna J. Mayton, Ph.D.
Science Applications International Corporation

APRIL 2007
Final Report

NOTICE

Using Government drawings, specifications, or other data included in this document for any purpose other than Government procurement does not in any way obligate the U.S. Government. The fact that the Government formulated or supplied the drawings, specifications, or other data does not license the holder or any other person or corporation; or convey any rights or permission to manufacture, use, or sell any patented invention that may relate to them.

This report was cleared for public release by the Air Force Research Laboratory [insert TD site] Public Affairs Office and is available to the general public, including foreign nationals. Copies may be obtained from the Defense Technical Information Center (DTIC) (http://www.dtic.mil).

THIS REPORT HAS BEEN REVIEWED AND IS APPROVED FOR PUBLICATION IN ACCORDANCE WITH ASSIGNED DISTRIBUTION STATEMENT.

*//signature//   //signature//

_____   _____
JUAN G. CALZADA, Program Manager   ROBERT T. MARSHALL, Asst. Branch Chief
NDE Branch   NDE Branch
Metals, Ceramics & NDE Division   Metals, Ceramics & NDE Division

//signature//

_____
GERALD J. PETRAK, Asst. Division Chief
Metals, Ceramics & NDE Division
Materials and Manufacturing Directorate

This report is published in the interest of scientific and technical information exchange and its publication does not constitute the Government's approval or disapproval of its ideas or findings.

*Disseminated copies will show "//signature//" stamped or typed above the signature blocks.

REPORT DOCUMENTATION PAGE			*Form Approved* *OMB No. 0704-0188*

The public reporting burden for this collection of information is estimated to average 1 hour per response, including the time for reviewing instructions, searching existing data sources, searching existing data sources, gathering and maintaining the data needed, and completing and reviewing the collection of information. Send comments regarding this burden estimate or any other aspect of this collection of information, including suggestions for reducing this burden, to Department of Defense, Washington Headquarters Services, Directorate for Information Operations and Reports (0704-0188), 1215 Jefferson Davis Highway, Suite 1204, Arlington, VA 22202-4302. Respondents should be aware that notwithstanding any other provision of law, no person shall be subject to any penalty for failing to comply with a collection of information if it does not display a currently valid OMB control number. **PLEASE DO NOT RETURN YOUR FORM TO THE ABOVE ADDRESS**.

1. REPORT DATE *(DD-MM-YY)*	2. REPORT TYPE	3. DATES COVERED *(From - To)*
April 2007	Final	08 May 2003 – 30 April 2007

4. TITLE AND SUBTITLE	5a. CONTRACT NUMBER
NONDESTRUCTIVE EVALUATION TECHNOLOGY INITIATIVES II Delivery Order 0002: Whole Field Turbine Disk Inspection	F33615-03-D-5204-0002
	5b. GRANT NUMBER
	5c. PROGRAM ELEMENT NUMBER 62102F

6. AUTHOR(S)	5d. PROJECT NUMBER
Donna J. Mayton, Ph.D.	4349
	5e. TASK NUMBER 41
	5f. WORK UNIT NUMBER 43494105

7. PERFORMING ORGANIZATION NAME(S) AND ADDRESS(ES)	8. PERFORMING ORGANIZATION REPORT NUMBER
Science Applications International Corporation 16701 West Bernardo Drive San Diego, CA 92127	

9. SPONSORING/MONITORING AGENCY NAME(S) AND ADDRESS(ES)	10. SPONSORING/MONITORING AGENCY ACRONYM(S)
Air Force Research Laboratory Materials and Manufacturing Directorate Wright-Patterson Air Force Base, OH 45433-7750 Air Force Materiel Command United States Air Force	AFRL/RXLP
	11. SPONSORING/MONITORING AGENCY REPORT NUMBER(S) AFRL-RX-WP-TR-2008-4004

12. DISTRIBUTION/AVAILABILITY STATEMENT
Approved for public release; distribution unlimited.

13. SUPPLEMENTARY NOTES
PAO case number WPAFB 07-0145, 22 October 2007. Report contains color.

14. ABSTRACT

This program sought to characterize and optimize the Sonic IR inspection technique for the inspection of Air Force aircraft components through empirical methods. As part of that effort, TF33 second stage turbine blades, F100 first stage high pressure turbine disks, various compressor blades, landing gear components, and a vane ring were inspected. Elongated scallop samples and fluorescent penetrant inspection (FPI) probability of detection (PoD) samples with known flaws were also tested in effort to understand the technique. Statistically designed studies were conducted on sets of some of these components and samples, with the analysis leading to definition of optimal operating regions for system operating parameter settings. These parameters may be used later to write test procedures for the specific components.

This report covers the assembly of the Sonic IR inspection system and interface materials selection, inspection of various scrapped Air Force aircraft components, and a specimen contamination study. Also covered are the rigorous testing and analysis of the scallop samples, FPI PoD samples, F100 turbine disks, and TF33 turbine blades.

15. SUBJECT TERMS
Thermosonics, Sonic IR, fatigue cracks, Nondestructive Evaluation, NDE

16. SECURITY CLASSIFICATION OF:			17. LIMITATION OF ABSTRACT:	18. NUMBER OF PAGES	19a. NAME OF RESPONSIBLE PERSON (Monitor)
a. REPORT Unclassified	b. ABSTRACT Unclassified	c. THIS PAGE Unclassified	SAR	318	Juan G. Calzada
					19b. TELEPHONE NUMBER *(Include Area Code)* (937) 255-9791

Standard Form 298 (Rev. 8-98)
Prescribed by ANSI Std. Z39-18

i

Table of Contents

List of Figures

List of Tables

Preface

The objective of this program is to establish the requirements and methodology for a Sonic Infrared turbine engine nondestructive evaluation (NDE) capability that will meet engine rotor life extension needs for whole field crack detection in complex geometries. The inspection of certain critical turbine engine components remains an important requirement and element of the Air Force's Engine Structural Integrity program (ENSIP), as well as meeting a need of the Engine Rotor Life Extension (ERLE) program initiative. In prior work for the Air Force during 2002 and earlier, Wayne State University researchers demonstrated the ability of the Sonic IR technique to image very small cracks. This method uses a pulsed low frequency ultrasonic source to infuse the material with sound, thus causing heating around cracks. An IR video camera images the thermal radiation, recording the crack image. In 2002, initial studies were performed by SAIC to define disk inspection methodology. This delivery order built on this earlier work. It addressed the more comprehensive tasks of defining/establishing the instrumentation/system design requirements and features, the systems applications issues, requirements and approaches, and a preliminary probability of detection (PoD) studies to provide a general characterization of the crack detection capability of the methodology.

On the previous subcontract, a thorough review of the state of the art of the Sonic IR technique was conducted through hands-on experience, a literature survey, attendance at technical conferences, extensive discussions with researchers in the field, and visits to laboratories. It quickly became apparent that there were a large number of variables that influence the outcome of Sonic IR measurements and that the effects of these variables were not well characterized and understood. As the objective was to develop the technique into a reliable, fieldable inspection technique for the Air Force, it was clear that these variables must be studied in a rigorous manner so that they could be understood, controlled, and optimized. A comprehensive list of such variables was developed during that earlier subcontract.

Experiments were designed to study the effects of these variables on the Sonic IR signal. Extensive testing was conducted on various components and specimens according to rigid plans, the data were analyzed, and optimal variable values were determined. This work involved designing and building fixtures, fabricating specimens, cracking components, and collecting and analyzing gigabytes of data.

The author acknowledges the following people for their contributions to the program:

- Thomas Moran, Gary Steffes (Air Force Research Laboratory)
- Carlos Alvarez, Bartolo Drennen, Mario Gajo, Robert Grills, Kevin Harkreader, Eric Lindgren, David Rose (Science Applications International Corporation)
- Steve Cargill (Aerospace Structural Integrity)
- Skip Favro, Xiaoyan Han (Wayne State University)
- Mike Ashbaugh, Floyd Spencer (Sandia National Laboratories)
- Chunwang Gao, William Meeker (Iowa State University)
- Cody Engstrand (San Diego State University [SDSU])
- Bob Cochoy, Don Forney (United Technology Corporation)
- Joe Chandler (Pratt and Whitney)
- Michael Makowicz (Tinker Air Force Base)

A difficult step in any nondestructive inspection program is obtaining specimens and components for testing. Special thanks are owed to the following people for obtaining and or loaning test materials to the program: Gary Steffes for the disks and wheels, Mike Makowicz for the turbine and compressor blades, and Joe Chandler for the elongated scallop specimens. Steve Cargill was with the program for the duration and proved to be a very valuable resource in many areas on many occasions. Carlos Alvarez tirelessly acquired the majority of the data used in the parameter studies and was absolutely invaluable in the laboratory. The author wishes to thank Dr. Floyd Spencer, Dr. William Meeker, and Chunwang Gao for conducting, and explaining, the data analysis for this program. My former colleagues at SAIC were a great help, as was Cody

1.0 Summary

The initial goals focused on the anti-rotation feature (ARF) of the F100 first stage high pressure turbine disk. A firm understanding of the Sonic IR technique was sought in order to devise an inspection procedure for this specific feature of this component. The inspection procedure would be necessary for a Probability of Detection (PoD) study and the successful completion of that study, in turn, would be necessary for depot use of the technique. After extensive testing and analysis of the disk by this program, Pratt & Whitney, the original equipment manufacturer, effectively removed the ARF from the list of uninspectable areas for that part. At that point, the focus of the program widened to incorporate other components such as blades and wheels.

The program was strongly committed to using Air Force aircraft components for testing. However, while waiting to compile statistically significant sample sets of these components, testing was performed on two manufactured specimen sets. This testing, and the analysis of the results from it, contributed to the overall understanding of the technique and helped refine the general testing and analysis protocols.

In addition to conducting thousands of Sonic IR tests on dozens of components and specimens, this program attempted to coordinate with other researchers in the field. The SAIC/AFRL Sonic IR program organized and conducted the following Sonic IR Working Group Meetings**:**

- March 12, 2003, Orlando, FL (2003 Spring ASNT)
- October 13, 2003, Pittsburgh, PA, (2003 Fall ASNT)
- April 14, 2004, Orlando, FL (Thermosense XXVI)
- November 18, 2004, Las Vegas, NV (2004 Fall ASNT)
- October 20, 2005, Columbus, OH (2005 Fall ASNT)
- July 31, 2006, Portland, OR (26th annual QNDE)

These meetings allowed workers in the field not only to stay abreast of recent developments, but also to interact with each other in a more informal

environment that invited questions and discussion. These meetings drew at least 83 unique attendees over the years.

Information on this program was presented at six conferences. The conference, title, presenter, and date are listed here:

- Aeromat Conference 2003, "Optimization of the Sonic IR Technique for the Inspection of Turbine Disks", Eric Lindgren, June 2003.

- UDRI Workshop on Ultrasonic Testing and POD Evaluation, "Comparisons of Binary Analysis to Response Surfaces using Design of Experiments", Floyd Spencer, March 2004.

- Thermosense XXVI, "A Design of Experiments Approach to Characterizing the Effects of Sonic IR Variables," Donna Mayton, April 2004.

- Review of Progress in Quantitative Nondestructive Evaluation, "Characterizing the Effects of Sonic IR Variables on Turbine Disk Inspection using a Design of Experiments Approach," Donna Mayton, July 2004.

- American Society of Nondestructive Testing Conference, "A Comparative Investigation of the Effects of Sonic IR Variables," Donna Mayton, November 2004.

- American Society of Nondestructive Testing Conference, "Application of Sonic Infrared NDE to Detection of Fatigue Damage in Military Aircraft Components," Steve Cargill, November 2007.

Three of the above listed conferences published proceedings. Technical papers, by the same titles as listed above, may be found for the UDRI Workshop, QNDE, and Thermosense conferences. These papers are listed in the Selected Bibliography.

2.0 Introduction

This report covers technical work performed on NTIP II, Contract # F33615-03-D-5204, Subcontract # 03-S508-002-C1. This subcontract was a continuation of work begun on an NTIP (I) subcontract the year before.

The report begins with the second part of a set of materials studies performed to determine the optimum interface materials to use with the Sonic IR inspection system. This material requirement stemmed from the fact that no metal-to-metal (horn-to-component or component-to-fixture) contact would be permissible in the Sonic IR inspection of Air Force components. Two materials are required in such testing. One material protects the specimen from direct contact with the ultrasonic horn. In this report, it is referred to as the "surface protection material." Another material is required between the specimen and the welder base, clamp, or fixture. It is referred to as the "vibration isolation material" since it also serves to isolate the specimen from the rest of the mechanical system, as well as protect the surface finish of the component.

Once the appropriate materials were selected for testing, the test system was assembled. The system is covered in Section 3.2. Unless stated otherwise, this is the Sonic IR system used for all testing covered in the report.

The testing and results of this program can be reviewed best when broken down by component or specimen. Several of these components and specimens were studied rigorously with the goal of optimizing the Sonic IR technique for future depot use, and others were studied much less rigorously, with the goal of merely determining the feasibility of Sonic IR testing.

The early sections of the report, Sections 4.X, will address testing conducted on scrapped Air Force aircraft components without the use of experimental design. Various wheels, turbine blades, compressor blades, and a vane ring are included in these sections. Most of these components contained marked fatigue cracks. The goal of these tests was to determine the feasibility of using Sonic IR inspection on the particular class of components. The components were clamped with either a vise or an existing fixture developed for

3

a similar component, but the clamping was not optimal. Operating system parameters were chosen because of brief feasibility testing or based upon experience. Even with these limitations, much knowledge was gained about inspection of these components.

Sections 5.X cover a different, more regimented, type of testing of components and specimens. Statistically designed testing matrices were used to study, systematically, the effects and interactions of some of the main variables in the Sonic IR inspection process. These test sets each comprise hundreds of individual tests and were the first such studies published in this field. Elongated scallop specimens, Inconel fluorescent penetrant inspection (FPI) probability of detection (PoD) specimens, artificially cracked engine disks, and rejected turbine blades were studied in depth. Analysis of the data obtained from this testing pointed to the optimal operating parameters for these components and specimens.

The final section of the report covers a study conducted to begin understanding the effects of contamination on the ability of the Sonic IR technique to detect cracks. Artificially cracked specimens of aluminum and Inconel were contaminated with various materials and tested with Sonic IR before and after this contamination. Results of this study indicate directions for future work in this area.

The Appendices include several reports on the fabrication and cracking of specimens and components, respectively, that were used during this program. The information they contain is necessary for a complete understanding of the testing performed and the results obtained. The Selected Bibliography is a list of papers consulted to varying degrees, during the course of the program. It is not intended to be a complete listing of work in the area.

3.0 Inspection System Preparation

3.1 Surface Protection and Vibration Isolation Material Study

3.1.1 Introduction to Materials Study

A series of tests was outlined by Floyd Spencer at Sandia and data were collected at San Diego State University by a graduate student. The objective of the study was to determine which consumable materials to use for the duration of the program. The work presented in this section is a continuation of an effort that was reported on previously (Reference 1).

3.1.2 Materials Study Experimental Design

This testing addressed issues of surface protection materials (SPM) and vibration isolation materials (VIM) and drew upon preliminary testing that was completed earlier in this program. The laser vibrometer was set up to measure velocity data of the test piece. The vibrometer data were captured and analyzed 5 times for each of the combinations of factors outlined in the test matrix. It should be noted that the ultimate efficacy of the Sonic IR technique is not measured by the vibrometer signal, but rather by whether or not a flaw would be adequately imaged by an IR camera.

Surface protection and vibration isolation materials need to possess necessary transmission and isolation properties, respectively, and for a field inspection environment, they need to be either durable or easily and inexpensively replaceable. It is likely that durability of the surface protection material will depend upon the tip shape and force applied by the welding horn. For this reason, these factors were included in this initial phase of the experiment. TABLE 1 shows the factors and levels tested.

TABLE 1. INITIAL FACTORS AND LEVELS.

Factor	Levels
Horn tip	2 – round, flat
Trigger force	2 – 20 lbs, 230 lbs
Surface Protection Material (SPM)	5 – Teflon, PFA, Nomex, Paper (Card Stock), Leather
Vibration Isolation Material (VIM)	3 – Cork, Dynamat, Rubberized cork

Two vibration isolation materials not covered in the previously reported testing were included here. "Dynamat," manufactured by Dynamat Control, is an engineered sound control material used in automobiles to reduce road noise and to improve sound system quality. Interim testing showed it to be a promising candidate material and it was added to the test matrix. This was also the case with the rubberized cork material, purchased from McMaster-Carr (stock number 9607 K63). It was found to be more durable than plain cork but still possess some desirable properties.   All other materials used were described in the earlier report.

3.1.3 Materials Study Experimental Setup

A Branson ultrasonic welder (Model 900 ma power supply, Model 921 AES actuator) and an Ometron laser vibrometer (Model VS 100) were used for this testing. The vibrometer data were collected with a National Instruments PCI-6052E multifunction I/O board and the data acquisition was controlled via a National Instruments LabVIEW program. For each test, 50,000 data points were collected at 200 kHz. The test piece used for these tests was a 3.5 inches diameter, 4.1 inches tall cylinder of mild steel. It was positioned on the base of the welder unit with the horn contacting it in the center.

A photograph of the welder and laser vibrometer equipment is shown in Figure 1. The photograph does not include the data acquisition computer, nor does it show the actual data acquisition configuration of the components.

Figure 1. Equipment used for vibration data acquisition.

The Branson welder unit was configured in the "Time" mode. The "Weld Time" was set to 200 ms, the air pressure was set at 36 psi, and the down speed parameter was 1.5. The energy and power levels varied for each test.

Since it is not yet known which frequency or frequency range produces the best Sonic IR signal, the alternating current (AC) root mean square (rms) average of the velocity data was calculated.

3.1.4 Materials Study Results

The digitized laser vibrometer velocity data were analyzed by calculating the AC rms average for each 250 ms waveform. This AC rms average gives a quantitative measure of vibration and it can be used to compare the behavior of the different combinations of factors. It was not possible to collect data for some of the combinations of factors since the welder unit locked up and gave an error prior to the completion of the 200 ms weld cycle.

The results are listed in TABLE 2. For each combination of factors, 5 data sets were collected and the AC rms value calculated. Data is listed in the following format:

Average of 5 data sets

(Highest value)

(Lowest value)

Cases in which the welder gave an error and data were not available are noted by "na".

TABLE 2. SPM AND VIM TEST RESULTS.

Horn Tip		Flat														
VIM		Cork					Dynamat					Rubberized Cork				
SPM		Pap	Tef	PFA	Nom	Lea	Pap	Tef	PFA	Nom	Lea	Pap	Tef	PFA	Nom	Lea
Horn Trigger Force (lbs)																
20		**1.190** (1.69) (1.04)	**1.154** (1.21) (1.11)	**1.062** (1.15) (1.01)	**1.004** (1.25) (0.83)	**0.262** (0.31) (0.20)	**1.093** (1.12) (1.07)	**1.179** (1.22) (1.14)	**1.062** (1.09) (1.04)	**0.992** (1.09) (0.85)	**0.285** (0.31) (0.24)	**0.936** (0.96) (0.89)	**1.008** (1.05) (0.96)	**0.902** (0.92) (0.89)	**1.031** (1.20) (0.89)	**0.355** (0.39) (0.28)
230		**3.230** (3.31) (3.11)	Na	na	**3.386** (3.62) (3.30)	**2.332** (2.37) (2.28)	na	na	na	**3.672** (4.29) (3.10)	**2.195** (2.42) (1.76)	**3.509** (3.74) (3.25)	na	na	**3.701** (4.11) (3.37)	**2.373** (2.58) (2.17)

Horn Tip		Round														
VIM		Cork					Dynamat					Rubberized Cork				
SPM		Pap	Tef	PFA	Nom	Lea	Pap	Tef	PFA	Nom	Lea	Pap	Tef	PFA	Nom	Lea
Horn Trigger Force (lbs)																
20		**1.072** (1.10) (1.05)	**1.053** (1.10) (1.02)	**1.061** (1.10) (1.03)	**0.839** (0.88) (0.79)	**0.095** (0.11) (0.08)	**1.184** (1.22) (1.14)	**1.254** (1.29) (1.22)	**1.518** (1.57) (1.48)	**0.933** (0.98) (0.89)	**0.104** (0.14) (0.09)	**0.924** (0.97) (0.87)	**0.969** (1.01) (0.94)	**1.187** (1.22) (1.15)	**0.911** (1.06) (0.86)	**0.098** (0.12) (0.08)
230		**3.804** (3.91) (3.70)	**3.795** (3.83) (3.76)	**3.605** (3.75) (3.47)	**3.605** (3.66) (3.44)	**1.338** (1.56) (1.22)	**2.962** (3.04) (2.86)	**2.050** (2.09) (2.00)	**1.962** (2.10) (1.86)	**2.833** (3.08) (2.43)	**1.349** (1.49) (1.23)	**3.848** (3.91) (3.76)	**3.874** (3.94) (3.82)	**3.744** (3.80) (3.65)	**3.614** (3.70) (3.54)	**1.644** (1.80) (1.53)

VIM = Vibration Isolation Material, SPM = Surface Protection Material, Pap = paper (card stock), Tef = Teflon film, Nom = 10 mil Nomex, Lea = leather.

3.1.5 Analysis of Materials Study Data

The factors studied were shown in TABLE 1. Sixty combinations of factors were studied by taking 5 shots for each combination. However, data were not obtained for 7 of the operating combinations, as noted by "n/a" in the table.

The response variable was the root mean square of the AC component of the laser vibrometer displacement data for the 200 millisecond waveform (denoted ACRMS). The first analysis considered whether there was a trend component to the shots taken at each set of conditions. That is, did the ACRMS have a consistent trend (increasing or decreasing) over the 5 shots? This was studied by coding each shot from 1 to 5 and modeling the data with "shot" as a covariate and including all "shot" interactions with the 4 factors listed in TABLE 1. There was no shot effect that was statistically significant. Thus, there was <u>no</u> indication of trends within the shots.

Since there was no detectable trend in the shots, the average ACRMS and the standard deviation within the 5 shots were viewed as response values. An initial look was provided by considering the box plots of the responses with respect to each of the design factors separately. These box plots are shown in Figure 2.
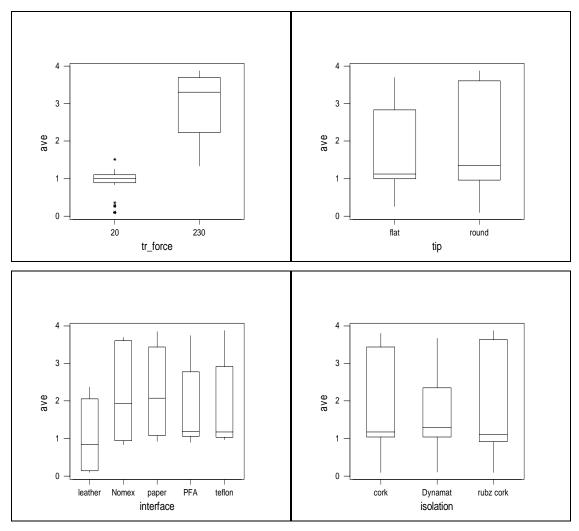
Figure 2. Box plot of the average ACRMS for main factors.

From the comparison of the factors in Figure 2, it is clear that the trigger force and the interface materials are the factors that have an effect on the average value of the ACRMS response. It is apparent that a trigger force of 230 lbs. results in a higher ACRMS value. For the interface materials, leather appears to be the most different from the other materials. However, recall that the PFA and Teflon levels of the interface material are the conditions that were missing at the trigger force of 230 lbs. due to lock up of the welder unit. An analysis of variance bears out the message from the box plots.

In addition to looking at the average ACRMS, standard deviation (actually the logarithm of the standard deviation) was also considered. Note that a high

value for standard deviation indicates that there is less repeatability in the shots within the conditions used to produce the shots. The standard deviation box plots are shown in Figure 3.
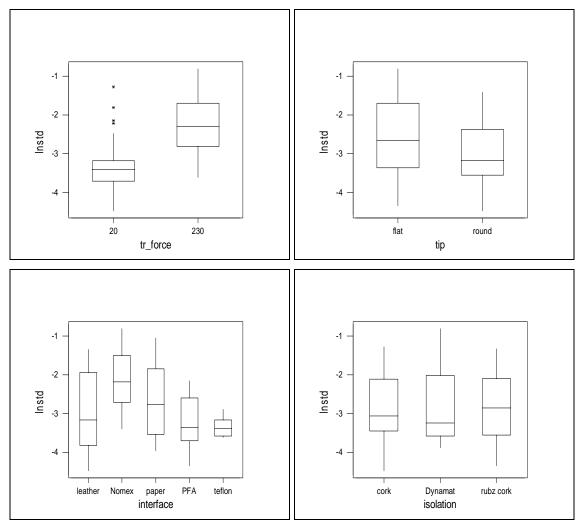
Figure 3. Box plots of natural logarithm of standard deviation of 5 shots by main factors.

The box plots of Figure 3 indicate that there is more shot–to–shot variability at the higher trigger force value and that the Nomex material, among the interface materials, exhibits more shot–to–shot variability than do the other materials. (Although, care must be taken in discussion of and comparison with PFA and Teflon materials, as it is these materials that are missing data at the

230 lbs. trigger force/flat tip settings.) In addition to the apparent differences seen in the plots in Figure 3, a formal analysis of variance showed that the observed differences in the level for the tip were also significantly different. On average, across the other conditions, the round tip showed less shot – to – shot variability than did the flat tip.

3.1.6 Materials Study Conclusions

Based on the test results and the cost of the surface protection and vibration isolation materials tested, paper and rubberized cork were chosen as the materials to use for the program. These materials are relatively inexpensive and performed well in testing. All testing conducted on this program and described in this report used fixtures lined with rubberized cork and 80 pound card stock paper between the horn and test specimen. The paper is used for one test only and the rubberized cork is changed on a prescribed basis.

3.2 Sonic IR System Assembly

A Sonic IR system based on the one originally developed by Gerd Busse (Reference 2) and later modified by researchers at Wayne State University (Reference 3) was assembled at SAIC. A 2000W Branson ultrasonic welder system, model 921aes actuator and 900MA controller, was used to generate the mechanical energy in the samples. An Indigo Merlin-Mid infrared (IR) camera, usually used with a half-inch extender ring, was used to monitor the sample surface. This camera acquires data at 60 frames per second. Data was collected from the IR camera and the ultrasonic welder using a customized version of the EchoTherm® VT program, from Thermal Wave Imaging, Inc (TWI), running on a dual drive, Pentium III, 1266 MHZ machine. The standard EchoTherm VT program, which is a component of the TWI Vibrothermography System, communicates with the welder system and actually controls the weld cycle in addition to acquiring the IR data. The version of the software used here

is passive and only acquires data from the IR camera and welder system. A Polytec PI laser vibrometer, model OFV 353 sensor head and model OFV 3001 controller, was used to measure surface motion. The vibrometer data was recorded using a LabVIEW 7 program running on a Dell workstation PWS 450 with a Xeon 2.66 GHz CPU.

A photograph of the experimental setup with a disk specimen on the welder base plate is shown in Figure 4. Unless noted otherwise, all testing discussed in this report was performed using this system.
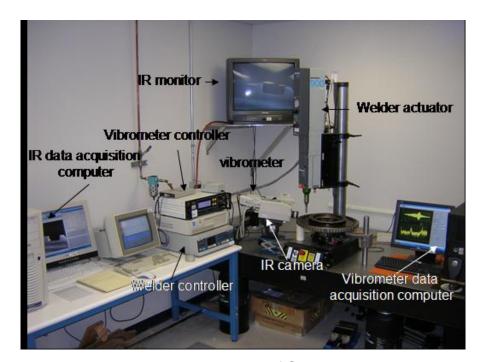
Figure 4. Experimental setup of Sonic IR equipment.

4.0 Components Inspected

Throughout this program, many scrapped aircraft components were sent to SAIC for inspection with the Sonic IR system. Some of these parts were considered for more extensive testing, with the intent of developing inspection procedures for probability of detection (PoD) testing. Other components were tested in the interest of determining the limits of the Sonic IR technique and our system in particular. The testing described in this section was conducted on rejected aircraft components with the latter goal. Section 5 of this report describes the more rigorous type of testing performed on several sets of components and samples.

4.1 Wheels

4.1.1 F-16 Main Landing Gear

An F-16 main landing gear (MLG) wheel half was received from the Air Force Research Laboratory (AFRL). This wheel, manufactured by Goodyear, has 2 fatigue cracks at the base of 4 of the 5 brake mounts. We were able to detect all 8 cracks with Sonic IR inspection. The cracks could be excited with the horn placed at any position along the flat outer rim, as indicated in Figure 5. The wheel rested on the welder base on a ring of rubberized cork and the horn was counterbalanced by a rubberized cork lined clamping rig on the opposite side of the wheel. A photograph of the wheel in the test setup is shown in Figure 6.

Figure 5. F-16 main landing gear wheel.
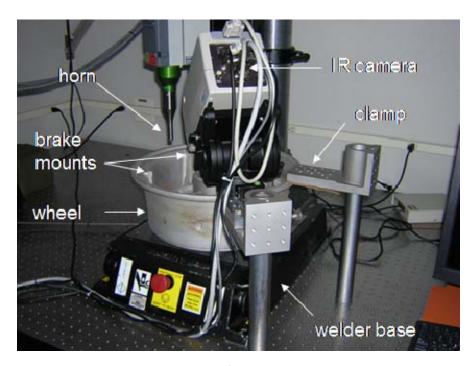
Figure 6. Experimental setup for F-16 main landing gear wheel.

Brake mount #1-4 each has 2 fatigue cracks at the base. Figures 7-10 are single frame images taken from a Sonic IR test of each brake mount, with arrows pointing to the cracks detected. No magnification was used. The frame selected shows the two cracks equally well, but earlier and/or later frames were better for viewing the cracks individually and as with most IR data, the images appear clearer on the computer screen than they do in reproduction. TABLE 3 contains the crack lengths, as determined by AFRL using fluorescent penetrant inspection (FPI). Sonic IR testing did not find any indications on brake mount #5.
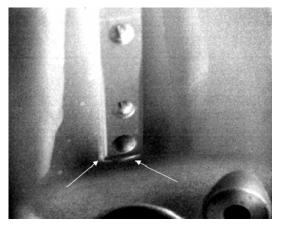
Figure 7. Brake mount #1.
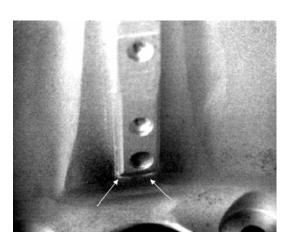
Figure 8. Brake mount #2.
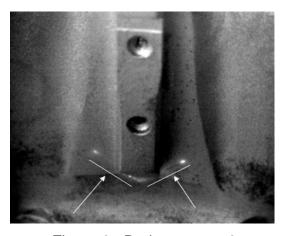
Figure 9. Brake mount #3.
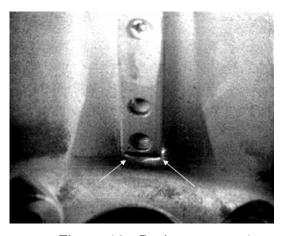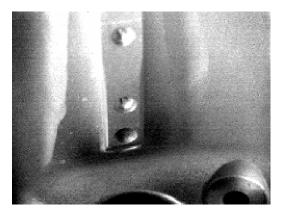
Figure 10. Brake mount #4.

TABLE 3. CRACK LENGTH MEASUREMENTS.

Brake Mount	Right of Brake Mount In image, crack length (in.)	Left of Brake Mount in image, crack length (in.)
1	0.270	0.080
2	0.300	0.280
3	0.890	0.970
4	0.310	0.220
5	None	None

After initial testing, the wheel was sent to AFRL, painted with "standard" Air Force wheel paint, returned to SAIC, and reinspected. All of the cracks detected prior to painting were found again after the part was painted. In addition, an anomaly was found on the bead seat that was not present prior to painting. The paint appeared to separate at several of the cracks and that effect highlighted the cracks, making them easier to detect. Sonic IR images, taken before and after the wheel was painted, are shown below in Figures 11 through 14. Optical images are included for cracks that could be visually detected after the application of paint. Note that the white colored rectangle in several of the Sonic IR images is a piece of foil tape that is used as a reference marker. The unknown feature found on the bead seat is shown in Figure 15. The Sonic IR images for the painted wheel were obtained at lower energy settings than those used for the unpainted wheel. The input energy was minimized to help protect the painted surface from the ultrasonic horn. While paint over an existing crack is not equivalent to a crack that formed under paint, this painting exercise was the first attempt by the program to look at the influence of the presence of paint on a component.
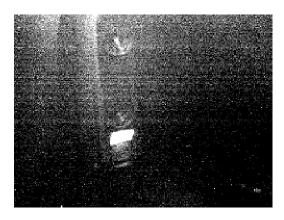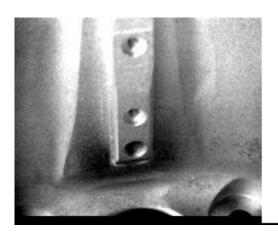
Figure 11. Sonic IR images of F-16 brake mount #1, unpainted (left) and painted (right).
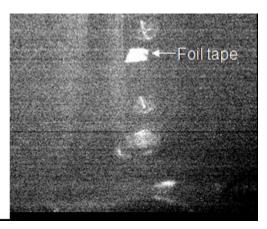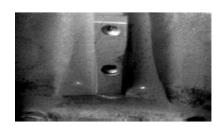
Figure 12. Sonic IR images of F-16 brake mount #2, unpainted (left) and painted (right).
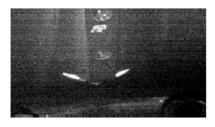
Figure 13. Sonic IR images of F-16 brake mount #3, unpainted (left), painted (middle), and optical image (right).

Figure 14. Sonic IR images of F-16 brake mount #4, unpainted (left), painted (middle) and optical image (right).
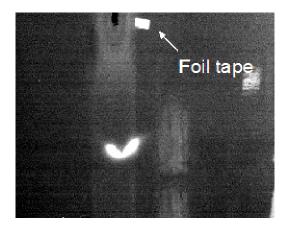
Figure 15. Optical image (left) and Sonic IR image (right) of "feature" found on F-16 bead seat.

4.1.2 A-10 Nose Wheel

An A-10 nose wheel half was received from AFRL and tested with our Sonic IR system. A through-wall crack on the bead seat was easily detected. This is the only defect in the part detected by FPI at the Air Force depot also. A photograph of the wheel is shown in Figure 16 and IR images of the two sides of the crack are shown in Figures 17 and 18.

Figure 16. Photograph of A-10 nose wheel with through-wall crack.
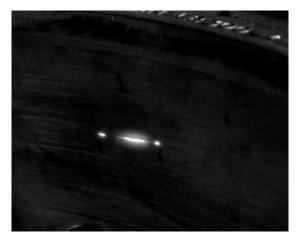
Figure 17. Sonic IR image of through-wall wheel crack, as viewed from inside the bead seat.
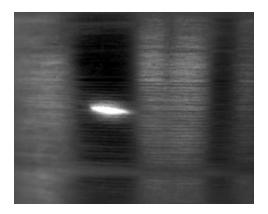
Figure 18. Sonic IR image of through-wall wheel crack, as viewed from outside the bead seat.

4.1.3 A-10 Nose Wheel Fixture

When several more rejected A-10 nose wheel halves were located by AFRL, this component was suggested as a candidate for future PoD testing. Towards that end, a clamping fixture for the component was developed. Design models of the fixture without and with the wheel half in place are shown in Figures 19 and 20, respectively.
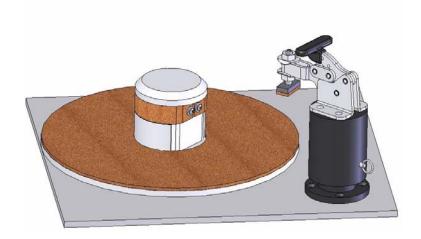
Figure 19. A-10 nose wheel fixture design model.
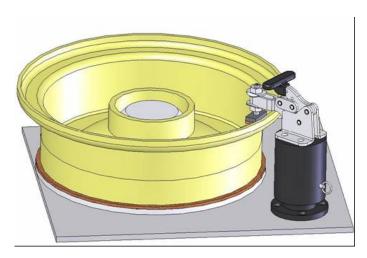
Figure 20. A-10 nose wheel fixture design model with wheel.

This fixture performed quite well. It met the design goals of ease of use and simplicity, and it secured the wheel without restricting the induced vibration

within it. The base plate of the fixture bolts to the base of the welder. The wheel rests on a rubberized cork lined pad and the post that fits in the center of the wheel is lined with rubberized cork, also. These surfaces can be replaced as needed. The height of the clamping mechanism can be adjusted to accommodate the differing heights of the two wheel halves by pulling a pin, sliding the post to the correct height, and reinserting the pin. The red handle flips the lined pad onto the rim of the wheel to counteract the force of the horn on the opposite side of the part. This simple design concept could be scaled easily to fit wheels of other sizes. Photographs of the fixture are shown in Figures 21 through 23.
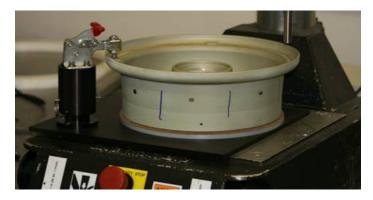
Figure 21. A-10 nose wheel half secured in fixture on welder base.

Figure 22. A-10 nose wheel fixture on base of welder.
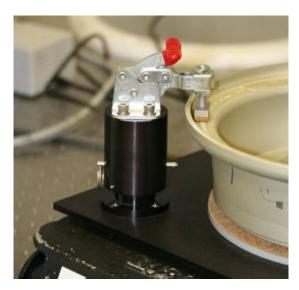
Figure 23. Close up view of clamping mechanism on A-10 nose wheel fixture.

4.1.4 KC-135 Nose Wheel

One half of a two-part decommissioned wheel was received from Hill Air Force Base through AFRL. This wheel is from the nose landing gear of a KC-135 aircraft and is painted with a glossy white paint, as shown in Figure 24. Initial testing revealed some Sonic IR indications, but the sources of these indications were unclear as no previous testing records were available.

Figure 24. Painted KC135 nose wheel section.

The KC-135 nose wheel was examined to determine the source of the five areas of Sonic IR indications recorded. Microscopic optical inspection revealed that most of the indications were caused by loose paint at the edge of a scratch or chip. Figure 25(a) shows the optical image and Figure 25(b) shows the corresponding Sonic IR image of the same area for one of these indications. These images were obtained at slightly different viewing angles. In each case, when the loose paint was flaked off, there was no longer a Sonic IR signal present. In another case, the Sonic IR signal was found to have been generated by a paint blister, and again, when the paint anomaly was removed, the signal vanished. Figure 26(a) shows the optical image and Figure 26(b) shows the corresponding Sonic IR image for this area. It was not known if any cracks were present in this part.

(a)   (b)
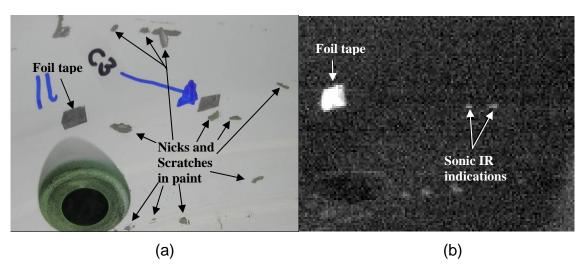
Figure 25. Painted KC-135 wheel near bolt hole #11, (a) optical image, (b) Sonic IR image.

(a)   (b)
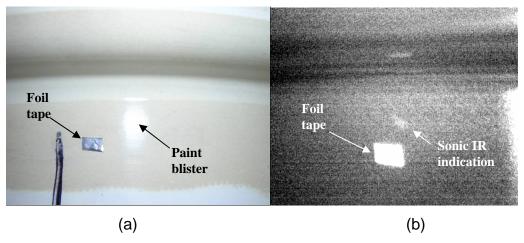
Figure 26. Painted KC-135 wheel on bead seat, (a) optical image, (b) Sonic IR image.

4.2 Turbine Blades

4.2.1 Turbine Blade Background

SAIC received seven condemned TF33 2nd stage turbine blades from Tinker Air Force Base. The parts each had at least one FPI indication marked, but we were advised that other indications may have been detected and not marked. Photographs, taken at various angles, of one of these TF33 blades are shown in Figures 27 through 29. The overall blade length is approximately 5.5 inches. The full field inspection of each of these parts will be reviewed here.

Figure 27. TF33 2nd stage turbine blade, edge view.

Figure 28. TF33 2nd stage turbine blade, airfoil view (90° rotation from Figure 27).
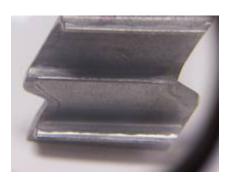
Figure 29. TF33 2nd stage turbine blade, tip shroud end view.

4.2.2 Turbine Blade Data Acquisition

The blades were tested extensively with Sonic IR and they were examined optically under magnification. In addition, they were inspected with FPI in-house at SAIC. Several blade positions were used during the Sonic IR testing to try to inspect the entire surface of each blade. The blades were tested while being held in position by a vise and were surrounded by rubberized cork at all contact points for all tests. The vise was hand-tightened to prevent the blades from tilting or twisting while being tested. Any further tightening of the vise, such as with a calibrated torque wrench, reduced or eliminated the Sonic IR signal. Unless otherwise stated, all Sonic IR testing was conducted with 60 pounds of force, 100 milliseconds (ms) pulse length, and 60% vibration amplitude. One of the test configurations is shown in Figure 30. Testing was also conducted with the same blade position but with the horn in contact with the shroud platform, as opposed

to the root platform as shown in the photograph. The blade was also positioned in the vise rotated 90° relative to the position shown in Figure 30 to image the airfoil.
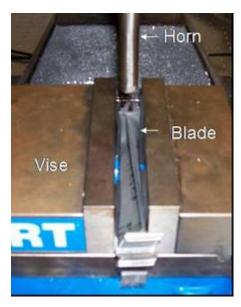
Figure 30. One test configuration for Sonic IR testing of TF33 blades.

All of the cracks marked on the parts by the Tinker FPI inspectors were detected with Sonic IR inspection. In addition, several cracks that were not marked by the Tinker FPI inspectors, but which could be seen using optical techniques with magnification, were detected with Sonic IR inspection. Sonic IR indications were also obtained in areas where there was no marked crack, no defect was visible under magnification, and no indication was seen during in-house FPI testing.

4.2.3 Turbine Blade Results

4.2.3.1 Summary of Turbine Blade Results

A summary of information obtained from each blade is listed in TABLE 4. A discussion of these results for each blade is presented in the next section of this report. The "Blade #" row in this table contains the serial number that is

stamped on the blade on the top, and the test number assigned to the blade for easier tracking in later tests below.

TABLE 4. TF33 2nd STAGE TURBINE BLADE SONIC IR TEST INFORMATION.

Blade #	VSSZ	TPN	L21636 (#7)	L21887 (#2)	L21447 (#4)	L22187 (#3)	L21638 (#1)
Crack location *	Tip shroud	Tip shroud	Airfoil l.e.	Airfoil l.e.	Airfoil l.e. & t.e.	Airfoil t.e.	Airfoil t.e.
Sonic IR detected?	Yes	Yes	Yes	Yes	Yes	Yes	Yes
Other Sonic IR indications	Tip shroud, airfoil t.e.	Tip shroud	Tip shroud, airfoil t.e.	Tip shroud, airfoil t.e.	Tip shroud, airfoil l.e.	Tip shroud, airfoil l.e.&t.e.	Tip shroud

* "Crack location" refers to the crack marked on the part. This crack was found by inspectors using FPI and its location/size met the condemnation criteria for the part. Other cracks may have been detected by FPI but not marked since the part had already been condemned.

4.2.3.2 Individual Blade Results

In this section, results from each of the seven blades tested will be discussed. First, there are some general observations to consider for all of the results.

The author is always reluctant to publish single frame IR images from Sonic IR tests because they can be confusing and misleading. Naturally occurring emissivity variations, especially on bare metal parts, can produce deceiving images. Reflections are also a problem on bare metal parts. The metal finish on most of the surfaces of the blades tested here is dull, matte, and dark grey. However, some areas appear more polished, some areas appear scratched, and some areas look worn, perhaps through contact with mating surfaces. When viewing a Sonic IR test sequence of many frames, the emissivity variations are present prior to the sonic pulse and it is easy for a human observer

to filter this uneven background against the temperature changes that occur due to a defect in the part being tested. When viewing a single frame from a Sonic IR test, however, it is not always possible to distinguish between an emissivity variation and a signal from a defect. Reflections are even more difficult to distinguish since they can have the same temporal profile as the pulse. They can be caused by the horn contact area or by a defect signal, both of which heat up synchronously with the sonic pulse.

The Sonic IR images shown in this section should be reviewed along with the accompanying text that explains the images. On occasion, an image that contains a reflection is shown, because it best demonstrates the signal from a defect. The "hot spot" labeled as a reflection was proven such in subsequent testing where the origin of the heat creating the reflection was shielded. These shielding tests do not always provide interesting images and therefore not all of them are included in the report. The cracks detected by FPI at Tinker, which caused the parts to be condemned, are labeled as "Marked Crack" in the images shown in this section. Sonic IR indications and reflections are labeled as such. Any other apparent "hot spot" seen in an image is either an emissivity variation or heat created by contact areas between the part and the horn or the part and the rubberized cork on the vise.

In some cases, multiple images from a single Sonic IR test are shown to illustrate interesting events that occurred as a function of time.

4.2.3.2.1 Part #VSSZ

This blade was condemned because of a crack in the tip shroud. Sonic IR testing detected the marked crack along with two other indications on one of the ridges on the tip shroud. The ridge indications were higher amplitude than the marked crack. Given the geometry of the part, it makes sense that the ridges will vibrate at higher amplitude than the base of the shroud and that defects in those regions may be easier to detect. The ridge geometry is somewhat similar to the anti-rotation feature (ARF) on the F100 1st stage high-pressure turbine disks,

discussed later in Section 5.3. Vibrometer measurements showed higher amplitude vibrations in the ARF than in the base of the disk.

Figure 31 shows an IR image of the tip shroud with indications labeled. A sequence of images is shown in Figure 32 to illustrate how the signals develop over time. The "hot spots" at the mid-plane of the tip shroud and under the top ridge were later proven reflections of the signal generated in the ridge directly above them.

Airfoil tests on this blade consistently produced indications along the trailing edge on both the convex and concave sides of the blade. These indications could not be correlated to any visible cracks or marks on the part. IR images of the airfoil are shown in Figure 33.
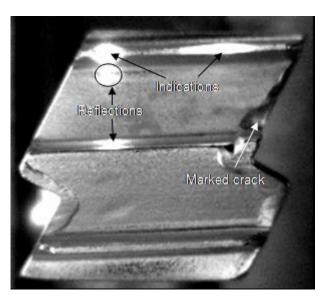
Figure 31. Part # VSSZ tip shroud IR image with labels.

| 17 ms | 33 ms | 50 ms | 67 ms | 83 ms | 100 ms |
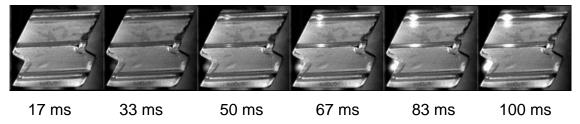
Figure 32. Part # VSSZ tip shroud Sonic IR image sequence, labeled with time in milliseconds after sonic pulse initiation.
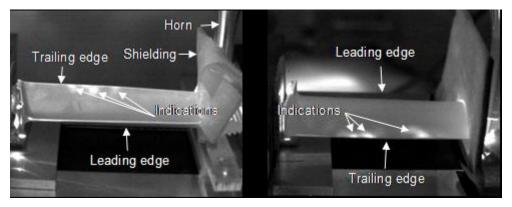
Figure 33. Part # VSSZ airfoil IR images, concave (left) and convex (right) sides, at 100 ms after sonic pulse initiation.

4.2.3.2.2 Part # TPN
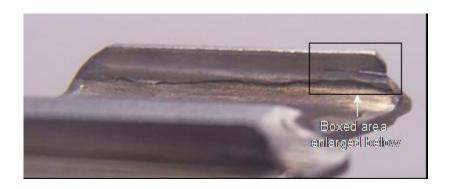
This part was condemned because of a crack in the tip shroud. Sonic IR testing detected the marked crack and another crack in one of the ridges on the shroud. Another Sonic IR indication was found on the other ridge. This indication did not correlate to any visual inspection or in-house FPI findings.

The unmarked crack detected in the shroud ridge was a through-wall crack approximately 0.15 inches in length. A photograph of the tip shroud with an enlargement of the cracked area is shown in Figure 34. After an estimated 40 - 50 Sonic IR tests on this part, a portion of the cracked ridge was liberated during a test. A sequence of images is shown in Figure 35 that captures this event. (The camera angles for Figures 34 and 35 are almost perpendicular to each other.) A photograph of the shroud ridge after the edge broke off is shown in Figure 36. The piece of material that broke off was not structurally sound prior to testing, so while it is somewhat disconcerting that the Sonic IR technique is capable of growing a crack to failure, in this case it did not matter. The part was already unfit for use prior to testing. This event does remind us of the importance of understanding the fundamental mechanism(s) responsible for generating indications with this technique. It is obvious that a damage threshold exists and

testing parameters must be understood and controlled sufficiently to stay below this threshold.

In-house FPI testing found an indication on the opposite end of the ridge that experienced the breakage. Sonic IR testing did not confirm this indication. Upon visual inspection, the area in question appears to be lap or some type of material buildup. These features are present on many of the shroud ridges on the blades. The origin of these features is not known to the author at this time. Photographs of some of these features are shown in Figure 37 and are visible in other tip shroud images as shown in Figure 36.

No Sonic IR indications were found on the airfoil portion of this part.
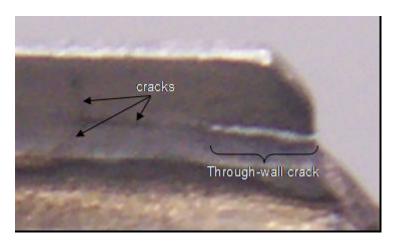
Figure 34. Part # TPN tip shroud (top) and enlargement showing cracks in the ridge (below).
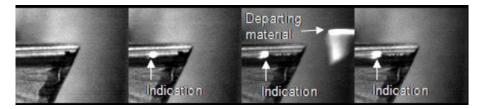
Figure 35. Part # TPN tip shroud Sonic IR sequence, 0ms, 33ms, 50ms, and 67ms after pulse initiation (left to right).
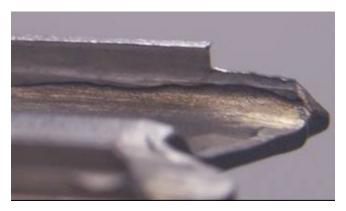
Figure 36. Part # TPN tip shroud ridge after failure.
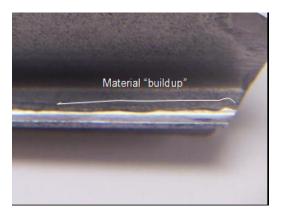
Figure 37. Tip shroud ridges showing buildup of material along edge.

4.2.3.2.3 Part # 7 (L21636)

This part was condemned because of a crack in the airfoil leading edge near the tip shroud. Sonic IR testing detected the marked crack and showed other indications along the trailing edge of the part, as shown in Figure 38. Some of the trailing edge indications were detected on both sides of the airfoil and

others were not. Figure 39 shows the tip shroud end with several Sonic IR indications. The airfoil trailing edge and tip shroud indications did not correspond to visible cracks or damage.
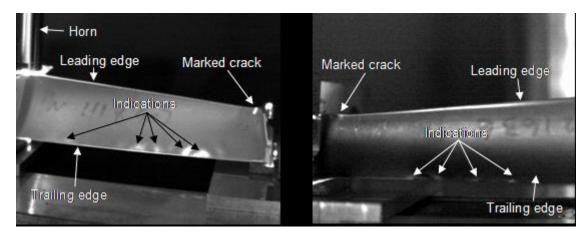
Figure 38. Part # 7 airfoil IR images, concave (left) and convex (right) sides, at 100 ms after sonic pulse initiation.
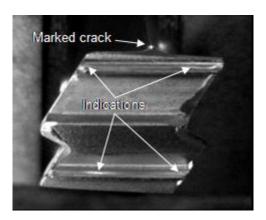
Figure 39. Part # 7 tip shroud IR image, 100 ms after sonic pulse initiation.

4.2.3.2.4 Part # 2 (L21887)

This blade was condemned because of a crack in the airfoil leading edge near the tip shroud in almost the same location as the marked crack in Part #7, discussed above. Sonic IR testing detected the marked crack along with three other indications on the ridges on the tip shroud. The airfoil crack is visible from the concave and convex sides of the airfoil in Sonic IR tests. IR images from

both sides of the airfoil are shown in Figure 40. No other indications were produced on the airfoil. Tip shroud IR images, taken prior to sonic pulse initiation for comparison and 100 ms after initiation, are shown in Figure 41. Faint indications are seen on the left and right on the top ridge and indications are seen intermittently across the bottom ridge. These indications are seen more clearly in the image sequence. The tip shroud indications do not correspond to the edge of the material build-up areas discussed in Section 4.2.3.2.2, but are between that edge and the base of the ridge. The marked airfoil crack is also visible in the top center of the 100 ms IR image in Figure 41.
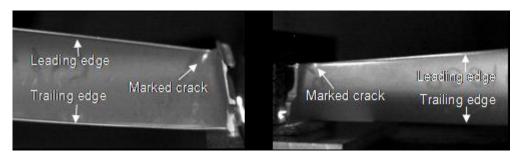
Figure 40. Part # 2 airfoil IR images, concave (left) and convex (right) sides, at 100 ms after sonic pulse initiation.
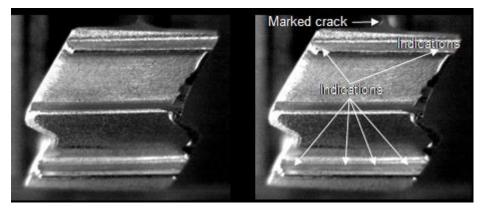
Figure 41. Part # 2 tip shroud IR image, prior to pulse initiation (left) and 100 ms after pulse initiation (right).

4.2.3.2.5 Part # 4 (L21447)

This blade was condemned because of cracks in the airfoil leading and trailing edges near the tip shroud. This blade is the only part in the current test set that contains 2 marked cracks. Sonic IR testing detected the marked cracks along with multiple other indications on the airfoil trailing edge. Figure 42 contains concave airfoil root end and tip shroud end IR images taken at 67 ms after sonic pulse initiation. (The indication with the **bold** arrow, seen in both images, can be used to align the two images.) Some of the trailing edge indications are barely visible under optical magnification. Figure 43 shows the IR image of the convex side of the airfoil. Both marked cracks are detected along with many indications along the trailing edge of the airfoil.

Sonic IR testing of the tip shroud produced a strong indication in the center of the top ridge. This signal does not correspond to anything visible on the part. A Sonic IR image of the tip shroud is shown in Figure 44.
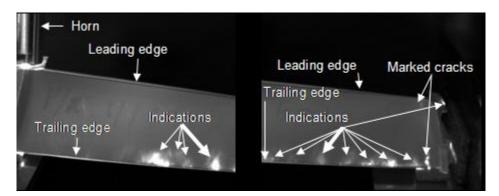
Figure 42. Part # 4 concave airfoil IR images, root end (left) and tip shroud end (right) at 67 ms after pulse initiation.
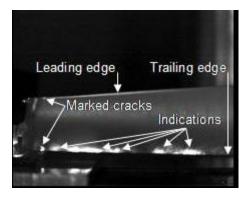
Figure 43. Part # 4 convex airfoil IR image at 67 ms after pulse initiation.
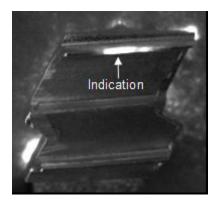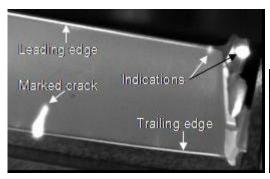
Figure 44. Part # 4 tip shroud IR image at 100 ms after pulse initiation.

4.2.3.2.6 Part # 3 (L22187)

This blade was condemned because of a crack in the airfoil trailing edge. Sonic IR testing detected the marked crack along with a series of other indications along the trailing edge. The marked crack was detected on the concave and convex sides of the airfoil. Some, but not all, of the other indications correlated with in-house FPI results. IR images of the airfoil are shown in Figure 45. Two other Sonic IR indications, one on the leading edge of the airfoil and one on the tip shroud, are also seen in the concave airfoil view and in both of these cases, small cracks can be seen under optical magnification. The tip shroud view, shown in Figure 46, contains these two indications along with other, uncorrelated, ones.
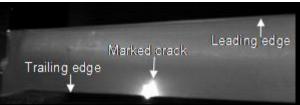
Figure 45. Part # 3 airfoil IR images, concave (left) and convex (right), taken at 50 ms after pulse initiation.
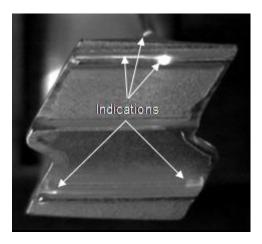
Figure 46. Part # 3 tip shroud IR image at 100 ms after pulse initiation.

4.2.3.2.7 Part # 1 (L21638)

This blade was condemned because of a crack in the airfoil trailing edge. Sonic IR testing detected the marked crack along with a series of other indications along the trailing edge. Some of these indications are visible under magnification and some were detected with in-house FPI. The marked crack was detected with Sonic IR testing from the concave and convex sides of the airfoil. Figure 47 shows IR images of the concave and convex sides of the airfoil taken at 50 ms after the sonic pulse initiation.

Sonic IR testing of the tip shroud of this blade produced an indication in one of the ridges. A crack was not found in this area by in-house FPI testing. Figure 48 shows the IR image of the tip shroud at 100 ms after pulse initiation.

Figure 49 contains an IR image of the bottom ridge (as viewed in Figure 48) with shielding in place and an enlargement of an indication detected on that ridge. This type of shielding test was performed whenever there was a question about the origin of a Sonic IR signal. Note that the IR camera was positioned at a higher angle, looking down on the part, in Figure 49 with respect to the image shown in Figure 48. This angle was necessary to image the indications shown.
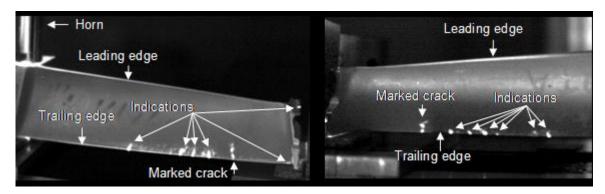
Figure 47. Part # 1 airfoil IR images, concave (left) and convex (right) sides, taken at 50 ms after pulse initiation.
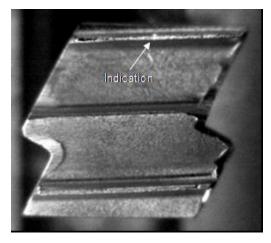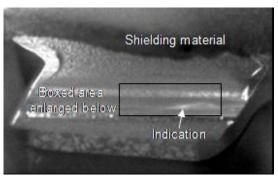
Figure 48. Part # 1 tip shroud IR image at 100 ms after pulse initiation.
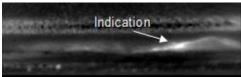
Figure 49. Part # 1 tip shroud IR image with shielding (top) and enlargement of indication area (bottom).

4.2.4 Conclusions for Turbine Blade Testing

The TF33 2nd stage turbine blade set contained marked and unmarked cracks on the leading and trailing edges of the airfoil and on the tip shrouds of the blades. All marked cracks were detected with Sonic IR inspection with differing levels of effort. The marked airfoil cracks were all detected quite easily. Low levels of excitation were possible and clamping and horn placement did not have to be precise. The marked tip shroud cracks, in contrast, did require some effort to determine the optimal clamping arrangement, horn placement, and excitation level, and the resulting Sonic IR signals were of much lower amplitude than the airfoil signals. These results are not surprising given the geometry of the part. The tip shroud area is thicker than the edges of the airfoil and the material is more confined by surrounding material than the airfoil edges.

Of particular interest in the blade test results is the detection of unmarked cracks and the Sonic IR indications that did not correlate to detectable cracks. First, the detection of cracks that are optically detectable but not known to exist prior to Sonic IR testing constitutes successful "blind test" cases. These successes lead to increased confidence in the technique. Second, the reproducible but uncorrelated Sonic IR signals obtained on some parts raise

41

questions as to their origins. The indications were not present on all of the parts, so it can be concluded that they are not the result of a simple geometric/resonant effect. The airfoil indications occurred along the leading and trailing edges, in the same areas that exhibit cracking on other parts. It is possible that the signals arise from cracks that are too small or tightly closed to be observed optically under magnification or enhanced with FPI. The uncorrelated indications for the tip shroud generally occurred between the material build-up region of the ridge and the ridge base (shroud platform), but in a few cases signals were obtained from the edge of the material build-up area. Many questions remain about these ridges and material build-up areas of the blade, so it is not prudent to speculate on the origin of the signals in those areas at this time.

4.2.5 TF33 2nd Stage Turbine Blade Fixture

In preparation for further work with these blades, a fixture was designed and built. Figure 50 shows the TF33 2nd stage turbine blade fixture model with a blade from a side view, and Figure 51 shows a top view.
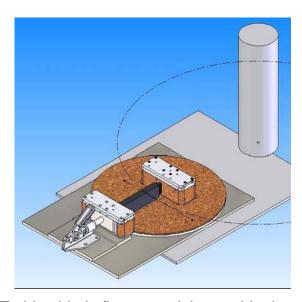
Figure 50. Turbine blade fixture model on welder base with blade.
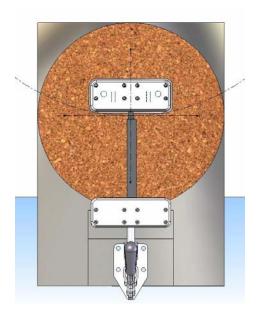
Figure 51. Turbine blade fixture with blade, top view.

Photographs of the fixture mounted on the welder base are shown in Figures 52 and 53. An IR image of a blade during testing is shown in Figure 54, with the crack indicated.
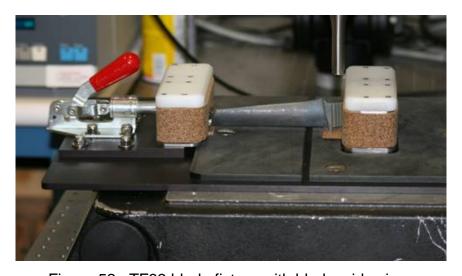
Figure 52. TF33 blade fixture with blade, side view.
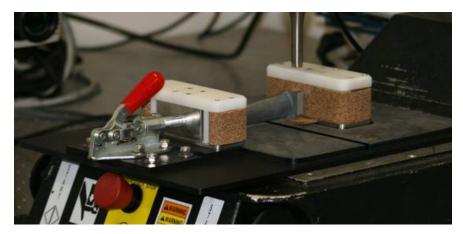
Figure 53. TF33 blade fixture and blade, front angled view.
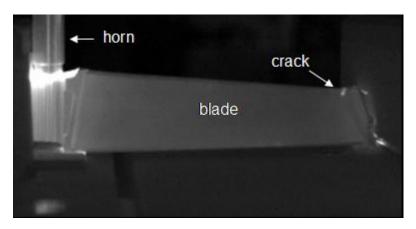
Figure 54. IR image of TF33 blade in fixture while excited by horn.

4.2.6 Spatial/Temporal Response Observation for Turbine Blade Data

While extracting data from the blade IR time sequence files, it was noted that the position of maximum contrast along the length of the crack, in some instances, varied as the operating parameters were varied. Examples of this observation are shown in Figures 55 and 56 below. The cropped IR images in Figure 55 were obtained from blade #3 with amplitude, pulse length, and trigger force settings of (a) 60, 150, 10 and (b) 60, 150, 60. The IR images in Figure 56 were obtained from blade #7 with amplitude, pulse length and trigger force settings of (a) 60, 217, 10 and (b) 60, 83, 10. This phenomenon illustrates the

44

danger of using any one frame of the Sonic IR data from which to draw all conclusions about the defect.
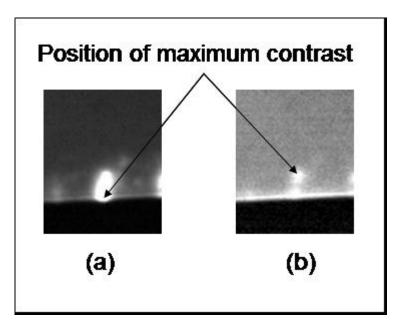
Figure 55. IR images of trailing edge crack in blade #3 acquired at different system operating parameters.
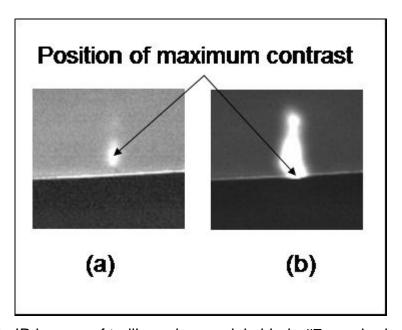
Figure 56. IR images of trailing edge crack in blade #7 acquired at different system operating parameters.

4.3 Compressor Blades

4.3.1 Compressor Blade Description

Forty compressor blades were received from Tinker Air Force Base by the program for Sonic IR testing. These blades had been rejected for fatigue cracks and the indications resulting from FPI were marked on the parts. An example of one of these compressor blades is shown in Figure 57.

Figure 57. F100 9th stage compressor blade.

Two examples of cracks in these small blades, from F100 compressors, are shown in Figures 58 and 59. The components were clamped in a vise.
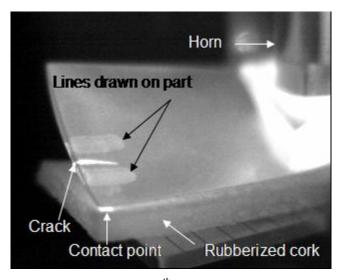
Figure 58. Crack in F100 9th stage compressor blade tip.
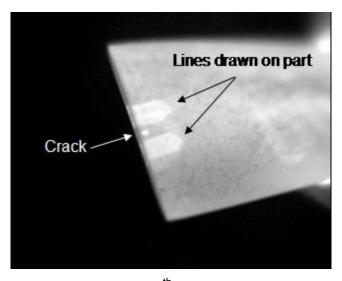
Figure 59. Crack in F100 7th stage compressor blade tip.

4.3.2 Compressor Blade Fixture

In preparation for possible future testing of these components, a small compressor blade fixture was completed and tested. A photograph of the fixture on the welder base is shown in Figure 60. The blades remain much more stable during testing in the fixture than they did in the vise. It may be possible to stabilize them even further by replacing the rubberized cork-lined metal jaws,

shown in Figure 61, with a soft nylon material. The blades are easily fixed and released in the fixture using the red handle on the right. The horn contacts the root of the blade. This fixture will accommodate several stages of TF33 and F100 compressor blades.
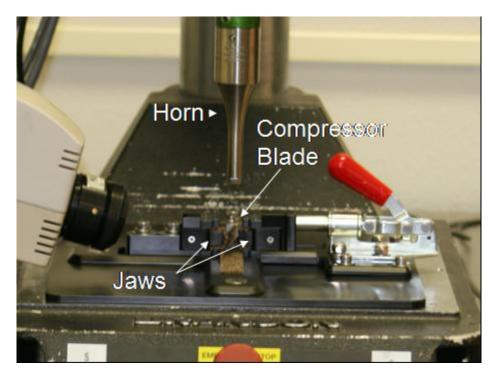
Figure 60. Small compressor blade fixture on welder base.

Figure 61. Jaws from the small compressor blade fixture.

While enough rejected F100 9th stage compressor blades exist for conducting parameter studies, these studies were not performed on this program.

4.3.3 Compressor Blade Anomaly

During testing of one of the compressor blades, a marked indication was not detected with Sonic IR. In an effort to understand this result, the blade was sent to Steve Cargill, a consultant on the program, for further investigation. The report of his findings is included below.

*BEGIN REPORT
Blade Evaluation-TF33 15th Stage Compressor Blade

A single blade, Part Number 464215J, was carried to Martin MetLabs in Stuart, Florida, on February 6th. Several experienced engineers surveyed the indicated area on the suction side of the blade, near the platform. None of the engineers could recall seeing a similar phenomenon on a blade. It is somewhat reminiscent of thermal mechanical fatigue (TMF), but this blade was probably run in a lower temperature environment than would produce TMF. Figure 62 shows the affected area at a magnification of 16X, while Figure 63 shows the same region at slightly higher magnification.

Figure 62. Indicated region at 16X magnification.

Figure 63. Indicated region at 25X magnification.

As magnification was increased, it became obvious that the nature of these indications is to have relatively large surface openings. When observed at 40X magnification, it was possible to see to the bottoms of some of the anomalies (Figure 64). These don't appear as normal fatigue cracks. Furthermore, it is easy to understand why Sonic IR does not produce any indications, considering the relatively large openings and apparent shallow nature of at least some of the anomalies. It does appear that the surface may have been etched to produce this effect. The next step in the investigation would be to break open some of these anomalies and obtain depth profiles.

Figure 64. Indicated region at 40X magnification.

The program did not pursue further study of this blade and returned it Tinker Air Force Base.

4.4 Vane ring

A vane ring of unknown origin with marked cracks in the trailing edges of several blades was inspected. Sonic IR images of all of the known cracks were obtained, but with difficulty. This part had a complex geometry and it was determined to be a poor candidate for future tests, given this complexity. The IR images with the cracks circled are shown in Figure 65.

| (a) | (b) | (c) |
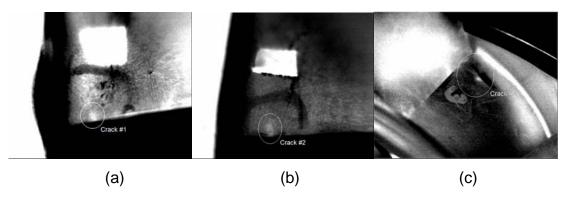
Figure 65. IR images of three cracks found in vane ring, (a) crack #1, (b) crack #2, and (c) crack #3.

5.0 Parameter Studies

In order to optimize defect detectability and minimize input energy in the components being tested, rigorous testing of specific components was conducted. High, low, and mid-range parameter settings were determined through empirical means, and hundreds of tests were performed based on a randomized matrix of operating parameter value combinations. The goal was to use the optimized parameter settings determined by this matrix testing to define an inspection procedure for a given component. This inspection procedure would then be used to conduct a PoD study on a statistically designed set of those components. This program studied 4 sets of components and specimens using this matrix testing method. These studies are described in the following sections.

5.1 Elongated Scallop Samples

The work on the specimens described in this section was presented at the Thermosense XXVI conference and published in the conference proceedings (Reference 4). A portion of the analysis was also presented at the March 2004 UDRI Workshop on Ultrasonic Testing and PoD Evaluation.

5.1.1 Scallop Sample Description

The samples used for this first round of matrix testing were obtained on loan from Pratt and Whitney. A sketch of the elongated scallop sample geometry with dimensions is shown in Figure 66. The samples are made of titanium and had fatigue cracks of various lengths placed in the scalloped region (on edge). The samples selected for our testing had cracks of lengths 0.0215 inch, 0.0115 inch, and 0.0175 inch, and were referred to as sample numbers 22, 12, and 18, respectively. All of these samples had the cracks placed in roughly the same

52

position along the scalloped region, as indicated in Figure 66. A photograph of the sample, with a pen for scale, is shown in Figure 67.
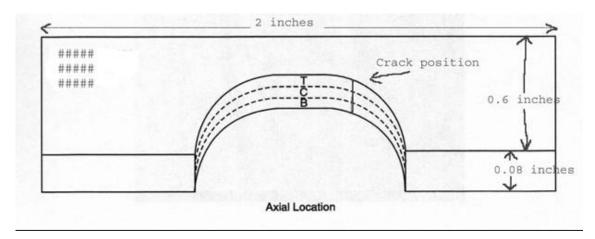
Figure 66. Sketch of scallop sample.

Figure 67. Photograph of scallop sample.

These specimens were subjected to hundreds of tests as part of the study. In order to ensure that the cracks had not lengthened during this testing, the samples were sent to Martin MetLabs, Inc. for crack length measurement. Excerpts from their report are included in Appendix A. The conclusion was that the cracks had not grown during the series of numerous Sonic IR tests.

5.1.2 Scallop Sample Experimental Setup

The standard Sonic IR test system was used for this testing. A photograph of the scallop specimen clamped in the vise for testing is shown in Figure 68.
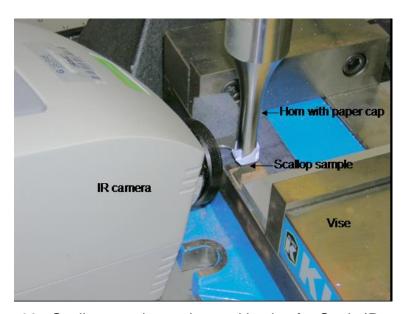
Figure 68. Scallop specimen clamped in vise for Sonic IR testing.

5.1.3 Scallop Sample Fixture

Originally, "clamping force" (of the fixture) was included as a test variable in the test matrix for the scallop samples. However, it was not possible, with readily available equipment, to fixture the scallop samples with any amount of measurable force and still excite the fatigue cracks. It is possible that a small, custom, precision clamp could have been manufactured to address this problem, but given the time constraints of the sample loan (one month) and the uncertainty of success with such a clamp, "clamping force" was dropped from the test matrix. Horn position was also dropped as a potential test variable because of the small size of the samples relative to the horn tip. Samples were only excited with one horn position, as shown in Figure 68, above. With the orientation of the sample

as shown in Figure 66, the half-inch diameter horn was positioned on the left area of the sample (with the # symbols in the corner).

The samples were secured as repeatably as possible in the following manner. The scallop sample rested horizontally on the base of a vise with a small (~0.5 inch x 0.5 inch) piece of rubberized cork under the same end of the sample that was contacted by the horn. That edge of the sample was positioned vertically against a piece of rubberized cork. The opposite edge of the sample was contained by a one-inch square piece of foam with a quarter-inch deep slit in it. The vise was hand tightened only to the point where the sample was stabilized. The cracks were located about two-thirds of the distance along the length of the sample from the horn contact point. This configuration allowed for support of the sample at the horn contact site and some motion of the sample at the other end. If this slight motion was prohibited, it was not possible to excite the cracks. However, if some constraint were not applied, the sample would rotate or translate under the horn. The samples were protected from marring by the horn by 80-weight card stock paper. To prevent the paper from slipping out from between the horn and sample, the edges of the one-inch square piece of the paper were folded up around the horn tip to form a shoe. This shoe can be seen in Figure 68.

NOTE: This clamping method would not be acceptable for any type of production testing, nor would this experimental setup ever be recommended for crack detection in such small parts. (The system was originally designed to test 40-pound engine disks.) However, for testing at least some of the technique variables, this experimental setup and fixture were acceptable.

5.1.4 Scallop Sample Data Acquisition

The experimental variables, or factors, included in the testing of the scallop samples are shown in TABLE 5 along with the levels of the factors. Three levels of each factor were used in the design. All of the horn tips were 0.5

inch in diameter, but had different tip geometries. The 3 levels for the horn tip "lift-off" were included that reflect the distance between the outer edges of the tip when the center of the tip first makes contact with a flat surface. Other representations of the curvature of the horn tip could be used, but it was felt that this representation was adequate to allow any dependency on the radius and also to allow for interactions between the Horn Tip factor and the other factors to be estimated.

TABLE 5. INITIAL FACTORS AND LEVELS FOR SCALLOP SAMPLES.

Factor	Level 1	Level 2	Level 3
Horn Tip (H) "lift-off"	Flat 0	5.9 inches radius 0.0053 inch	3.35 inches radius 0.0094 inch
Pulse Amplitude (A) in % of maximum	15	28 [33[+]]	40 [50[+]]
Pulse Length (P) in milliseconds	75	125	200
Trigger Force (T) in pounds	50	65 [80[+]]	80 [110[+]]
Flaw length (L) in inches	0.012	0.018	0.022

[+]Values used for the flat horn tip only

There are 243 (35) combinations of the factors shown in TABLE 5. In addition, we collected 3 data sets for each combination of factors for nominally 729 total data sets.

All tests for a given horn tip geometry were run consecutively on each of the three samples and then the tip was changed. The other variables were changed through the welder controller for each test as prescribed in the test matrix. After each test, it was verified that IR, vibrometer, and welder data were obtained successfully before proceeding to the next test. Foam positioning material and the rubberized cork materials were replaced daily. The interface

material was replaced for each test since it became compressed during the excitation pulse.

The first test on each day of testing was conducted on a verification sample, chosen from the scallop sample set. This sample had a 0.015 inch crack in approximately the same location as the cracks in the test samples, eliminating repositioning of the IR camera. The test variables were fixed at prescribed levels known to excite the crack. Running this test every morning and detecting the crack helped assure that all of the equipment was functioning properly. After the verification run, the test sample was clamped and the matrix testing began.

One problem that was encountered in the testing was a *General Alarm* in the welder system. When this alarm occurs, the welder aborts the test, yielding a pulse length that is shorter than the one prescribed. The most common cause of this alarm in our testing was a lock-up condition at the welder/sample interface. There is a protective feedback loop in the welder that shuts off the power to the horn if the horn does not have adequate freedom of motion. This condition often occurs at higher trigger force and vibration amplitude settings, but it has been observed to occur at lower settings as well. To minimize gaps in the data set, a protocol was developed to handle the alarm situation. If any one of the three tests at a given set of variable values produced an alarm, the trigger force was reduced to the midpoint between the existing value and the next lowest value in the matrix. Three tests at the new set of variable values were then conducted. If one of those test resulted in an alarm, the set was skipped. Each time there was an alarm, the welder system had to be recalibrated, according to the manufacturer's instructions, before continuing. Alarms, therefore, slowed down data acquisition as well as altered the original test matrix.

5.1.5 Scallop Sample Data Extraction

Data extraction was performed after all of the tests were completed. For each IR data file, the following parameters were recorded:

- maximum contrast

- time to maximum contrast

- maximum vibration amplitude

- time to maximum vibration amplitude

- recorded pulse length

- contrast at the end of the pulse

- contrast at the end of the pulse + 500 ms

Of these data, recorded pulse length was obtained from the built-in EchoTherm VT *Capture Information* feature. This recorded length sometimes varied slightly from the prescribed length. The maximum vibration amplitude and time to maximum vibration amplitude data were obtained from the program's *Amplitude-Power* graph. All other data had to be obtained from the IR image sequence. A very useful feature of the EchoTherm software, the *T-t Profile*, was of no help in the data extraction for these samples. The *T-t Profile* plots the amplitude-time history of the signal at the position indicated by a cursor, which can be a single point or NxN points. This feature would have allowed for easy extraction of the remaining parameters. However, because the sample moved slightly during testing, this feature could not be used. This data extraction method proved to be a very time-consuming process.

Maximum contrast and time to maximum contrast were determined by positioning a background cursor, 3 x 3 pixels in size, and 15 pixels to the left of the single pixel cursor positioned over the peak amplitude point on the crack. The *Contrast* option in the program's *T-t Profile* feature was used to plot out the difference between these two cursor values as a function of time. The cursors had to be repositioned in several frames in order to find the true maximum contrast value and time since the sample moved slightly during testing. The contrasts at the end of the pulse and at 500 ms after the end of the pulse were extracted using the cursors in two specific frames – the last frame of the pulse and 500 ms after the end of the pulse, respectively. This last value will be used as a baseline value since the part has cooled to ambient by that time. Often in thermal nondestructive evaluation, a frame prior to the heating of the part would

be used as the baseline. In this testing, however, the part moved when contacted by the horn so there was no spatially stable frame to use as a baseline prior to the pulse initiation. A "dwell time" was used on the welder to hold the horn in contact with the part after the acoustic pulse had turned off. This method kept the part spatially stable long enough to obtain a baseline reading.

5.1.6 Scallop Sample Data Analysis

The question of whether a flaw is detected using Sonic IR is, of course, related to the amplitude of the signal when the sonic energy is imparted to the part. This detection of a flaw occurs when a change is observed in the image of the flaw over time. A particular flaw may or may not be detectable at all, resulting in binary data (detected/not detected) to characterize the inspection. However, if it is detectable, the signal amplitude can be used as a response to be studied in relation to the various input variables. These sets of data (detect/no detect and amplitude response) are analyzed by different statistical techniques. The binary data are analyzed using binary logistic regression and yield a probability of detection as a function of the design variables. The response data are fit to a quadratic function of the design variables.

The purpose of the analysis presented here is to estimate probability of detection (PoD) from the binary data and to compare that to the mean response surface fit to the contrast change variable. If the IR image contrast variable (amplitude) is directly related to the probability of detection then the areas of the design space that yield lower mean responses should also yield lower estimates of probability of detection.

It should be clear that the probability of detection that is calculated here would not be applicable to field inspections. In the data analyzed here, the experimenter is aware of the presence of a flaw and therefore the slightest amount of change in the IR image in the flaw area is interpreted as a detection. Therefore, no consideration has been given to the inherent background noise in the full view of the IR image. Incorporating the noise in the background image

changes would require the raising of the threshold for making calls. This, in turn, would lead to lower PoD estimates for field implementation. The data analyzed here were gathered on three flaws of different sizes. Therefore, flaw–to–flaw variation is also not adequately known to be able to provide a realistic field applicable PoD estimation.

5.1.6.1 Response Surface Analysis of Scallop Sample Data

The initial response variable analyzed was the maximum contrast change. This response was calculated by taking the difference in the maximum contrast near the flaw during the pulse and the contrast value 500 milliseconds after the pulse. This quantity reflected how much the crack "lit up" from the background and should be directly related to the detectability of a flaw. Figure 69 contains a histogram showing the distribution of this quantity over all the shots.
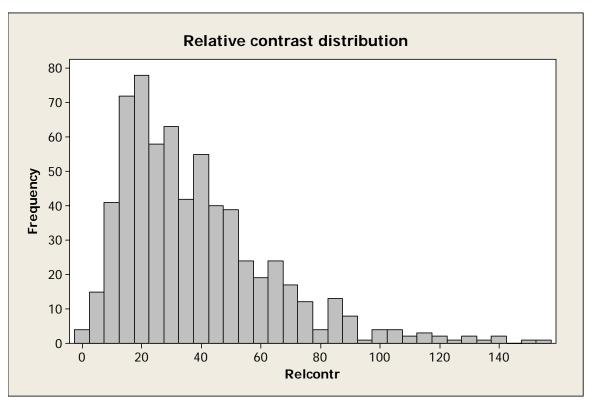
Figure 69. Histogram of relative contrast distribution for all experiments.

The actual model fitting was performed using the square root transform of the relative contrast variable, as it provided residuals that are more consistent with the usual Normality assumptions. The initial distribution for the square root transform is given in Figure 70 below.
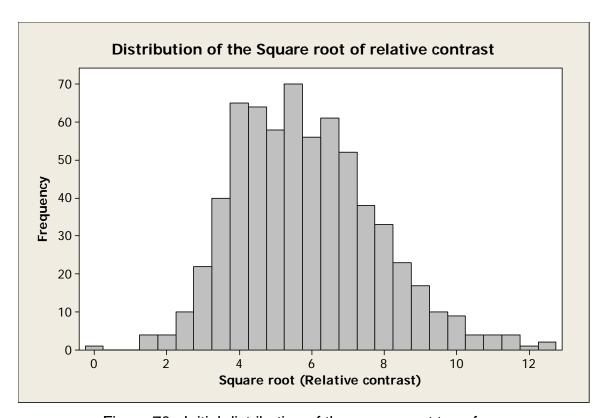
Figure 70. Initial distribution of the square root transform.

Initially, a full quadratic model was fit to the response using the five variables shown in TABLE 6. That is,

$$resp = c_0 + c_1 x_1 + c_2 x_2 + c_3 x_3 + c_4 x_4 + c_5 x_5$$
$$+ c_{12} x_1 x_2 + c_{13} x_1 x_3 + c_{14} x_1 x_4 + c_{15} x_1 x_5 + c_{23} x_2 x_3 + c_{24} x_2 x_4 + c_{25} x_2 x_5 + c_{34} x_3 x_4 + c_{35} x_3 x_5 + c_{45} x_4 x_5$$
$$+ c_{11} x_1^2 + c_{22} x_2^2 + c_{33} x_3^2 + c_{44} x_4^2 + c_{55} x_5^2, \tag{1}$$

where the coefficient, $c's$, are all estimated from the data. However, the coefficients that were not statistically significant at the 0.05 level were eliminated. TABLE 6 shows the combination of terms remaining in the model using this procedure. Note that the first order terms are all retained in the model as a result of being statistically significant in combination with at least one additional factor.

The resulting fit is of the form:

$$resp = c_0 + c_1 x_1 + c_2 x_2 + c_3 x_3 + c_4 x_4 + c_5 x_5 + c_{14} x_1 x_4 + c_{15} x_1 x_5 + c_{23} x_2 x_3 + c_{25} x_2 x_5 + c_{45} x_4 x_5$$
$$+ c_{11} x_1^2 + c_{22} x_2^2 + c_{55} x_5^2, \tag{2}$$

where the subscripts are determined from the numbering of TABLE 6.

TABLE 6. COMBINATION OF VARIABLES USED IN MODEL.

	Probe radius	Vibration amplitude	Pulse length	Trigger force	Flaw length
1. Probe radius (as lift-off)	X				
2. Vibration amplitude		X			
3. Pulse length		X			
4. Trigger force	X				
5. Flaw length (log transform)	X	X		X	X

The distribution of residuals after the model fit are shown in Figure 71 and indicate that approximately 50% of the variation has been explained by the model. This residual variation can be used to obtain preliminary probability of detection values when combined with the assumption that a certain level of relative contrast is needed in order to make a call.
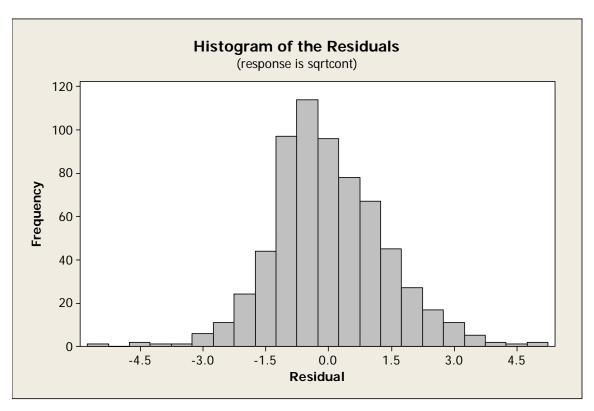
Figure 71. Residuals of square root (relative contrast) after model fit.

To visualize the effect that the various factors have on the contrast, pair-wise contour plots are given in Figure 72 for the large flaws. For example, the upper left plot of "lnlength*Pr_Lo" shows the contour lines for the response as a function of the flaw size (expressed as natural logarithm of size) in the vertical axis and the probe lift–off factor in the horizontal axis. For this plot, the other three factors are set at the levels shown in the "Hold Values" box. These values are: Pr_Lo = 0.0912, lnLength = -3.817, VIBR = 50, PULSE = 200, and TR_FO = 50. They are the levels that produce the overall high values for contrast for the large flaws. Figure 73 shows the same set of contours where the hold values are those that produce the maximum contrast for the small flaws. Those hold values are: Pr_Lo = 0.2143, lnLength = -4.423, VIBR = 50, PULSE = 200, and TR_FO = 110.
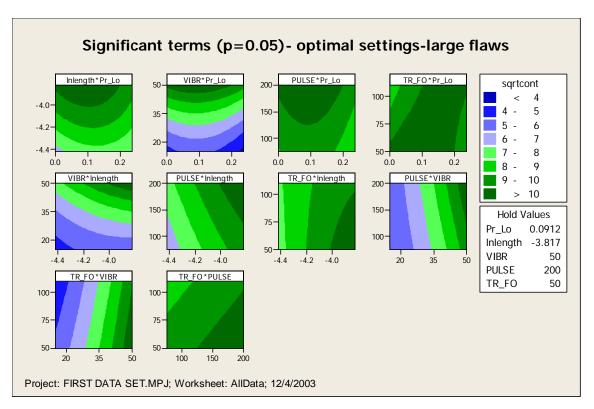
Figure 72. Pair wise contours at optimal settings for large flaws.
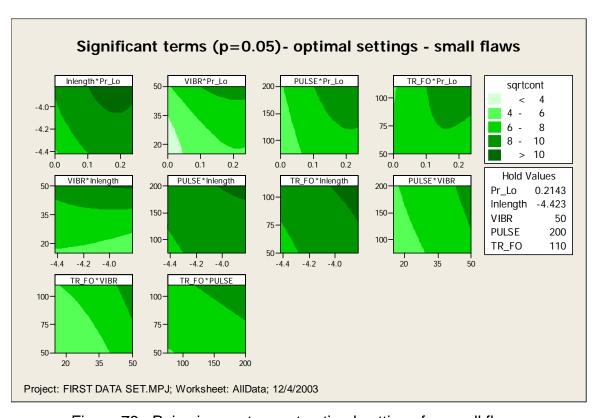
Figure 73. Pair wise contours at optimal settings for small flaws.

The most apparent factor in the plotted contours is the role of the vibration amplitude (VIBR) factor. This factor is the largest contributor as is evidenced by the full range of contrast values being present in the contour plots involving it. The contour plots show that, as expected, maximum relative contrast occurs at largest pulse length and the largest vibration amplitude for the full range of all other conditions. Trigger force did not exert a large effect on the results, but the model suggests that the lower trigger force is slightly better for flat probes and higher trigger force is better for the more curved probe. This transition for the effect of trigger force implies that a probe tip curvature between the two extremes employed in this experiment could be effective in removing any effect due to trigger force.

5.1.6.2 Binary Analysis of Scallop Sample Data

The binary data of detections and non-detections are analyzed using a binary regression model with the probit link function. This model is consistent with a latent, continuous variable that determines detectability. Used for the analysis is a complete quadratic in the five independent variables given in TABLE 6. The full model is given in equation (3).

$$
\begin{aligned}
\pi = \Phi(c_0 &+ c_H x_H + c_A x_A + c_P x_P + c_T x_T + c_L x_L + c_{HA} x_H x_A + c_{HP} x_H x_P + c_{HT} x_H x_T \\
&+ c_{HL} x_H x_L + c_{AP} x_A x_P + c_{AT} x_A x_T + c_{AL} x_A x_L + c_{PT} x_P x_T + c_{PL} x_P x_L + c_{TL} x_T x_L \\
&+ c_{HH} x_H^2 + c_{AA} x_A^2 + c_{PP} x_P^2 + c_{TT} x_T^2 + c_{LL} x_L^2)
\end{aligned}
\tag{3}
$$

where H = probe radius, A = vibration amplitude, P = pulse length, T = trigger force, and L = flaw length.

The model of equation (3) contains 21 terms covering the overall mean, 5 linear terms, 10 factor interaction terms, and 5 squared terms. Once these terms are estimated from the data it is apparent that many of them contribute little to explaining the data. That is, the estimates of the coefficients do not differ from 0 by a statistically significant amount. The model was reduced to only those terms showing statistically significant contributions resulting in equation (4).

$$\pi = \Phi(-68.252 + 15.222x_H + 0.4174x_A - 0.0273x_T - 31.736x_L + 0.2512x_H x_T$$
$$+ 4.937x_H x_L + 0.08124x_A x_L - 50.96x_H^2 - 3.628x_L^2) \qquad (4)$$

The variable P (pulse length) does not significantly contribute to the probability of detection and therefore does not appear in equation (4).

      The fit of equation (4) allows for the estimation of a probability of detection after specifying the various input values for the given parameters. One can also specify the set up parameters (H, A, and T), in which case the argument becomes a function of L, the size parameter. This allows for the estimation of the traditional probability of detection as a function of the flaw size. For example, consider the case where H=0 (flat probe), A = 50% of maximum amplitude, and trigger force, T = 50 pounds. With these values, the argument of equation (4) is a quadratic in the one remaining parameter, L, which is the logarithm of the flaw length. This function is graphed along with two others in Figure 74, for flaw sizes up to the largest included in the experiment.

      The coefficient for x_L^2 is negative, which implies that for arbitrarily large and arbitrarily small flaws the function argument in equation (4) will become negative and the PoD will therefore go to zero. This is a desired result for the small flaws, but is not believable for the large flaws. This illustrates the problem with this model for extrapolating results to larger flaws.
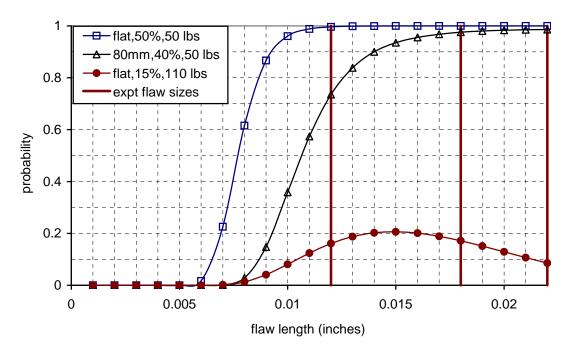
Figure 74. Specific PoD functions (probe, amplitude, trigger force).

It is also the case that an increasing PoD in the region covered by the experimental design is not imposed by the model form of equation (4). One consequence is the possibility of a PoD curve such as that given by the conditions using flat probe, A = 15% of maximum amplitude, and trigger force, T = 110 pounds. The resultant estimated PoD curve is shown in Figure 74 where it is apparent that a monotonic structure is not imposed. One should take the fit as an indication that there was little difference in the three flaws and the overall detection rate under these conditions was approximately 15% independent of the flaw size. A similar argument could be made for the conditions of a flat probe at 50% amplitude and 50 pounds of trigger force. The resultant PoD curve for flaw length is as one would expect, but it should be clear from the curve in Figure 74 that the portion of increase in the PoD is in an extrapolation region. However, these results indicate that a future design for further characterizing inspections on these specimens should include flaw lengths in the 0.005 to 0.007 inch range.

5.1.6.3 Comparison of Scallop Sample Binary Analysis to Contrast Response

In addition to the binary data reflecting whether the flaw was detectable, data also yield a response variable as to amplitude of the signal. The response used for analysis is the difference of the maximum contrast during the pulse and the contrast at the end of the pulse + 500 milliseconds. The contrast was measured as the difference between peak value at the crack and a background value measured 15 pixels to the left of the peak. With this response labeled "R," the same quadratic model used in the binary analysis was fit to the square root of R and those factors that were not statistically significant were eliminated. (The square root transform was used in order that the residuals from the fit come closer to having a Gaussian distribution.) The resultant fitted equation is given in equation (5).

$$\sqrt{R} = -37.8 - 30.4x_H + 0.492x_A - 0.00168x_P - 0.154x_T - 22.3x_L$$
$$+ 0.192x_H x_T - 8.7x_H x_L + 0.000246x_A x_P + 0.125x_A x_L - 0.0317x_T x_L$$
$$- 68.2x_H^2 + 0.00146x_A^2 - 2.89x_L^2 \tag{5}$$

The starting point for the explanatory variables in fitting the binary PoD argument and the mean response level for $\sqrt{R}$ is the same. However, the resulting explanatory functions are different. Although differences would be expected, we also expect the probability of detection to have a monotonic relationship with the response value. Comparing the form of equation (5) to that of equation (4) four additional terms are added. There are more data available for the response fits so it is not unexpected that there would be additional resolution for the fits.

Although the equations differ between the response surface and the binary PoD argument, can we say that the response fit is telling the same story about detectability as the binary fits? In order to answer this question we compare the equi-probability contours from the PoD fits to response surface contours. This is done in the array of graphs shown in Figure 75, where the different probes and flaw sizes are reflected in the 9 different contour plots and

the contours of trigger force versus amplitude are given. In all cases, the pulse length (important in the response model but not in the binary analysis model) is set to the maximum of 200 milliseconds. The levels for the response contours were chosen arbitrarily, with only a criterion that they are in the same regions as the probability contours from the binary analysis.

There is overall good agreement between the two analysis. Both analyses predict the best operating conditions to be high amplitude, low trigger force for the flat probe and high amplitude, high trigger force for the 0.0053 inch curved probe and the 0.0094 inch probe for the smaller of the flaws. The two methods differ on the prediction of the best conditions for the 5.9-inch probe and the two large flaws. The difference is in the best choice for the trigger force. However, from Figure 75 it is seen that the contours for both models are nearly vertical for these two operating conditions (bottom two graphs in center column). This indicates that there is very little dependence on trigger force for these conditions and that with the amplitude at the high value, trigger force is not important.
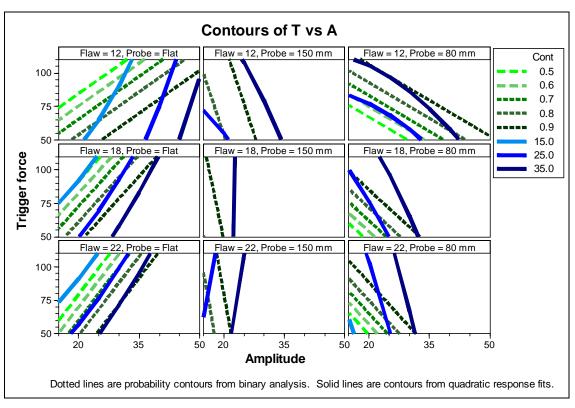
Figure 75. PoD contours compared to response contours (P=200 milliseconds).

The response surface values can be equated to probabilities of detection by considering that detection is made only if the response exceeds a certain threshold, T. This is done by using the variation in the residuals after fitting the mean responses. The residual standard deviation was 1.872 in this example. We would therefore estimate the probability of detection along a mean contour of "m" for the response R to be given by equation (6):

$$POD = \Pr(\sqrt{R} > \sqrt{T}) = \Pr\left(\frac{\sqrt{R} - \sqrt{m}}{1.872} > \frac{\sqrt{T} - \sqrt{m}}{1.872}\right) = \Phi\left(\frac{\sqrt{m} - \sqrt{T}}{1.872}\right) \quad (6)$$

where $\Phi(\cdot)$ is the standard normal distribution function. The last equality in equation (6) assumes that the quantity $\left(\dfrac{\sqrt{R} - \sqrt{m}}{1.872}\right)$ is adequately modeled by a Gaussian random variable and therefore the probability of being greater than x is equal to the probability of being less than negative x.

Let $T = 15$ and equation (6) results in PoD values of 0.50, 0.73, and 0.86 associated with $R = 15$, 25, and 35, respectively. These values are in rough agreement with the PoD contours in the case of the flat probe and the largest flaw (lower left graph of Figure 75).

5.1.7 Summary of Scallop Sample Study

We have shown agreement between a binary analysis and response surface analysis in predicting the best operating conditions within the operating conditions incorporated into a design of experiments. The binary analysis uses only the information that flaws are detected or not detected. The response surface analyses uses signal amplitude information to characterize the influence of the operating regime on the inspection results. We have also shown how the

mean response data would be converted to probability of detection using a threshold for the response that must be met before a flaw is "detected."

The analysis was performed on data gathered in the laboratory by an experimenter who knew where the flaws were located and was characterizing the impact of the various operating conditions on the flaws. Therefore, the probability of detection as presented here cannot be considered to apply to conditions where the presence or absence of a flaw is unknown.

The model of the response surface does provide the ingredients to make an estimation of PoD when the presence or absence of a flaw is unknown. This would be accomplished by characterizing response changes in a wide variety of specimens with no flaws and then setting the threshold, T, to a value that would preclude making false calls.

5.2 FPI PoD samples

A set of Inconel 718 samples with artificial fatigue cracks that was used as a fluorescent penetrant inspection (FPI) PoD test set by Goodrich Aerospace was obtained on loan by the program for testing.

5.2.1 FPI PoD Sample Fabrication

The specimen fabrication process began with 0.25 inch x 4.25 inches x 18 inches blanks of Inconel material. For each desired fatigue crack, two half-inch wide notches of material were removed to a depth of 0.020 inch, with a 0.010 inch wide "rib" of remaining material between them. An EDM notch was machined across (perpendicular to) this rib to a depth of 0.007 inch. This rib technique was used to expedite the cracking process and to produce a more natural length-to-depth aspect ratio in the final crack. Individual notch locations were selected so that the final specimens could be cut out with 0°, 90°, +45°, and -45° crack orientations.

The fatigue cracks were grown in tension-tension cantilever bending. The loads varied, but most samples were processed at roughly 90 pounds minimum and 1000 pounds maximum with a 4 inch moment arm. After cracking, the specimen blanks were milled to near final thickness and cut lines for the individual specimens were scribed into the blanks. The 4 inches x 1.25 inches specimens were then water-jet cut from the blanks and ground to a final thickness of 0.25 inch.

A photograph of one of the samples, with a pencil for scale, is shown in Figure 76.

Figure 76. FPI PoD specimen with pencil.

5.2.2 FPI PoD Sample Experimental Setup and Design

Samples were clamped for this testing lengthwise in a vise, as shown in Figure 77.
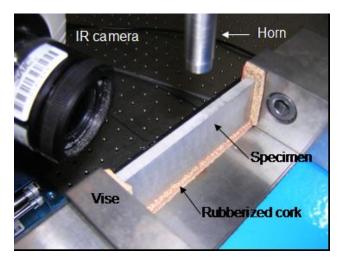
Figure 77. FPI PoD specimen clamped in vise.

Four factors, vibration amplitude, trigger force, pulse length, and clamping torque, and three levels of each factor were used in the testing of seven specimens. The factor levels are shown in TABLE 7. Crack lengths in the samples were 0.028 inch, 0.042 inch, 0.069 inch, 0.093 inch, 0.116 inch, 0.182 inch, and 0.252 inch.

TABLE 7. FACTOR LEVELS FOR FPI POD SPECIMENS.

Factor	A- Vibration amplitude (% max)	T- Trigger force (pounds)	P- Pulse length (milliseconds)	C- Clamping torque (foot-pounds)
Low level	50	20	83	5
Mid level	75	45	150	7.5
High level	100	65	217	10

5.2.3 Analysis of FPI PoD Sample Data

5.2.3.1 Response Surface Analysis of FPI PoD Sample Data

As in the scallop sample data sets, the initial look was to determine if there was statistical evidence of a "shot" effect. With each setup of conditions, three shots were taken one after the other. There was a statistically significant (p = 0.009) shot–to–shot effect, with the second shot producing a lower response on average than the first shot ($\Delta\sqrt{R} = -0.14$) and the third shot was, on average, halfway between the first two shots. The shot-to-shot estimate of the standard deviation for the response was $\hat{\sigma}_{\sqrt{R}} = 0.650$.

The shots were averaged and the averages were fit to the quadratic model in the remaining factors. The seven flaws were crossed with each of the factors of TABLE 7 and all their 2nd order interactions. The non-significant factors were removed from the fit. The final fit had the form given by equation (7), where the subscript i signifies that the estimated coefficient was different for flaw "i". That is, the coefficients of equation (7) were fit, where the x terms are the levels of each of the factors and the ε term is the residual or unexplained portion of the response.

$$\sqrt{R} = c_{0i} + c_{Ai}x_A + c_{Ti}x_T + c_{Pi}x_P + c_{Ci}x_C + c_{AC}x_Ax_C + c_{PPi}x_P^2 + \varepsilon \qquad (7)$$

The estimated coefficients for equation (7) are given in TABLE 8. The residual error is estimated to be $\hat{\sigma}_{\varepsilon} = 0.8377$. The flaws are ordered in TABLE 8 from the lowest to highest responses. Contour plots for each flaw are given in the same order in Figure 78 through Figure . Each of the pair-wise contours graphs are given with the other variables held the level that produced the highest responses. This occurred at the highest vibration amplitude (A), longest pulse length (P), and highest trigger force (T) for all the flaws. However, the flaws behaved differently with respect to clamping. Flaws 28 and 69 had higher

responses when clamped at the high pressure level, whereas the remaining flaws all achieved maximum response levels when clamped at the smallest pressure level. Other than the smallest flaw having the smallest response there was no evidence of a strong monotonic relationship of response to flaw size, as is evidenced by the order of the flaws in TABLE 8.

TABLE 8. ESTIMATED COEFFICIENTS FOR FPI POD SAMPLES.

Flaw	28	93	182	252	69	43	116
Const	2.86442	-2.80825	4.24399	-0.03694	-2.33840	0.82734	0.42756
A	-0.01309	0.02989	0.00489	0.02429	0.02904	0.00998	0.08592
P	-0.02782	0.03592	-0.01656	0.01520	0.01175	0.05151	0.00208
T	0.02040	0.03798	0.02707	0.03683	0.05320	0.04572	0.02203
C	-0.18012	-0.35138	-0.36636	-0.29546	0.14443	-0.56479	-0.47831
A*C	0.00234	0.00234	0.00234	0.00234	0.00234	0.00234	0.00234
P*P	-0.0001078	0.0000529	0.0001092	-0.0000020	-0.0000049	-0.0000865	0.0000124
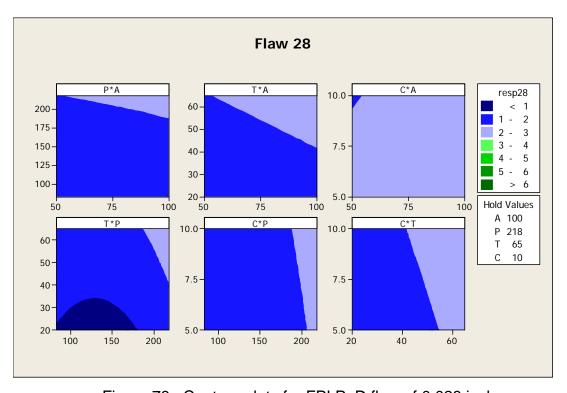
Figure 78. Contour plots for FPI PoD flaw of 0.028 inch.
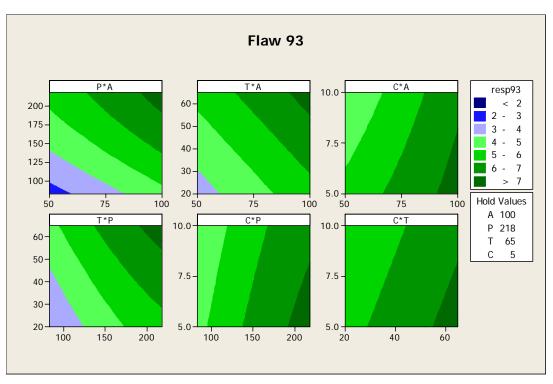
Figure 79. Contour plots for FPI PoD flaw of 0.093 inch.
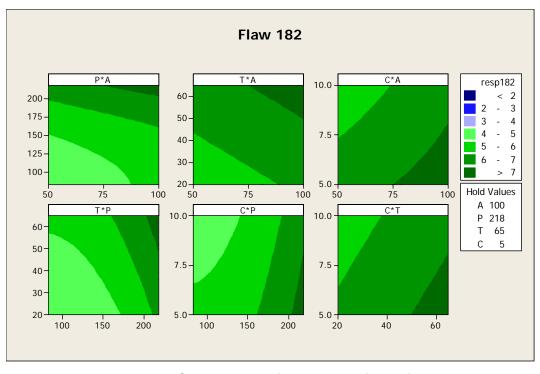
Figure 80. Contour plots for FPI PoD flaw of 0.182 inch.
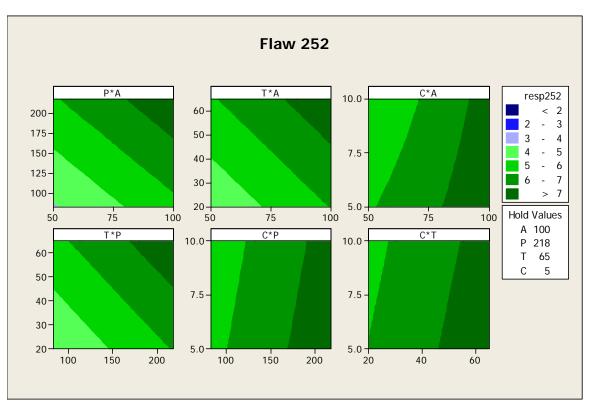
Figure 81. Contour plots for FPI PoD flaw of 0.252 inch.
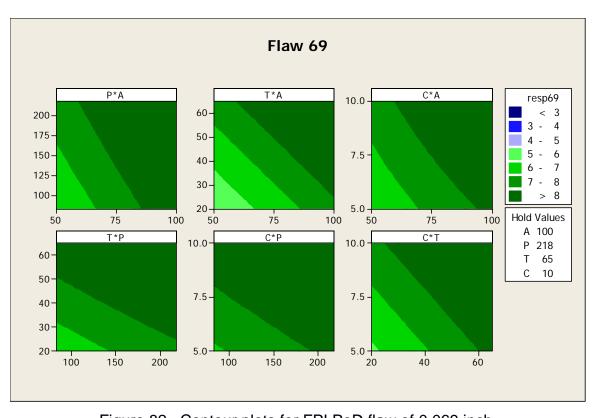
Figure 82. Contour plots for FPI PoD flaw of 0.069 inch.
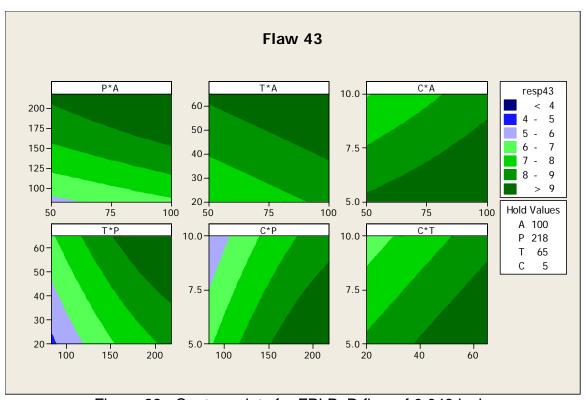
Figure 83. Contour plots for FPI PoD flaw of 0.043 inch.
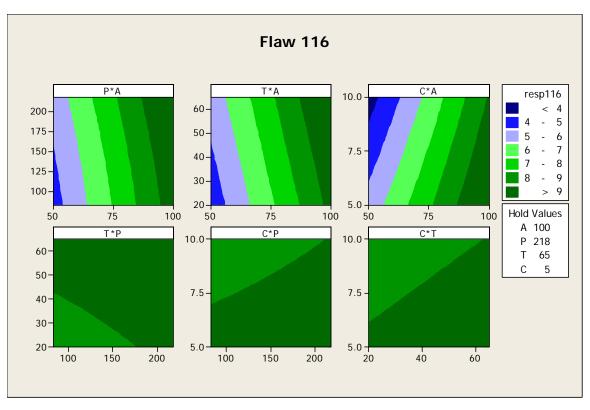
Figure 84. Contour plots for FPI PoD flaw of 0.116 inch.

Flaw 28 was hardest to detect and was not clearly present in the captured images over much of the input space. It is clear from Figure 78 that there was not much variation in the response. However, the general tendencies, other than clamping, are consistent with the other flaws.

As already noted, flaw 69 exhibits a distinctly different behavior with respect to the clamping force than do the other flaws. Flaw 116 is also atypical in that it exhibits a much different response range than do the other flaws. Flaw 116 is more responsive to vibration amplitude as is evidenced by the wider range of contour bands in the top row (all containing A as a factor) of Figure . Similarly, with the vibration amplitude held constant at the high level, the other factors made little difference in the response, as is evidenced in the small number of contours in the bottom row of Figure .

5.2.3.2 Alarm Condition Analysis of FPI PoD Sample Data

The times at which alarms occurred were recorded. These time values were analyzed as failure times regressed on amplitude, trigger force, and clamping pressure. Those times where no alarm occurred were treated as right-censored data, censored at the value of the pulse length. In addition, there were 16 occurrences of alarms were recorded but the time of alarm was not. These values were treated as left-censored data, with the pulse length being the censoring value.

A full quadratic model was considered in the three variables, but the clamping variable was not statistically significant and was therefore removed. The resultant best fit to this model was such that the mean time to alarm is given by $\hat{\mu} = 131.983 - 1.782 \cdot A + 3.6457 \cdot T - 0.1121 \cdot A \cdot T + 0.07747 \cdot A^2$ milliseconds with standard deviation of 18.40 milliseconds.

For a given pulse length combined with an amplitude and trigger force, an alarm occurs only if the value given above is less than the given pulse length. Therefore the probability that an alarm occurs is equivalent to the probability that the alarm time is less than the pulse length, where the alarm time has a Normal

79

distribution with above mean and standard deviation. Figure 85 shows the z-levels associated with the probability. The small values are the low probabilities, whereas the high values (z> 2) are associated with high probability of General Alarm.
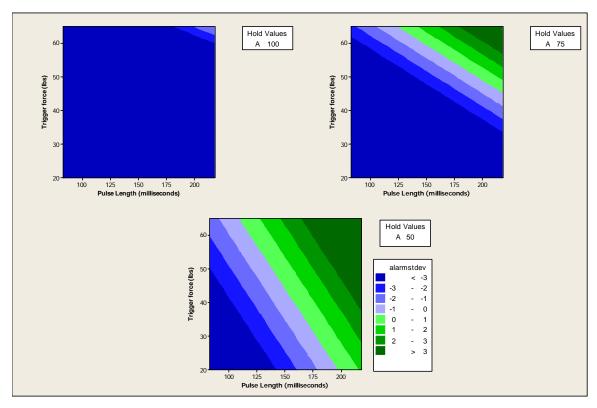
Figure 85. Normal Z-values for probability of alarm - FPI PoD flaws.

The working range with respect to obtaining an adequate response from the flaw but maintaining a low probability of General Alarm is shown in Figure 86. Only the contour for flaw 93 is shown because if it is imaged all the flaws (except flaw 28) will also be imaged. Different amplitude values are reflected in the columns and different clamping values are shown in the rows. The contour value of $\sqrt{R} = 3.16$ was chosen to be conservative in thinking that the contrast in imaging the flaw should be at least 10. The contour for the alarm standard deviation level (-2.326) was chosen to give a probability of 0.01 of a General Alarm or 99% probability of no General Alarm.

80
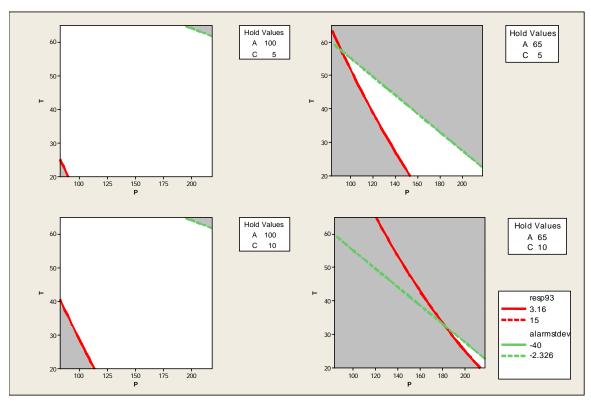
Figure 86. Regions for Adequate response and Low Alarm probability – FPI PoD flaws (flaw 28 not included and only contour value for flaw 93 shown).

5.2.4 FPI PoD Sample Study Summary and Observations

Analysis of General Alarm conditions gave similar results in all the cases considered. The conditions leading to alarms were large trigger force, long pulse lengths, and lower vibration amplitudes. However, when the vibration level is at 100% the probability of a General Alarm is very low with the pulse lengths and larger trigger forces used in these experiments.

Flaw –to –flaw variation with respect to the level of responses was highly variable. Detectability as reflected by the response level did not correlate well with the flaw lengths. The FPI PoD sample population had one flaw that was detectable only in a limited range of the experimental setup. The results of the experimental design approach demonstrate that even though there may be substantial evidence for the best operating range for the input variables in

81

performing a Sonic IR inspection, probability of detection will be very dependent on the flaw-to-flaw variation, which may have little relationship to flaw size.

General Alarms were minimized with vibration amplitude at higher values. In all the cases considered here this was also the conditions that led to the higher responses from flaws. However, there may be reason to reduce amplitude to ensure that no damage is being imparted to the test specimens. In this case, we have shown that there may be a lower amplitude limit to have an effective inspection. With the lower amplitudes, the combination of other factors, specifically trigger force and pulse length, need to be considered to guarantee an effective inspection free of General Alarms. The relationship between trigger force and pulse length is near linear with a negative slope (that is, increasing pulse length requires decreasing trigger force). For a given pulse length and trigger force setting the probability of a General Alarm has a strong dependency on the vibration amplitude.

5.2.5 Clamping Torque vs. Crack Orientation in FPI PoD Samples

Earlier data indicated that the clamping torque parameter influenced the signal from perpendicular cracks differently than cracks with other orientations. An example of this difference is shown in Figure 87. Figure 87a shows the signal response as a function of clamping torque and trigger force for a crack oriented perpendicular to the horn. Figure 87b shows the signal response as a function of clamping torque and trigger force for a crack oriented at 45° to the horn. Increased clamping torque is seen to improve the signal from the perpendicular crack while diminishing the signal from the 45° crack. This trend was observed for clamping torque verses all other operating parameters as well. The samples were clamped as shown in Figure 88. Cracks with -45° and parallel orientations to the horn showed the same trend in the signal analyses as the 45° orientation example shown in Figure 87b. Only one other perpendicular crack was included in the matrix test set and the data were comparable to Figure 87a.
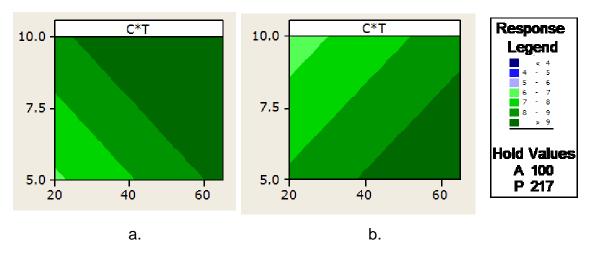
Figure 87. Relative signal amplitude for clamping torque vs. trigger force for cracks at orientations (a) perpendicular and (b) 45° to the horn.
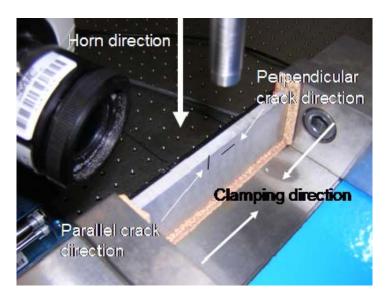
Figure 88. Orientation of FPI PoD sample, cracks, and clamping torque.

Prompted by analysis of the test matrix data, additional testing was conducted on the FPI PoD samples with cracks oriented perpendicular to the driving direction of the horn. Fifteen cracks, all with perpendicular orientation and lengths ranging from 0.048 inch to 0.305 inch were tested with all operating parameters fixed except for clamping torque. The range of clamping torque values was expanded beyond that used for the matrix testing. The goal was to

observe relative signal amplitude as a function of clamping torque for these cracks.

In the initial matrix data set, cracks with this orientation displayed increased relative signal amplitude versus increased clamping torque. However, when other perpendicular cracks were tested over a larger range of clamping torque values, this trend was not evident. One major difference between this data and the earlier data is that the analysis performed earlier included all of the parameter settings used in the DoE matrix. Therefore, the analysis included a large amount of results that were averaged to obtain the trends. For this additional testing performed on other specimens with perpendicular cracks, all parameters except clamping torque were held constant near the optimal settings and only 3 tests were performed for each clamping torque value. It may be necessary to acquire more data to see the signal decrease with increasing clamping torque in those specimens.

Data were also acquired, extracted and analyzed from samples with parallel cracks. Relative maximum signal amplitude as a function of clamping torque for 3 of these samples is shown in Figure 89. These samples have crack lengths of 0.167 inch, 0.177 inch, and 0.226 inch. Increased clamping torque, acting to close the crack, decreases signal amplitude for each sample. Also, note that the relative maximum signal amplitudes measured under the same operating conditions for the 0.167 inch crack and the 0.177 inch crack are quite different. These data again illustrate our earlier finding that the Sonic IR signal amplitude does not correspond to crack length.

Clamping Torque Influence on Sonic IR Crack Signal
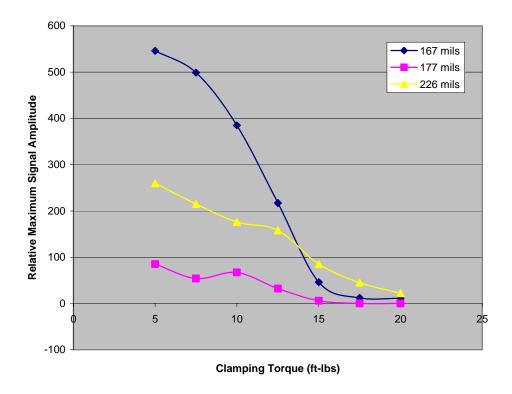
Figure 89. Relative maximum signal amplitude vs. clamping torque for parallel cracks.

5.3 F100 First Stage High Pressure Turbine Disks

The anti-symmetric anti-rotation feature (ARF) on the F100 1st stage high pressure turbine disk was identified as the original target component of interest to this program by the Air Force COTR. Unless a component can be inspected fully, its life cannot be extended by the Air Force Engine Rotor Life Extension (ERLE) program. The ARF on this component had been flagged as "uninspectable" by existing NDE techniques, thus preventing the component from being considered for life extension.

Information on the effort described in this section was presented at the 2004 Review of Progress in Quantitative Nondestructive Evaluation Conference and was published in the conference proceedings (Reference 5).

5.3.1 Turbine Disk Description

A photograph of a scrapped F100-PW-220 1st-stage high pressure turbine disk is shown in Figure 90. The 48 pound disk is 18.5 inches in diameter with an inner bore diameter of 7.25 inches. Each disk contains two ARFs of interest; one is shown in Figure 91.
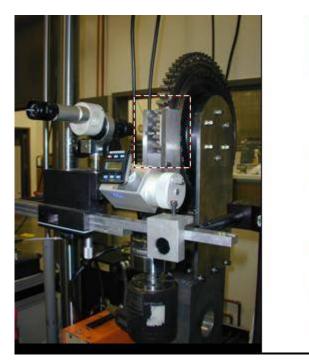
Figure 90. F100 1st stage high pressure turbine disk, with ruler for scale.

Figure 91. Anti-rotation feature on F100 1st stage high-pressure turbine disk.

No scrapped disks with fatigue cracks of interest were available for study, so cracks had to be artificially introduced. Fatigue cracks were grown to specified lengths in the base of the ARF, two per disk on five disks, using a specially designed fixture that was inserted into a standard fatigue machine. The fixture included a key that pressed against the ARF in a similar manner as the mating part would contact it in service. Photographs of a disk in the load cell are shown in Figure 92a, with an enlarged view of the key fitted into the anti-rotation window shown in Figure 92b. This work was performed under subcontract at Fatigue Technology, Inc. in Seattle, WA. A report covering their effort is contained in Appendix B.
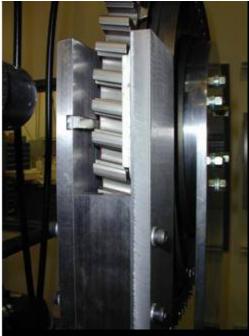
Figure 92 (a) Disk mounted in test frame, (b) Close-up view of key on load bar.

Tests were conducted on a practice disk prior to growing the specified cracks for the test matrix. A photograph of one of the cracks in the practice disk is shown in Figure 93.
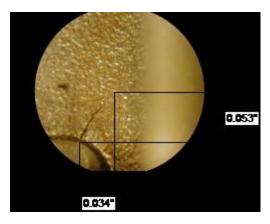
Figure 93. Fatigue crack in ARF of practice disk.

5.3.2 Experimental Setup and Design for Turbine Disk Study

The standard Sonic IR inspection system was used for this testing. A photograph illustrating the placement of the horn relative to the ARF is shown in Figure 94. As shown in the photograph, the horn contacted the disk on the thin ridge next to the cracked ARF wall.

Figure 94. Ultrasonic horn in contact with disk next to ARF.

The experimental variables included in the disk testing are listed in TABLE 9. Three values for each variable were included to allow non-linear effects to be estimated in the response surface modeling. This response surface design method was described in Reference 4. Each of the combinations of values was tested three times in order to determine if there existed a temporal trend in the

data. No such trend was found and the three results for each combination were averaged.

TABLE 9. VARIABLES AND VALUE FOR TURBINE DISK TESTING.

Variable	A Vibration Amplitude (% max)	T Trigger force (pounds)	P Pulse length (msec)	C Clamping torque (inch-pounds)
Low level	50	20	83	25
Mid level	75	40	150	55
High level	100	65	217	75

5.3.3 Preliminary (3-Crack) Turbine Disk Study Data Analysis

The fatigue crack growing process took some time to accomplish for the whole set of 10 cracks. While waiting for the later cracks to be placed in the disks, testing began on 3 of the cracks, 0.009 inch, 0.021 inch, and 0.040 inch in length. All 10 cracks were later tested, with a reduced test matrix, and that analysis is reported in Section 5.3.4.

5.3.3.1 Response Surface Analysis of 3-Crack Data

Data was extracted from the infrared image sequence for each test by recording the contrast between the maximum amplitude pixel at the crack and a background area nearby at the time of maximum signal amplitude. The same contrast was recorded 500 milliseconds later, when the sample had returned to room temperature. The difference in contrast at the crack between these two times was used as the response, R, in the analysis. Equation 8 was used to fit the first four variables in TABLE 9 to the square root of R for each of the crack

lengths tested. Nonsignificant factors below 0.05 were eliminated, which simplified this equation.

$$\sqrt{R} = c_0 + c_A x_A + c_T x_T + c_P x_P + c_C x_C + c_{AT} x_A x_T + c_{AP} x_A x_P + c_{AC} x_A x_C + c_{TP} x_T x_P +$$

$$c_{TC} x_T x_C + c_{PC} x_P x_C + c_{AA} x_A^2 + c_{TT} x_T^2 + c_{PP} x_P^2 + c_{CC} x_C^2 + \varepsilon \qquad (8)$$

where c = constant

                 ε = residual

                 x_Y = value of variable Y, where

                 A = Vibration amplitude

                 T = Trigger force

                 P = Pulse length

                 C = Clamping torque

The clamping torque (C) variable was not significant for any of the crack lengths tested. Clamping was accomplished by a 6-finger lathe chuck in the inner bore of the disk. The disk originally rested on a small platform ring around the inner bore, but this fixture had to be modified by the addition of three nylon support posts because of flexure problems. In the new configuration, apparently the only "clamping" of significance occurred between the horn and the support posts.

There was no correlation found between the flaw length and the measured response. There may be several reasons for this result. The "length" of the flaw was measured on the side face of the ARF, but every crack in the test set extended across the width of the ARF also. Therefore, the "length" measurement may be more of a crack depth indication. However, tests on both naturally occurring and artificially grown cracks have yielded similar results with respect to true crack length, indicating that factors other than crack length may be dominant in determining Sonic IR signal amplitude. Tightness of the crack and stress state of the material are two such possible factors. In this study, flaws are referenced by their flaw length value (Flaw21, for example, indicates a 0.021 inch crack as measured on the side face of the ARF).

To visualize the relationships between the three remaining significant variables, vibration amplitude, trigger force, and pulse length, X-Y plots of Variable1 vs. Variable2 were generated, with Variable3 held at a constant value. Three of these plots were generated for each flaw and they are shown in Figures 95 through 97. The magnitude of the square root of the response is shown in constant contour bands and the hold values of the variables not shown in a given graph are listed in the legend. These hold values were chosen to produce the maximum response for each flaw.
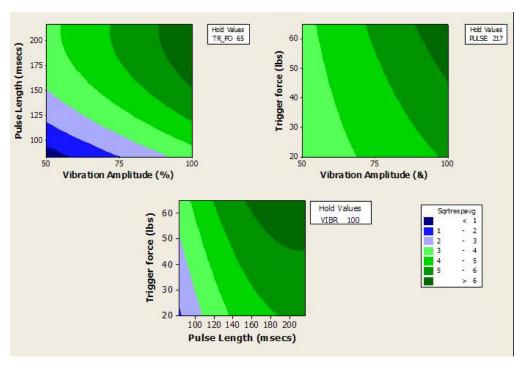
Figure 95. Response contour plots for Flaw 9.
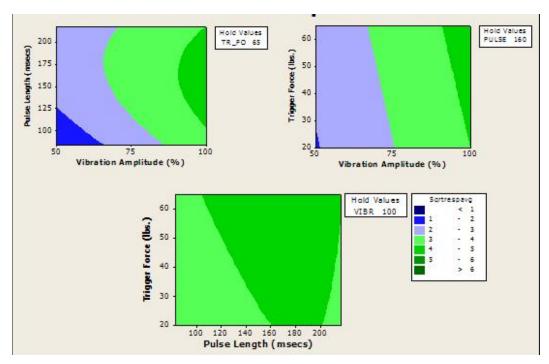
Figure 96. Response contour plots for Flaw21.
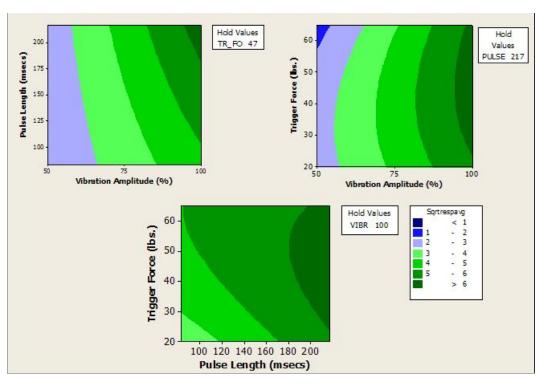
Figure 97. Response contour plots for Flaw40.

5.3.3.2 Alarm Condition Analysis of 3-Crack Data

Fifty-six tests produced a General Alarm on the Branson welder unit. The conditions at which the alarms occurred are given in TABLE 10. In that table the first number is the number of times an attempt at those conditions produced an alarm and the second number is the number of times shots were made alarm free.

TABLE 10. ALARM/NO–ALARM COUNTS BY AMPLITUDE, TRIGGER FORCE, AND PULSE LENGTH.

Amplitude	Trigger Force	Pulse length		
		83 msec	150 msec	217 msec
50%	20 lbs.	0/63	0/27	7/6
50%	45 lbs.	0/27	4/16	9/0
50%	65 lbs.	0/27	9/0	9/0
75%	20 lbs.	0/27	0/27	0/27
75%	45 lbs.	0/27	0/54	0/27
75%	65 lbs.	0/27	9/0	9/0
100%	20 lbs.	0/27	0/27	0/27
100%	45 lbs.	0/27	0/27	0/27
100%	65 lbs.	0/27	0/27	0/63

The times at which alarms occurred were recorded and these values were analyzed as failure times regressed on amplitude and trigger force. Those times where no alarm occurred were treated as right censored data, censored at the value of the pulse length. That is, the "time to alarm" was considered to have a normal distribution with mean as a function of amplitude and trigger force. The best fit to this model was such that the mean time to alarm is given by

$\hat{\mu} = 104.57 + 2.800 \cdot amplitude - 0.7412 \cdot trigger\_force - 0.0234 \cdot (trigger\_force)^2$ and

the estimate of the scale parameter is 16.7689. For a given pulse length an
alarm occurs only if this value is less than the given pulse length. Therefore the
probability that an alarm occurs is equivalent to the probability that the alarm time
is less than the pulse length. The plots in Figure 98 through Figure 100 show
these contours and are in agreement with the outcomes reflected in TABLE 10.
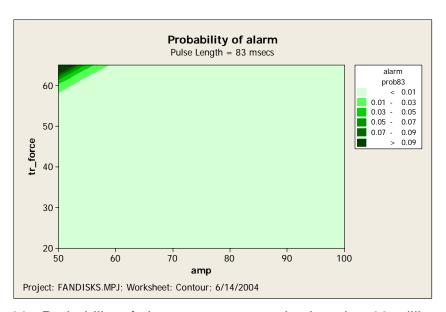
Figure 98. Probability of alarm contours at pulse length = 83 milliseconds.
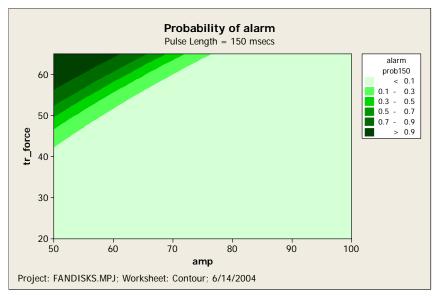
Figure 99. Probability of alarm contours at pulse length = 150 milliseconds.
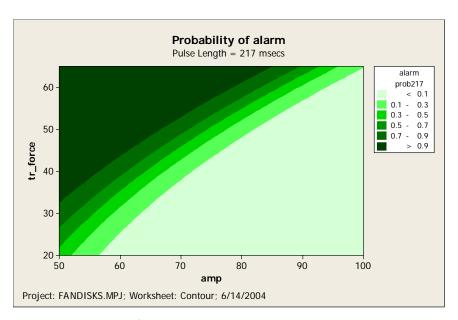
Figure 100 Probability of alarm contours at pulse length = 217 milliseconds.

5.3.3.3 Combining Response Information with Alarm Possibilities for 3-Crack Study

Models have been developed for the contrast response as a function of the set – up factors for the sonification of the flaw area. They have also been developed for alarm conditions. Here they are combined to yield regions of operation that have reasonable assurance of producing a response for a flaw, if it is present, but are unlikely to produce an alarm.

Equi-contours of probability of alarm – free shots are given by $\Pr(noalarm) = \Phi(z)$, where $\Phi(\cdot)$ is the standard normal distribution function and z is given by

$$z = \frac{104.57 + 2.800 \cdot amplitude - 0.7412 \cdot trigger\_force - 0.0234 \cdot (trigger\_force)^2 - pulselength}{16.7689}$$

(9)

A high probability (> 0.99) of no alarm would result for all values where $z > 2.33$. As discussed earlier, the level of response for detecting a flaw is taken to be $\sqrt{R} > \sqrt{10} \cong 3.2$. Response models were different for each of the flaws. Using

the information from all three flaws, regions are shown in Figure 101, Figure 102, and Figure 103 that satisfy the above criteria for all three flaws. The regions satisfying all the conditions are shown in white. The hold values in Figures 101-103 are set at the high levels. Each of the contour plots show the 3.2 response contours for each flaw and the $z = 2.33$ for the probability of no alarm. Note that the upper right corner (high trigger force and high pulse length) in Figure 101 is not included in the region of operation. This might seem inconsistent with the fact that these conditions did not produce alarms in the data. However, the probability of no alarm was set high (0.99) and the model predicts that the upper right region has probability of no alarm that goes as low as approximately 0.91.
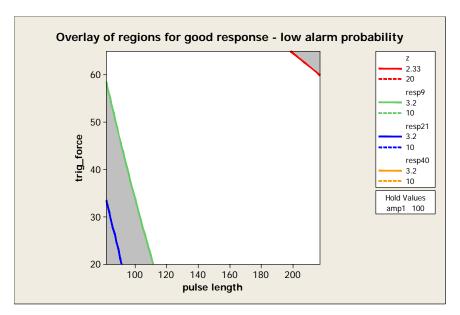
Figure 101. Trigger force – Pulse length region of operation for Amplitude = 100%.
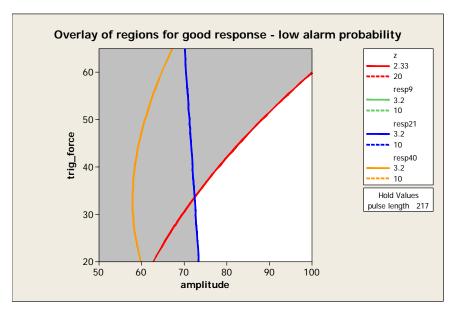
Figure 102. Trigger force – Amplitude region of operation for Pulse length = 217.
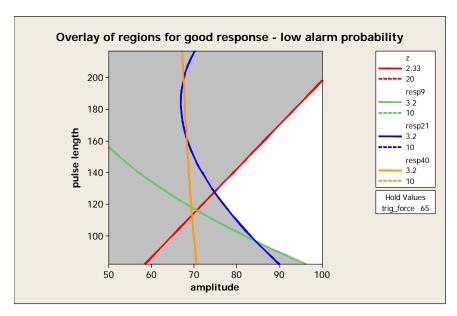
Figure 103. Pulse length – Amplitude region of operation for Trigger force = 65.

The regions in both Figure 102 and Figure 103 indicate that the amplitude can not be reduced to lower than about 75% while keeping the pulse length and trigger force at 217 milliseconds and 65 pounds, respectively. Fixing the amplitude at 75% the relationship between pulse length and trigger force that would produce a good inspection is shown in Figure 104.
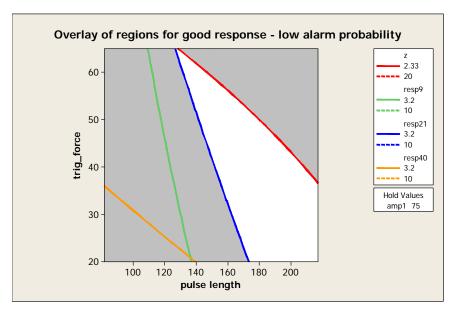
Figure 104. Trigger force – Pulse length region of operation for Amplitude = 75%.

What lower limit for vibration amplitude is implied by the analysis? Figure shows side-by-side the regions when setting the amplitude at 71% and 70.2%. The modeling suggests that the vibration amplitude should not go below approximately 70.2% and if amplitude is set at these levels then the pulse length should be set around 180 milliseconds and the trigger force at 45 pounds in order to have good response combined with a low probability of alarm.
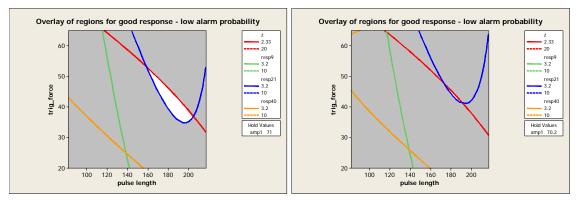
Figure 105. Trigger force – Pulse length operation region for Amp=71% (left) and 70.2% (right).

It is apparent from Figure 105 that the constraint on the trigger force and pulse length that is being imposed when the vibration amplitude is around 71% is from flaw 21. There is a much broader operating region that generates adequate response levels for the other two flaws. If this process was followed with a larger population of flaws, the criteria of finding a region that could adequately image all the flaws present may not be able to be met. However, the basis of a probability of detection estimation process is established by considering the distribution of responses for the given set – up values.

5.3.4 Full (10-Crack) Turbine Disk Study Data Analysis

In Section 5.3.3 above, the results of a 4 – factor experimental design were presented where the full design was repeated on three different flaws contained within the ARFs in F100 1st stage high-pressure turbine disks. One of the factors, clamping torque, proved to be an insignificant factor. The flaws were of lengths 0.009 inch, 0.021 inch, and 0.040 inch. There was not a monotonic relationship of the ability to detect flaws with the size of the flaw. The smallest of the flaws, 0.009 inch, proved to be more detectable over the range of inputs than was the 0.021 inch flaw.

Seven additional flaws of lengths 0.011 inch, 0.013 inch, 0.015 inch, 0.017 inch, 0.026 inch, 0.029 inch, and 0.036 inch became available for testing. The clamping force variable was removed from the designs and a 78 run experiment in the 3 remaining variables was performed on each of the seven additional flaws. The tests were conducted at the 3 x 3 x 3 combinations of the levels shown in TABLE 11, except for the combination of the lowest levels, which was believed to be producing very little useable data and was therefore eliminated. Three (3) replicate tests were run at each combination of factors.

TABLE 11. FACTOR LEVELS – EACH COMBINATION TESTED 3 TIMES.

Factor	A- Vibration amplitude (% max)	T-Trigger force (pounds)	P- Pulse length (milliseconds)
Low level	50	20	83
mid level	75	45	150
High level	100	65	217

As in the previously reported experiments, the difference of the maximum contrast and the contrast at the end of the pulse + 500 milliseconds was the response taken from thermal time images.

5.3.4.1 Surface Response Analysis of 10-Crack Data

The initial look at the data was to determine if there was statistical evidence of a "shot" effect. With each setup of conditions, three shots were taken one after the other. There was no evidence of a shot effect. The 3 replicates were therefore averaged and the averages were fit to the remaining factors. The shot-to-shot estimate of the standard deviation for the response was $\hat{\sigma}_{\sqrt{R}} = 0.370$, a little less than was observed in the first 3 flaws (0.460).

The data from the seven flaws are shown in Figure 106. In that figure, the design points are ordered by vibration amplitude (A), then pulse length (P), followed by trigger force (T). It is seen that the relationships in the response across the design space is consistent between flaws. That is, there may be a different level of response for each flaw, but the patterns are roughly the same. The flaw of length 0.029 inch was detected only at a limited number of the runs. However, where it was detected is consistent with the part of the design space at which the flaws were exhibiting their highest responses.
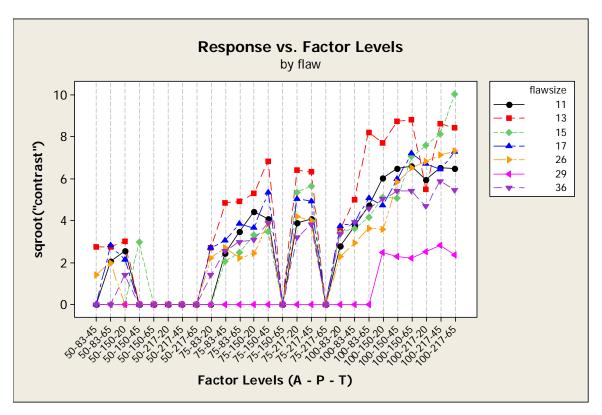
Figure 106. Responses at the experimental design points.

The "zeroes" shown in Figure 106 are those design points that produced welder alarms and therefore no images were obtained for post-inspection analysis. These points consistently produced alarm situations across all of the flaws.

For each flaw, a full quadratic model was fit to the $\sqrt{R}$ using the three variables shown in TABLE 11 plus allowing for a different level for each flaw. That is, the coefficients of equation (10) were fit, where the x terms are the levels of each of the factors and the ε term is the residual or unexplained portion of the response.

$$\sqrt{R} = c_{0i} + c_A x_A + c_T x_T + c_P x_P + c_{AT} x_A x_T + c_{AP} x_A x_P + c_{TP} x_T x_P$$

$$+ c_{AA} x_A^2 + c_{TT} x_T^2 + c_{PP} x_P^2 + \varepsilon \qquad (10)$$

In equation (10) the subscript "i" for the leading coefficient allows for a different level to be fit for each flaw. Before fitting the data, the flaw of length 0.029 inch was removed from the data. This was done so as not to have an undue

101

influence by the fact that the flaw was unobservable for much of the design space and therefore would only lessen the ability to estimate the significance of the factors in equation (10). Not all of those coefficients were statistically significant. The coefficients that were not statistically significant ($p > 0.05$) were sequentially eliminated. The resulting model reduced to

$\sqrt{R} = c_{0i} + c_A x_A + c_T x_T + c_P x_P + c_{PP} x_P^2 + \varepsilon$, where the coefficient fits are given in

TABLE 12 and the contour plots for the highest response flaw (0.013 inch), lowest response flaw (0.026 inch), and the average response across all flaws are shown in Figures 107-109.

TABLE 12. COEFFICIENTS FOR EACH FLAW FOR MODEL.

	Coefficients
Flaw 13	-6.78696
Flaw 17	-8.14453
Flaw 36	-8.35244
Flaw 15	-8.54274
Flaw 11	-8.57848
Flaw 26	-8.85253
VIBR(A)	0.070811
PULSE(P)	0.058138
TR_FO(T)	0.035516
PULSE(P)*PULSE(P)	-0.000127
Residual $\hat{\sigma}$	0.8444
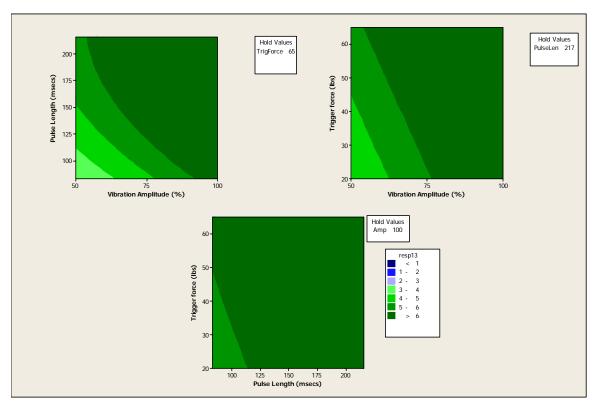
Figure 107. Response contour plots for Flaw 13.
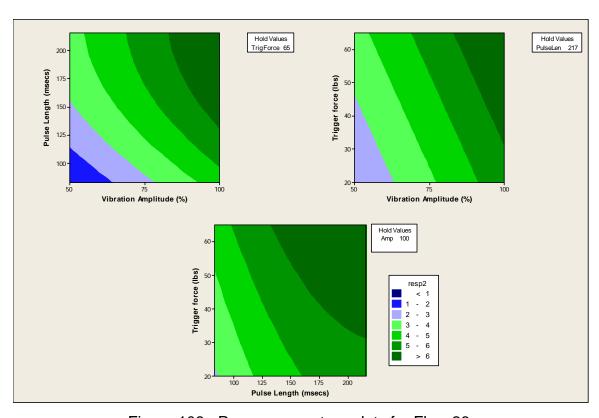
Figure 108. Response contour plots for Flaw 26.
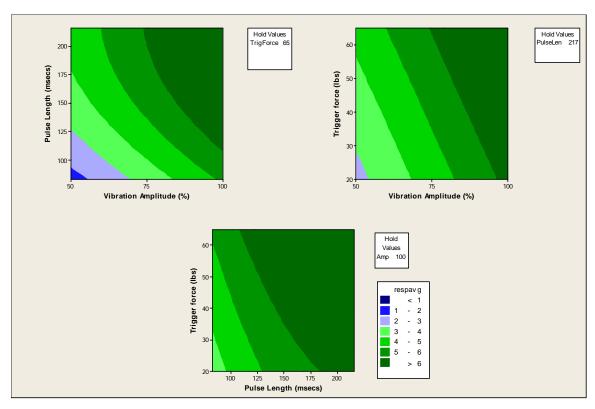
Figure 109. Average response contour plots for 6 flaws.

5.3.4.2 Alarm Condition Analysis of 10-Crack Data

As noted in the graph of Figure 107, the "zeroes" for all the flaws occur at conditions where alarms were generated on the welder unit. The times at which alarms occurred were recorded and these values were analyzed as failure times regressed on amplitude and trigger force. Those times where no alarm occurred were treated as right censored data, censored at the value of the pulse length. That is, the "time to alarm" was considered to have a normal distribution with mean as a function of amplitude and trigger force. The best fit to this model was such that the mean time to alarm is given by

$$\hat{\mu} = 78.467 + 2.723 \cdot amplitude + 0.04114 \cdot trigger\_force - 0.02920 \cdot (trigger\_force)^2$$

milliseconds with standard deviation of 16.50 milliseconds. For a given pulse length combined with an amplitude and trigger force, an alarm occurs only if the value given above is less than the given pulse length. Therefore, the probability

104

that an alarm occurs is equivalent to the probability that the alarm time is less than the pulse length, where the alarm time has a Normal distribution with above mean and standard deviation.

Figure 110 shows the contours for the standard Normal z-values for the probability of an alarm. TABLE 13 shows the probability levels associated with the z-values.
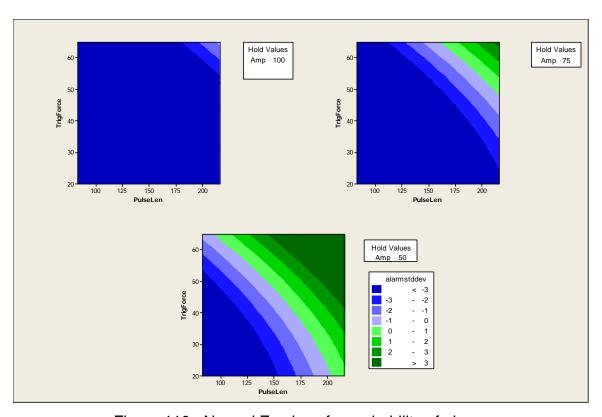
Figure 110. Normal Z-values for probability of alarm.

TABLE 13. PROBABILITY LEVELS FOR NORMAL Z-VALUES FOR PROBABILITY OF ALARM.

z-value	-3	-2	-1	0	1	2	3
probability	0.0013	0.0228	0.1587	0.5	0.8413	0.9772	0.9987

5.3.4.3 Combining Response Information with Alarm Possibilities for 10-Crack Study

As outlined for the 3-crack study in Section 5.3.3.3 above, response surface data and probability of alarm data were combined to determine regions of desirable operability for Sonic IR inspection of the ARF regions of the disks. Overlay plots of these data are shown in Figure 111. All ten cracks were used in this analysis but fewer are shown in the plots for clarity.
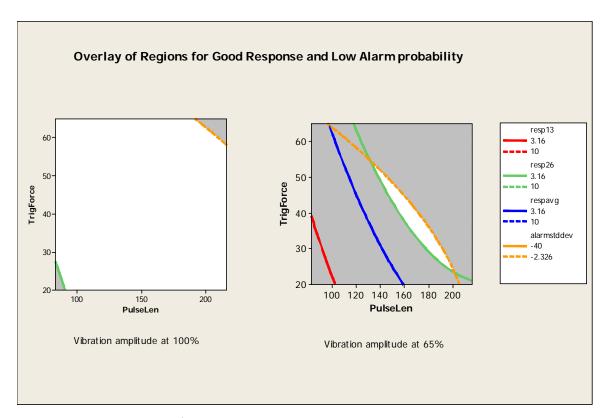
Figure 111. Regions for adequate response and low alarm probability at 100% vibration amplitude (left) and 65% amplitude (right).

5.3.5 Conclusions for Turbine Disk Studies

An extensive experimental plan covering the technique variables for the Sonic IR inspection system has enabled the characterization of operating regions that are likely to result in good inspections with a low probability of welder alarms.

Test results indicated that the crack signal response increased with increasing vibration amplitude, trigger force and pulse length over most of the operating region for the flaws tested. There were only two exceptions to this trend. The response did not scale with "crack length" although the term may be a misnomer in this case. Clamping torque was found to be an insignificant factor in the final test configuration, owing to the addition of the three support posts in the fixture. This factor was eliminated in the testing of the total test set of 10 cracks. General Alarms of the welder unit occurred at high trigger force/low vibration amplitude combinations and the probability of an alarm increased with pulse length.

5.4 TF33 Second Stage Turbine Blades

5.4.1 Turbine Blade Introduction

A collection of TF33 2nd stage turbine blades, described in Section 4.2, was used to produce a sample set for matrix testing of system operating parameters. The blades selected contained service-induced fatigue cracks in the leading and trailing edges of the airfoils. Preliminary testing, discussed in the same section referenced above, indicated that Sonic IR testing may be a viable inspection method for these components. It is the intent of the parties involved to publish the work on this component at the upcoming 2007 QNDE conference.

5.4.2 Experimental Setup and Design for Turbine Blade Study

The standard Sonic IR experimental setup was used to test the turbine blades along with the fixture described in Section 4.2.5. A photograph of a blade undergoing testing is shown in Figure 112.
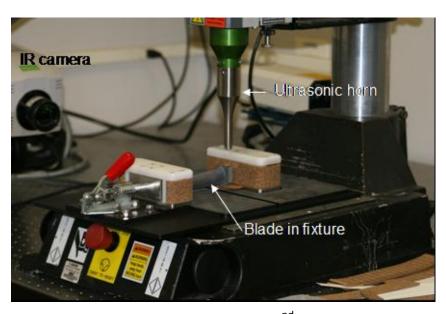
Figure 112. Sonic IR testing of TF33 2nd stage turbine blade.

The experimental test matrix in TABLE 14 was used to test seven TF33 second stage turbine blades containing a total of 10 cracks (2 cracks were tested on Blade #4 and 3 cracks were tested on Blade #7). Maximum contrast data, defined as the difference between the peak amplitude at the crack and the background value (3 x 3 pixel area 15 pixels to the left of the peak), were manually extracted for each of the tests. The test matrix consisted of the experimental factors vibration amplitude, pulse length and trigger force. All three experimental factors have 3 levels as shown in TABLE 14.

TABLE 14. TURBINE BLADE TEST MATRIX.

Level	Vibration Amplitude	Pulse Length	Trigger Force
low	10	83	10
mid	35	150	35
high	60	217	60

There were 32 tests (27 full factorial combinations plus one additional test at 10-83-10, two additional tests at 35-150-35, and two additional tests at 60-217-

60) for each crack. For each of the 32 tests there were 3 replications, which were conducted in sequence. These three responses were averaged for each test.

5.4.3 Determination of Optimal System Parameters for Turbine Blades

5.4.3.1 Analysis of Turbine Blade Signal Response Data

5.4.3.1.1 Models for the Maximum Contrast Response for Turbine Blade Data

A log transformation was used on the data. For an individual crack *b*, the linear model for the maximum contrast response (denoted by *m*) can be expressed in the form of (11):

$$\log(m+1) = \beta_{0,b} + \beta_{1,b}\log(v) + \beta_{2,b}\log(p) + \beta_{3,b}\log(tr) + \beta_{4,b}\log(v)\log(tr)$$
$$+\beta_{5,b}\log(v)\log(p) + \beta_{6,b}\log(p)\log(tr) + \beta_{7,b}\log(v)^2 + \beta_{8,b}\log(p)^2 + \beta_{9,b}\log(tr)^2 + \varepsilon \quad (11)$$

Here *v* represents Vibration Amplitude, *p* represents Pulse Length, *tr* represents Trigger Force. We use b to index the 10 cracks. The maximum contrast values were increased by 1 before taking logs to avoid having log(0). Function lm() in the statistical software in Reference 6 was used to fit the model. The fitting results for the first four coefficients are listed in TABLE 15. The results indicate large variability from crack to crack. That suggests that crack-to-crack differences should be described by a model in which parameters are random.

TABLE 15. FITTING RESULT OF MODEL (11) FOR INDIVIDUAL CRACKS.

Crack *b*	$\beta_{0,b}$	$\beta_{1,b}$	$\beta_{2,b}$	$\beta_{3,b}$
1	-6.580	-7.651	2.068	5.428
2	-20.505	-4.909	8.423	0.287
3	38.022	-5.006	-11.639	-4.157
4	12.915	-3.180	-4.118	-1.793
5	-27.055	-7.914	15.356	-1.762
6	6.967	0.326	-5.131	-2.438

7	11.945	-3.160	-3.948	-0.155
8	-37.345	-0.495	10.730	6.463
9	4.654	-1.119	-3.567	0.153
10	-179.016	1.227	59.186	23.576

5.4.3.1.2 Mixed Effects Model for Turbine Blade Data

In order to describe a larger population of cracks using one model, we fit a linear mixed effects model, as described in References 7 and 8, in which the intercept and main effect (linear) model terms are modeled as random effects to describe the crack to crack variability in response. The final model for the maximum contrast is:

$$\log(m+1) = \beta_{0,b} + \beta_{1,b}\log(v) + \beta_{2,b}\log(p) + \beta_{3,b}\log(tr) + \beta_4\log(v)\log(tr)$$
$$+ \beta_5\log(v)\log(p) + \beta_6\log(p)\log(tr) + \beta_7\log(v)^2 + \beta_8\log(p)^2 + \beta_9\log(tr)^2 + \varepsilon \quad (12)$$

Here, again, v represents Vibration Amplitude, p represents Pulse Length and tr represents Trigger Force. The random error ε is assumed to have a normal distribution with mean 0 and variance σ_ε. To describe the crack-to-crack variability, random effects are put on the mean effect coefficients, i.e., $\beta_{0,b}, \beta_{1,b}, \beta_{2,b}$ and $\beta_{3,b}$ together have a multivariate normal distribution with mean $\bar{\mu}_{\beta b}$ and covariance matrix $\Sigma_{\beta b}$, where $\bar{\mu}_{\beta b} = (\beta_0, \beta_1, \beta_2, \beta_3)$ is a 4-dimenstional vector and $\Sigma_{\beta b}$ is a 4×4 matrix. The model assume that $\beta_{0,b}, \beta_{1,b}, \beta_{2,b}$ and $\beta_{3,b}$ are independent of the error ε. The $\beta_0, \beta_1......\beta_9$ are means of the fixed effect coefficients. The parameter estimates, which are calculated by package "nlme" in Reference 6, are given in TABLE 16.

TABLE 16. THE FITTING RESULT FOR THE FIXED EFFECT OF THE MIXED-EFFECT MODEL.

$\hat{\beta}_0$	$\hat{\beta}_1$	$\hat{\beta}_2$	$\hat{\beta}_3$	$\hat{\beta}_4$	$\hat{\beta}_5$	$\hat{\beta}_6$	$\hat{\beta}_7$	$\hat{\beta}_8$	$\hat{\beta}_9$	$\hat{\sigma}_\varepsilon$
-7.833	-3.579	2.888	1.137	0.671	0.0916	-0.299	0.214	-0.264	0.129	0.749

$$\hat{\Sigma}_{\beta b} = \begin{pmatrix} 19.1 & 1.00 & -3.68 & -2.11 \\ 1.00 & 0.117 & -0.214 & -0.126 \\ -3.68 & -0.214 & 0.721 & 0.420 \\ -2.12 & -0.126 & 0.420 & 0.281 \end{pmatrix}$$

5.4.3.1.3 Contour Plot of Probability of Detection (PoD) for Turbine Blades

Under model (12), for a given test condition (fixed values of Vibration Amplitude v, Pulse Length p, and Trigger Force tr), the log transformation of response plus 1, i.e., $\log(m+1)$ has a normal distribution with mean expressed in (13) and variance in (14), where X_l is a vector with four components:

$$X_l = \begin{pmatrix} 1 \\ \log(v) \\ \log(p) \\ \log(tr) \end{pmatrix}.$$

$$mean_{\log(m+1)}(v,p,tr) = \beta_0 + \beta_1 \log(v) + \beta_2 \log(p) + \beta_3 \log(tr) + \beta_4 \log(v)\log(tr)$$
$$+ \beta_5 \log(v)\log(p) + \beta_6 \log(p)\log(tr) + \beta_7 \log(v)^2 + \beta_8 \log(p)^2 + \beta_9 \log(tr)^2 \tag{13}$$

$$Var_{\log(m+1)}(v,p,tr) = \sqrt{X_l^T \Sigma_{\beta b} X_l + \sigma_\varepsilon^2} \tag{14}$$

where the superscript T is used to indicate vector transpose.

Probability of detection (PoD) is defined as the probability that the maximum contrast m in an image sequence exceeds a threshold for a crack taken at random from some population of cracks. PoD can be calculated in the form of (15).

$$\text{POD} = \Pr(m > m_T) = 1 - \Phi_N \left(\frac{\log(m_T+1) - mean_{\log(m+1)}(v,p,tr)}{Var_{\log(m+1)}(v,p,tr)} \right) \tag{15}$$

$\Phi_N(x)$ is the cumulative distribution function of standard normal distribution. We can estimate the PoD by evaluating (15) using the estimates of the model parameters in TABLE 16.

A reasonable threshold was chosen as $m_T = 10$. Figure 113, Figure 114 and Figure 115 are contour plots that illustrate the output of our mix-effects model for the PoD. Green regions have low PoD values and the light color regions have high PoD values as the color bars on the right side of the plots indicate.
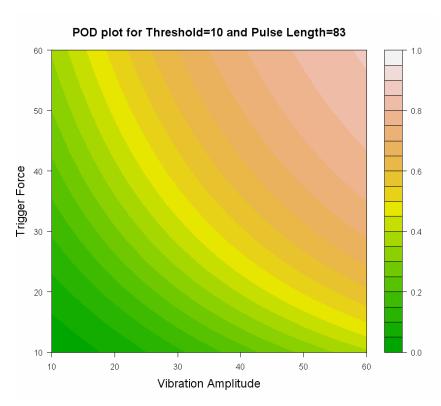
Figure 113. PoD plot for Pulse Length = 0.083 inch.
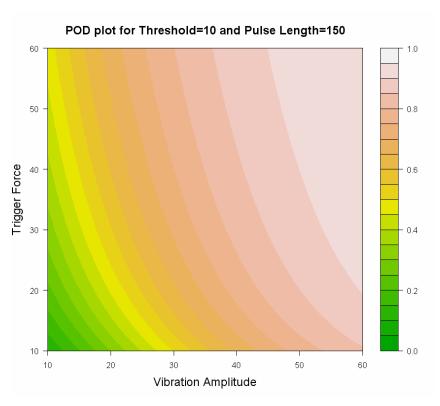
Figure 114. PoD plot for pulse length = 0.150 inch.
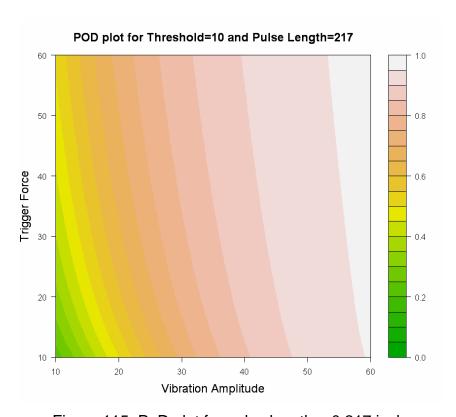
Figure 115. PoD plot for pulse length = 0.217 inch.

5.4.3.2 Analysis of Turbine Blade Alarm Data

Some tests ended with an alarm condition. When there was an alarm, the time to alarm data were recorded. When there was no alarm, the alarm time observation was right censored at the length of the pulse. A log normal regression model was fitted to the time-to-alarm data to assess the probability of alarm as a function of the test conditions.

5.4.3.2.1 Log Normal Model for Turbine Blade Data

Let T_A denote the time of an alarm. The data suggest that the T_A can be described by a lognormal distribution expressed as:

$$\text{POA} = \Pr\left(T_A < p\right) = \Phi_{nor}\left[\frac{\log(p) - \hat{\mu}_a}{\hat{\sigma}_a}\right]$$

(16)

Here $\mu_a = \beta_0^a + \beta_1^a v + \beta_2^a tr$. As in the model for maximum contrast, v stands for Vibration Amplitude, p stands for Pulse Length and tr stands for Trigger Force. β_0^a , β_1^a and β_2^a are estimated by using the maximum likelihood method in SPLIDA in Reference 9. Higher order terms (like those in the maximum contrast model) are ignored because they are not statistically significant. The estimated parameters are listed in TABLE 17:

TABLE 17. ALARM MODEL FITTING RESULT.

$\hat{\beta}_0$	$\hat{\beta}_1$	$\hat{\beta}_2$	$\hat{\sigma}$
6.027	-0.0188	0.00531	0.1629

5.4.3.2.2 Contour Plots of Probability of Alarm for Turbine Blade Data

Contour plots in Figure 116, Figure 117 and Figure 118 illustrate the probability of alarm for the three fixed values of pulse length in model (16).

Probability of alarm is defined here as the probability of having an alarm condition before the end of the pulse.
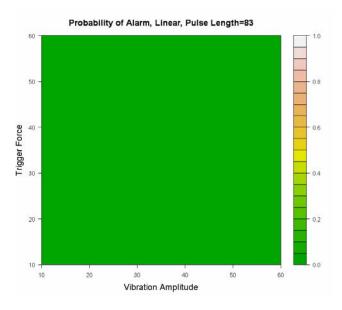
Figure 116. Probability of alarm for pulse length = 0.083 inch.
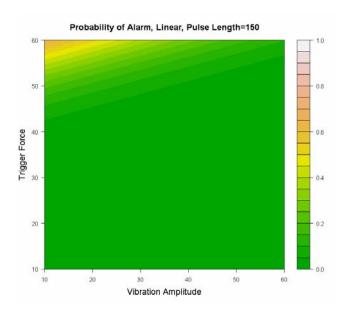
Figure 117. Probability of alarm for pulse length = 0.150 inch.
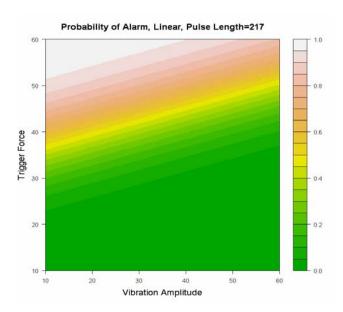
Figure 118. Probability of alarm for pulse length = 0.217 inch.

5.4.3.3 Combining Turbine Blade Response and Alarm Information

We combined the information in the probability of detection and probability of alarm contour plots to create "overlay" contour plots in Figure 119 and Figure 120 which show the test conditions where the probability of detection is expected to be high and probability of alarm is expected to be low (the green regions). In addition to a signal threshold, these overlay plots require specification of acceptable PoD and PFA thresholds (chosen to be >.90, <0.05, respectively, in the following study). In both plots, the green regions meet both conditions. The white regions meet neither condition.
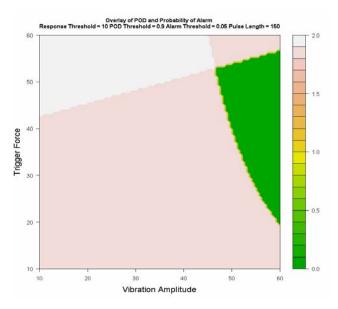
Figure 119. Overlay plot for pulse length = 0.150 inch.
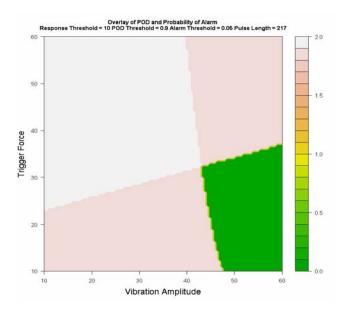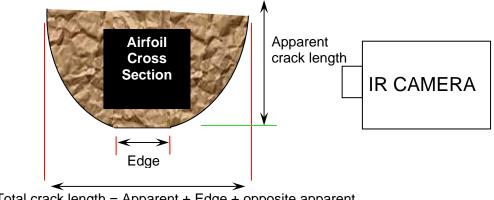
Figure 120. Overlay plot for pulse length = 0.217 inch.

5.4.4 Estimation of Probability of Detection versus Crack Length for Turbine Blades

TABLE 18 lists the crack length information that was obtained by subcontractor Martin MetLabs, Inc. using acetate replication. A report covering their work on this task is included as Appendix C. As illustrated in Figure 121, 'apparent' length is the portion of the total wrap-around crack length visible from the same side of the airfoil as the IR camera. 'Edge' length is the portion of the crack length that wraps around the edge of the airfoil but is not visible from either side of airfoil. 'Opposite apparent' is the portion of the crack that would be visible from the opposite side of the airfoil.

TABLE 18. SIZE INFORMATION FOR THE 10 TURBINE BLADE CRACKS.

Crack	Crack Length (inches)			
	Apparent	Opposite Apparent	Edge	Total
1	0.04	0	0.0039	0.0439
2	0.1058	0.0304	0.021	0.1572
3	0.2903	0.228	0.0153	0.5336
4A	0.0793	0.1875	0.0313	0.2981
4B	0.2907	0	0	0.2907
5	0.0935	0.1129	0.0163	0.2227
6	0	0.0718	0.0066	0.0784
7A	0.2781	0.2449	0.0156	0.5386
7C	0.0962	0.1321	0.01	0.2383
7D	0.1039	0.0503	0.0126	0.1668

Figure 121. The crack size definition for airfoil cracks.

5.4.4.1 Quadratic Mixed-Effect Model with Effective Crack Length for Turbine Blade Data

To reflect the effects of the crack length on the response value, two extra terms with apparent length and edge length information are added into the model described above in Section 5.4.3.1.3. The new model is:

$$\log(m+1) = \beta_{0,b} + \beta_{1,b}\log(v) + \beta_{2,b}\log(p) + \beta_{3,b}\log(tr) + \beta_4\log(v)\log(p) + \beta_5\log(v)\log(tr) +$$
$$\beta_6\log(p)\log(tr) + \beta_7\log(v)^2 + \beta_8\log(p)^2 + \beta_9\log(tr)^2 + \beta_a L_a + \beta_e L_e + \varepsilon \tag{17}$$

Here v represents Vibration Amplitude, p represents Pulse Length, tr represents Trigger Force, m represents Maximum Contrast, L_a stands for Apparent length and L_e stands for Edge length. The random error ε is assumed to have a normal distribution with mean 0 and variance σ_ε. The intercept and main effect (linear) model terms are modeled as random effects to describe the crack-to-crack variability in response, i.e., $\beta_{0,b}, \beta_{1,b}, \beta_{2,b}$ and $\beta_{3,b}$ together have a multivariate normal distribution with mean $\bar{\mu}_{\beta b}$ and covariance matrix $\Sigma_{\beta b}$, where $\bar{\mu}_{\beta b} = (\beta_0, \beta_1, \beta_2, \beta_3)$ is a 4-dimenstional vector and $\Sigma_{\beta b}$ is a 4×4 matrix. The model also assume that $\beta_{0,b}, \beta_{1,b}, \beta_{2,b}$ and $\beta_{3,b}$ are independent of the error ε. The fitting results of the model (17) show that the effect of edge length is statistically significant and the apparent length is not. This might suggest using only edge

length in the model. However, TABLE 18 indicates that one value of the edge length is zero and its response value is not. To avoid the "zero-size-crack" problem, we define an effective crack length, which is the convex combination of apparent length and edge length to be used in the model.

We define effective crack length as:

$$L_N = \alpha L_a + (1-\alpha)L_e$$

(18)

Here α is in the range from 0 to 1 and it needs to be decided by the model fitting to the data. The model with the effect crack length can be described as in (19).

$$\log(m+1) = \beta_{0,b} + \beta_{1,b}\log(v) + \beta_{2,b}\log(p) + \beta_{3,b}\log(tr) + \beta_4\log(v)\log(p)$$
$$+\beta_5\log(v)\log(tr) + \beta_6\log(p)\log(tr) + \beta_7\log(v)^2 + \beta_8\log(p)^2 + \beta_9\log(tr)^2 + \beta_{10}L_N + \varepsilon$$ (19)

For different fixed α values, the maximum likelihood of fitting model (19) will be different. Figure 122 shows the relationship between the fixed α and the maximum log likelihood of fitting model (19). The final value for α is chosen such that it will maximize this function, which is $\hat{\alpha} = 0.0179$.
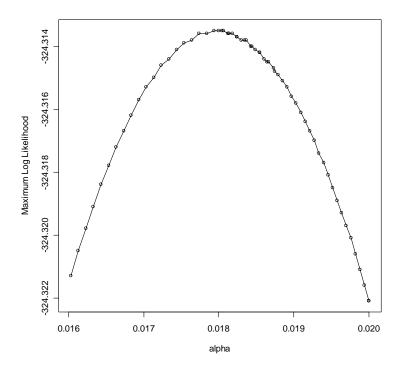
Figure 122. Maximum log likelihood of model (19) vs. α.

The parameter estimates of model (19) with $\hat{\alpha} = 0.0179$ are given in TABLE 19.

TABLE 19. MODEL (19) FITTING RESULT.

$\hat{\beta}_0$	$\hat{\beta}_1$	$\hat{\beta}_2$	$\hat{\beta}_3$	$\hat{\beta}_4$	$\hat{\beta}_5$	$\hat{\beta}_6$	$\hat{\beta}_7$	$\hat{\beta}_8$	$\hat{\beta}_9$	$\hat{\beta}_{10}$	$\hat{\sigma}_\varepsilon$
-9.344	-3.529	2.940	1.207	0.664	0.0880	-0.303	0.213	-0.266	0.123	78.20	0.754

$$\hat{\Sigma}_{\beta b} = \begin{pmatrix} 21.5 & 0.916 & -3.86 & -2.31 \\ 0.916 & 0.114 & -0.206 & -0.129 \\ -3.86 & -0.206 & 0.716 & 0.431 \\ -2.31 & -0.129 & 0.431 & 0.274 \end{pmatrix}$$

5.4.4.2 Estimation of Probability of Detection for Turbine Blades

Under model (19), for a given test condition (fixed values of Vibration Amplitude v, Pulse Length p and Trigger Force tr) and a given size, the log transformation of response plus 1, i.e., $\log(m+1)$, has a normal distribution with mean expressed in (20) and variance in (21), where X_l is a vector with four

components: $X_l = \begin{pmatrix} 1 \\ \log(v) \\ \log(p) \\ \log(tr) \end{pmatrix}$.

$$mean_{\log(m+1)}(v, p, tr) = \beta_0 + \beta_1 \log(v) + \beta_2 \log(p) + \beta_3 \log(tr) + \beta_4 \log(v)\log(tr)$$
$$+ \beta_5 \log(v)\log(p) + \beta_6 \log(p)\log(tr) + \beta_7 \log(v)^2 + \beta_8 \log(p)^2 + \beta_9 \log(tr)^2 + \beta_{10} L_N \quad (20)$$

$$Var_{\log(m+1)}(v, p, tr) = \sqrt{X_l^T \Sigma_{\beta b} X_l + \sigma_\varepsilon^2}$$

$$(21)$$

PoD vs. effective crack length plots are drawn in Figure 123, Figure 124 and Figure 125 for different specified test conditions. The two dotted vertical lines show the range of the effective crack length for the 10 cracks used in the experiments and the small circle indicates where those 10 cracks are according to their sizes. PoD values estimated outside of these lines involve extrapolation and are questionable. These plots show that the PoD can be close to 1, even for small cracks, if test conditions are chosen carefully, such as the test conditions in Figure 124 and Figure 125.
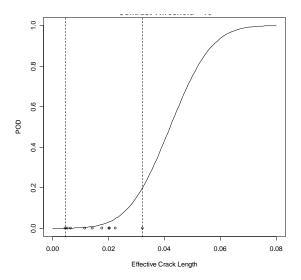
Figure 123. PoD vs. Effective Crack Length, Vibration Amplitude=10, Pulse Length=83 and Trigger Force = 10.
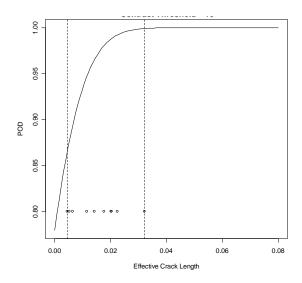
Figure 124. PoD vs. Effective Crack Length, Vibration Amplitude=55, Pulse
Length=150 and Trigger Force = 40.
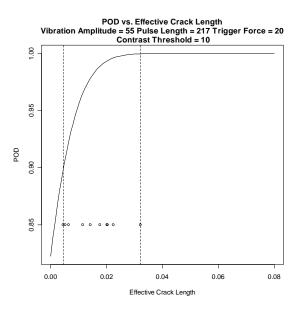
Figure 125. PoD vs. Effective Crack Length, Vibration Amplitude=55, Pulse
Length=217 and Trigger Force = 20.

5.4.5 Conclusions for Turbine Blade Study

The PoD vs. effective crack length analyses demonstrate that proper
selection of operating parameters for a given component can greatly improve the
probability of detecting a defect. These optimal parameters can determined by

combining results from a mixed effect model for the response data and a log normal reliability model for the time-to-alarm data from a parameter study such as the one outlined here.

5.5 Summary and Conclusions from Parameter Studies

Summary:
- General (across all four sample sets):
    – Defect signal increased with increasing amplitude, trigger force, and pulse length for most cases
    – Defect signal amplitude did not scale with flaw size
- For elongated scallop samples:
    – Trigger force did not have a large effect on defect signal
    – Defect signal increased for lower trigger force/flat horn tip combination and higher trigger force/curved horn tip combination
- For FPI PoD samples:
    – Increased clamping torque produced opposite results in responses, depending on crack orientation in sample
- For disks:
    – Alarms occurred at higher trigger force/low vibration amplitude combination
    – Alarm probability increased with pulse length
    – Clamping torque was not significant factor due to final fixture configuration
- For blades:
    – Optimal operating parameters increase the PoD of cracks

Conclusions:
- It is possible to characterize operating regions that produce reliable responses and low probabilities of welder alarms using the test method described here.

- Differences in responses from the flaws tested cannot be characterized by a single size variable in all cases.
- Clamping force can influence the crack signal depending on crack orientation.
- When using the optimal operating parameters, hit/miss PoD results from the Sonic IR technique are encouraging.

6.0 Crack Contamination Study

6.1 Crack Contamination Study Introduction

Many questions about factors influencing Sonic IR testing results have surfaced during the course of this program. Some of these questions concern the cleanliness of the scrapped engine components that have been studied. Most scrapped parts tested by this program have been rejected based on FPI results. The materials used in that testing could potentially affect the Sonic IR signal produced in our tests. There are anecdotes both supporting and contradicting this hypothesis. In addition, since engine and structural components are exposed to a wide variety of potentially contaminating materials while in use, general cleanliness requirements for parts removed from an airplane would have to be included in any Sonic IR inspection procedure for those components.

At the time this work was performed, there had been no published studies examining the effect of contaminants on Sonic IR results. This study was designed and performed to help understand if the presence of contaminants in fatigue cracks could influence the Sonic IR signal from those cracks. Inconel and aluminum specimens were produced and fatigue cracks of various lengths were placed in them. These specimens were exposed to several contaminants that aircraft structural and engine components might encounter in service. The specimens were then subjected to Sonic IR testing. While the number of samples in the study was limited due to budget considerations, the study was a first step towards understanding cleanliness requirements for this NDE technique.

6.2 Specimen Development and Contamination

6.2.1 Specimen Specifications for Crack Contamination Study

SAIC subcontracted Metcut Research, Inc. to produce the specimens for this study. Reports on the sample production are included in Appendices D and E. Inco 718 and Al 7075-T6 materials were used. A sketch of the sample dimensions is shown in Figure 126. Fourteen plates of each material were prepared, but only 12 of those plates for each material were cracked.
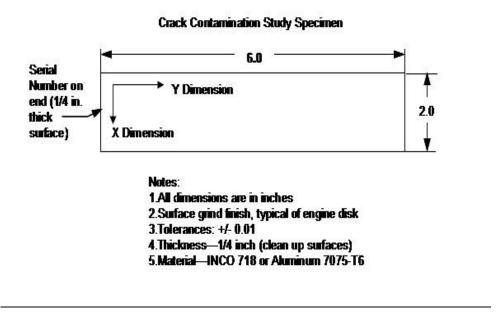
Figure 126. Specimen sketch and production notes.

A single EDM starter notch was positioned on each plate. Sixteen of the 24 test plates had the starter notch placed on the flat surface of the specimen at x = 1.0 inch and y = 1.75 inches, as defined in Figure 126. Eight of the specimens had the starter notch placed on the edge of the sample at x = 2.0 inches and y = 1.75 inches. All of the notches were oriented such that cracks would propagate parallel to the x direction in the specimen.

Fatigue crack development in the samples was described in the Metcut final report (Appendix D) as follows: "Crack development was performed using an MTS servo-hydraulic test frame in a 3-point bend mode of fatigue. The notched area of the plates was oriented directly under the load fulcrum such that the tensile moment would propagate the cracks as a function of elapsed cycles. The span of the fixturing was held constant at 3.5 inches. The maximum stress used to initiate the cracks was help constant at 80-100 ksi for the Inco-718 plates and 30.0-40.0 ksi for the aluminum plates. The plates were cycled at a frequency of 10 Hz using a sinusoidal wave shape. The load ratio for cycling was held constant at R=0.10."

Crack lengths were measured using a linearly traveling Gaertner microscope. Once the cracks reached their target lengths, the EDM notches were removed using low stress grinding.

The original goal was to have 4 samples for each material with surface cracks ~0.03 inch in length, 4 of each with surface cracks ~0.25 inch in length, and 4 of each with edge cracks ~ 0.03 inch in length. Unfortunately, one half of the cracks produced at the initially requested lengths could not be detected with Sonic IR, prior to any contamination. The samples were sent back to Metcut to have the crack lengths increased and brought back in and retested. It took several such iterations to develop a sample set with cracks that could be detected reliably with Sonic IR. A table of the initial and final crack lengths for the complete sample set is shown in TABLE 20, along with contaminants.

TABLE 20. INITIAL, FINAL CRACK LENGTHS AND CONTAMINANTS.

Sample #	Crack Type	Initial Crack Length	Final Crack Length[2]	Contaminant
1A	Surface	0.027	0.183	Paint
2A	Surface	0.028	0.188	Lubricant
3A	Surface	0.030	0.182	CPC
4A	Surface	0.028	0.177	None (control)
5A	Surface	0.295	(same)	Paint

Sample #	Crack Type	Initial Crack Length	Final Crack Length[2]	Contaminant
6A	Surface	0.247	(same)	Lubricant
7A	Surface	0.249	(same)	CPC
8A	Surface	0.249	(same)	None
9A	Edge	0.029	0.121	Paint
10A	Edge	0.028	0.122	Lubricant
11A	Edge	0.029	0.118	CPC
12A	Edge	0.037	0.118	None
1N	Surface	0.027	0.058	Fuel
2N	Surface	0.036	0.059	Lubricant
3N	Surface	0.029	0.60	Anti-gallant
4N	Surface	0.029	0.60	None
5N	Surface	0.258	(same)	Fuel
6N	Surface	0.249	(same)	Lubricant
7N	Surface	0.249	(same)	Anti-gallant
8N	Surface	0.248	(same)	None
9N	Edge	0.027	(same)	Fuel
10N	Edge	0.027	(same)	None
11N	Edge	0.029	(same)	Anti-gallant
12N	Edge	0.028	(same)	Lubricant

6.2.2 Specimen Contamination

As was shown in the table above, for each specimen material, 3 contaminants were chosen. The Inco specimens were contaminated with a jet fuel, a lubricant, and an anti-gallant compound. The aluminum specimens were contaminated with paint, a lubricant, and a corrosion preventive compound (CPC). [Note that the paint used on the Al specimens as a contaminant was an Air Force specified wheel paint. This paint is not to be confused with the tempura paint used to reduce specimen reflectivity for Sonic IR testing, discussed in the

next section.] Martin MetLabs, Inc. (MML) was subcontracted for this contamination work and a report on their effort is included in Appendix F.

The three Al specimens that were to be contaminated with paint were sent to the AFRL at Wright-Patterson Air Force Base and processed through an in-house paint line. The system used was "typical" of paint used on wheels of Air Force aircraft. This contamination procedure was intended to duplicate the condition of an existing crack, missed by the current inspection method, painted over, returned to use, and later inspected using Sonic IR testing. It is possible that the paint could prevent the crack from being detected with Sonic IR. This test does not address the question of detecting a crack that had formed under paint. Other testing would be required to determine the effect of paint on a crack formed in service, and whether Sonic IR can be performed successfully on painted parts in general.

For the specimens sent to MML for contamination, all specimens were individually set up on a fatigue machine with 3-point bend fixturing for a "winking" contamination procedure. This step simulated in-service stress likely to be encountered by an aircraft component. The contaminants were applied to roughly one square inch around the crack location and loaded in 3-point bending for several cycles. The specific materials used were:

- Jet fuel - JP-4
- Lubricant - WD-40$^®$
- CPC – Corban$^®$ 35 Corrosion Preventative Compound
- Anti-gallant – Permatex$^®$ High Temperature Anti-Seize Lubricant (#80078)

Following the contamination process, the Inco specimens were run through a bake cycle to simulate engine usage. The specimens were heated to 800° F and allowed to cool to less than 200° F. This contamination and baking cycle was conducted 4 times.

6.3 Test Procedure for Crack Contamination Study

The fatigue-cracked specimens from Metcut were examined with Sonic IR. They were too reflective in the infrared wavelengths to detect the cracks. Samples of Inconel and aluminum with ~0.25 inch cracks were tested, painted with flat black tempura paint and retested, and then washed and tested again with the same operating parameters. The cracks were not found initially, were detected when painted, and again were not found after washing in an ultrasonic water bath. These results indicated that painting the samples was required, and that painting and cleaning the samples did not improve crack detectability. Sonic IR images of the crack in Inconel, bare and with paint, are shown in Figure 127. The signal amplitude of the crack increased by roughly an order of magnitude when the sample was painted. Sonic IR images of the crack in aluminum, bare and with paint, at lower magnification than the Inco images, are shown in Figure 128. The crack was not visible in the bare sample, as shown in Figure 128(a).

(a) Bare   (b) Painted
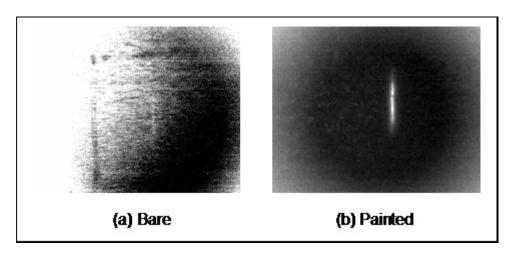
Figure127. Inconel sample with 0.25 inch fatigue crack, (a) bare and (b) painted.
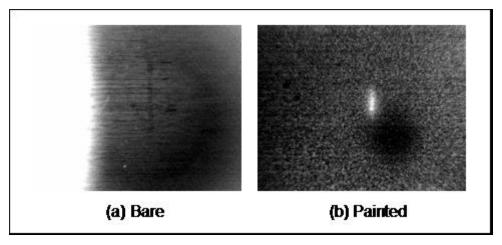
Figure 128. Aluminum sample with 0.25 inch fatigue crack, (a) bare and (b) painted.

For the results presented here, all Sonic IR tests were conducted using the same operating parameters. These parameters were: Amplitude – 100%, Pulse length – 90 milliseconds, and Trigger Force – 100 pounds. Other parameter combinations of lower values were tested in an attempt to quantify the influence of the contaminant on the detectability of the crack. However, the signal amplitudes were too small to allow any statistically significant differences to be observed. All specimens were painted with the black tempura paint to minimize reflections prior to each Sonic IR test. The specimens were washed with water in an ultrasonic bath after each Sonic IR test to remove this paint. The specimens were clamped in a rubberized cork-lined vise for these tests and 80 pound card stock (paper) was used as an interface material between the horn and the specimen.

The steps comprising this study are listed here:

- Specimens were tested with Sonic IR to verify that the fatigue cracks placed in them could be detected. (test "a")
- Specimens were subjected to fluorescent penetrant inspection (FPI). The materials used for this inspection were Zyglo ZL-27A penetrant and ZP-9F developer (Level III, post-emulsifiable). This step involved spraying the samples with a penetrant fluid, waiting 10 minutes, wiping off the fluid, spraying on a developer, and waiting ~10 minutes to read the results.

After the results were recorded, the samples were wiped clean. FPI
materials (penetrant and developer) were the first contaminant system
tested and all specimens were tested with these contaminants.

- Specimens were tested with Sonic IR to determine the effect of the FPI
"contaminants." (test "b") After testing, the samples were washed with
water to remove the tempura paint and then placed in an ultrasonic
acetone bath for 2 hours to remove the penetrant materials.

- At this point, the specimens were sent to either AFRL or Martin Metlabs
for further contamination. When the samples were returned to SAIC, they
were again tested with Sonic IR. (test "c")

6.4 Crack Contamination Study Results and Discussion

The results of the study described above are summarized in TABLE 21.
Notes on abbreviations used in the table are listed below the table.

TABLE 21. CONTAMINATION STUDY RESULTS.

Sample #	Crack Type	Crack Length (in.)	Sonic IR test "a"	Visible w/FPI?	Sonic IR test "b"	Contaminant	Sonic IR test "c"
1A	S	0.183	Yes	Yes	Yes	Paint	Yes
2A	S	0.188	Yes	Yes	Yes	Lubricant	Yes
3A	S	0.182	Yes	Yes	Yes	CPC	Yes
4A	S	0.177	Yes	Yes	Yes	None	N/A
5A	S	0.295	Yes	Yes	Yes	Paint	Yes
6A	S	0.247	Yes	Yes	Yes	Lubricant	Yes
7A	S	0.249	Yes	Yes	Yes	CPC	Yes
8A	S	0.249	Yes	Yes	Yes	None	N/A
9A	E	0.121	Yes	Yes	Yes	Paint	Yes
10A	E	0.122	Yes	Yes	Yes	Lubricant	Yes
11A	E	0.118	Yes	Yes	Yes	CPC	Yes
12A	E	0.118	Yes	Yes	Yes	None	N/A
1N	S	0.058	Yes	Yes	Yes	Fuel	Yes
2N	S	0.059	Yes	Yes	Yes	Lubricant	Yes
3N	S	0.060	Yes	Yes	Yes	Anti-gallant	Yes
4N	S	0.060	Yes	Yes	Yes	None	N/A
5N	S	0.258	Yes	Yes	Yes	Fuel	Yes

Sample #	Crack Type	Crack Length (in.)	Sonic IR test "a"	Visible w/FPI?	Sonic IR test "b"	Contaminant	Sonic IR test "c"
6N	S	0.249	Yes	Yes	Yes	Lubricant	Yes
7N	S	0.249	Yes	Yes	Yes	Anti-gallant	No
8N	S	0.248	Yes	Yes	Yes	None	N/A
9N	E	0.027	Yes	No	Yes	Fuel	No
10N	E	0.027	Yes	No	No	None	N/A
11N	E	0.029	Yes	No	Yes	Anti-gallant	No
12N	E	0.028	Yes	No	Yes	Lubricant	No

Notes: A = Aluminum 7075-T6
   N = Inconel 718
   S = Surface crack
   E = Edge crack
   test "a" = baseline Sonic IR test
   test "b" = Sonic IR test after FPI materials contamination
   test "c" = Sonic IR test after other materials contamination
   Paint = Air Force "wheel paint"
   Lubricant = WD-40®
   CPC = Corban® 35 Corrosion Preventative Compound
   Fuel = JP-4
   Anti-gallant = Permatex® High Temperature Anti-Seize Lubricant (#80078)

The first result of note is the difficulty encountered in conducting Sonic IR tests on polished bare metal specimens. While this is a well-known problem in traditional thermography, it is one that had not plagued this program because we dealt with scrapped parts instead of polished samples. A common solution for this problem is coating the metal with water-based flat black paint. It was not desirable to add another potential contaminant into the mix, given that the point of this study was to look at the effects of various contaminants, but no other acceptable workaround could be found for the problem. Most parts that have been in service on an airplane will not be as polished and reflective in the infrared as these samples were, so this is not a problem to be expected in depot use of the Sonic IR technique.

There was no need to "read" the FPI results when the penetrant materials were used as contaminants on the specimens. However, since the standard FPI procedure was being followed anyway, the results were recorded. It is interesting to note that the smallest cracks in the specimen set, roughly 0.030 inch in length, were <u>not</u> detected with penetrant. These same cracks were detectable with Sonic IR prior to FPI materials contamination (test "a"). The

crack in sample 10N could not be detected with Sonic IR after the penetrant materials were applied (test "b"). Although this step was not part of the test matrix, sample 10N was retested with Sonic IR after going through the acetone ultrasonic bath to remove the penetrant materials. Again, the crack was not detected. At that point, 10N became the control sample for the edge-cracks-in-Inco subset and received no further contamination or testing.

With further contamination, the other 3 smallest edge cracks in Inco were no longer detectable with Sonic IR (test "c"). The surprising result was the final test of sample 7N. This sample had a surface crack that was almost a quarter of an inch in length and it was not detected after contamination. The sample was tested numerous times to verify this result.

6.5 Conclusions for Crack Contamination Study

There were a limited number of samples and contamination materials in this study because of the expense of generating such samples. Global conclusions cannot be drawn from such a small sample set. However, some trends and anomalies were observed that warrant further study.

Sonic IR outperformed Level III post-emulsifiable fluorescent penetrant inspection in the detection of small (~0.03 inch) corner cracks in the 4 uncontaminated Inco 718 specimens. A properly designed probability of detection (PoD) study could determine if this result can be expected.

Scrapped parts used for Sonic IR studies are often rejected based upon FPI results. When received by the Sonic IR laboratory, the parts are usually not subjected to an acetone ultrasonic bath to remove the penetrant materials residue. The results of this study indicate that FPI materials are not a problem for the cracks larger than ~ 0.06 inch. However, in one case for a 0.030 inch corner crack in Inco (test "b"), the presence of the FPI materials <u>did</u> prevent the detection of the crack with Sonic IR. This is only one datum and further study is needed to determine the significance of it.

The "winking" contamination and bake procedure using fuel, anti-gallant, and WD-40 materials prevented Sonic IR detection of the 0.03 inch corner cracks in the Inco specimens (test "c"). Taken together with the results of the post-FPI materials contamination test (test "b"), these results do indicate a trend. If confirmed, this result would indicate that contaminants are more likely to interfere with Sonic IR testing of small cracks (<0.03 inch) than with testing of larger ones (>0.06 inch). Recall, however, that the smallest cracks were corner cracks, not surface cracks, so that difference must be taken into account, also.

The most puzzling result of this study was the post-contamination Sonic IR test of specimen 7N (test "c"). The large surface crack, almost 0.25 inch in length, was not detectable after contamination with the anti-gallant compound. The smaller surface crack in specimen 3N, which was only 0.06 inch in length, was detectable after anti-gallant contamination, as were the other 2 longer cracks in specimens 5N and 6N. The result from specimen 7N does not fit a pattern of any sort nor is it easily explained. Further testing is recommended in this area.

To reiterate, the sample size used in this study was relatively small. Given that fact, the strongest conclusion that can be drawn here is that contaminants can potentially prevent the Sonic IR detection of cracks at or below 0.03 inch in length. It would be interesting to determine if these specimens could be cleaned sufficiently to produce a Sonic IR signal again. That investigation could lead to pre-Sonic IR inspection cleaning requirements for aircraft parts. All of the specimens used in this study are available for further testing.

7.0 References

1.   Mayton, Donna and Eric Lindgren, "Advanced Thermosonic Methods (Sonic IR)," Final Report for Nondestructive Evaluation (NDE) Technology Initiatives Program (NTIP) delivery order 0029, USAF report # A684524, July 2003.

2.   Busse, G., M. Bauer, W. Rippel, and D. Wu, "Lock-in Vibrothermal Inspection of Polymer Composites," *QIRT 92*, Editions Europeenes Thermique et Industrie, Paris, 1992, p.154.

3.   Favro, L.D., Xiaoyan Han, Zhong Ouyang, Gang Sun, and R.L.Thomas, "Infrared Imaging of Defects Heated by a Sonic Pulse," *Review of Scientific Instruments*, Vol. 71, No. 6, June 2000, pp. 2418-2421.

4. Mayton, D. and F. Spencer, "A Design of Experiments Approach to Characterizing   the Effects of Sonic IR Variables," *Thermosense XXVI*, D.D. Burleigh, K.E. Cramer, and G.R. Peacock, eds., SPIE vol. 5405, Bellingham, WA, 2004, pp. 322-331.

5. Mayton, Donna, Floyd Spencer, and Carlos Alvarez, "Characterizing the Effects of Sonic IR Variables on Turbine Disk Inspection using a Design of Experiments Approach," *Review of Progress in Quantitative Nondestructive Evaluation*, Donald O. Thompson and Dale Chimenti, eds., Vol. 24A, 2004, pp. 642-649.

6. R Project for Statistical Computing, http://www.r-project.org.

7. Venables, W.N. and B.D. Ripley, Modern Applied statistics with S, Springer, New York, 2003.

8. Davidian, M. and D.M. Giltinan, "Nonlinear models for repeated measurements: An overview and update," *Journal of Agricultural, Biological, and Environmental Statstics* 8, 2003, pp. 387-419.

9. Meeker, W.Q. and L. A. Escobar, SPLIDA (S-PLUS Life Data Analysis). http://www.public.iastate.edu/~splida, 2004.

8.0 Appendices

Appendix A
Crack Length Measurements for Scallop Samples

(Excerpts from MML report. The complete report is not included because it reveals part numbers. The sample set is used in the NDE community as a blind test, so part numbers and crack lengths cannot be revealed.)

…
Four F100-220 eddy current reliability specimens were sent to Martin MetLabs for microphotograph documentation and crack length measurements. Each sample had a crack transversely oriented in the scalloped detail. These particular samples had been subjected to Sonic IR testing and required verification that cracks did not propagate any further. Pre-test 100X microphotographs and crack length measurements of each sample were also included for comparison. These images appeared to have been captured from cellulose acetate replicas.

Results:
Each sample was reviewed at 100X magnification using conventional microscopy. Image analysis software was employed to determine all crack length measurements and were recorded in the following data matrix.

Reliability Demo Specimen Crack Measurement Data			
Sample ID	Crack Length Measurement (in.)		Comments
	Before Sonic IR	After Sonic IR	
A	0.0215	0.0211	Additional surface crack continuity
B	0.0115	0.0113	None
C	0.0175	0.0180	None
D	0.0145	0.0149	Additional surface crack continuity

Microphotographs were also captured of sample crack and annotated with the crack length measurements. 'Before and after' images were represented in Figures 1a – 1d for visual comparison. It should be noted that although cracks did not propagate any further in length, there was what appeared to be some increased surface crack continuity on Sample A and Sample D. These particular cracks had multiple surface crack ligaments that apparently linked up as depicted in the comparison images.
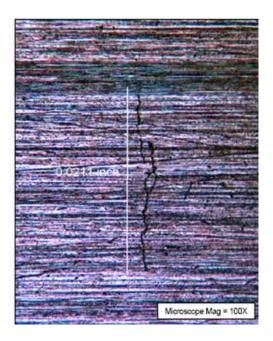
FIGURE 1a. *LEFT IMAGE:* 100X microphotograph of Sample A before Sonic IR testing (0.0215 inch crack length). NOTE: Original image was rotated and horizontally inverted for accurate comparison. *RIGHT IMAGE:* 100X microphotograph of Sample A after Sonic IR testing (0.0211 inch crack length).
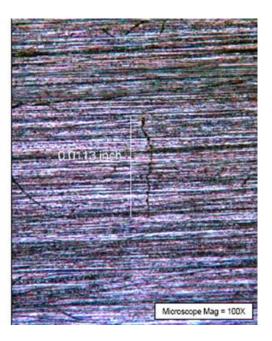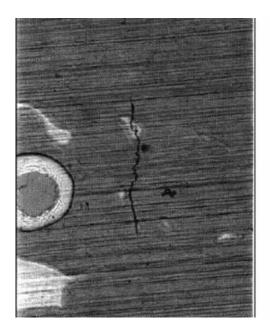
FIGURE 1b. *LEFT IMAGE:* 100X microphotograph of Sample B before Sonic IR testing (0.0115 inch crack length). NOTE: Original image was rotated and horizontally inverted for accurate comparison. *RIGHT IMAGE:* 100X microphotograph of Sample B after Sonic IR testing (0.0113 inch crack length).
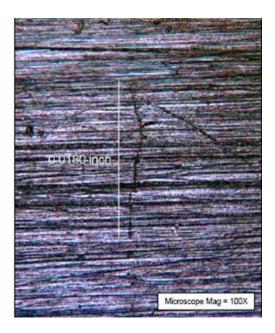
FIGURE 1c. *LEFT IMAGE:* 100X microphotograph of Sample C before Sonic IR testing (0.0175 inch crack length). NOTE: Original image was rotated and horizontally inverted for accurate comparison. *RIGHT IMAGE:* 100X microphotograph of Sample C after Sonic IR testing (0.0180 inch crack length).

FIGURE 1d. *LEFT IMAGE:* 100X microphotograph of Sample D before Sonic IR testing (0.0145 inch crack length). NOTE: Original image was rotated and horizontally inverted for accurate comparison. *RIGHT IMAGE:* 100X microphotograph of Sample D after Sonic IR testing (0.0149 inch crack length).

FATIGUE TECHNOLOGY INC.

401 Andover Park East
Seattle, Washington 98188-7605
USA   (206) 246-2010

FATIGUE TECHNOLOGY INC.

FTI TECHNICAL REPORT #153505

Crack Generation in Turbine Disks for
Non-Destructive Inspections at
Scientific Applications International Corporation

October 22, 2003

Beverly Franada
Materials Test Facility Assistant
Manager

Copy Number: _____

Issued To: _____

FATIGUE TECHNOLOGY INC. - REPORT DOCUMENTATION PAGE

1. Report Title and Subtitle	2. Report No.
Crack Generation in Turbine Disks for Non-Destructive Inspections at Scientific Applications International Corporation	153505
	3. Performing Organization Report No.
	N/A

4. Author(s)	5. Date
Beverly Franada	October 22, 2003

6. Performing Organization Name and Address	7. Type of Report	
Fatigue Technology Inc.	Test Report	
401 Andover Park East	**8. Log Number**	**8a. Project Number**
Seattle, WA 98188-7605	2927	SO64785

9. Sponsoring Organization Name	10. Contract No.	
Iowa State University (ISU) and Science Applications International Corporation (SAIC)	ISU Subcontract #404-25-91 SAIC Subcontract #44000071759	
	11. Keywords / Subject Terms	

12. Supplementary Notes	
None	Fatigue crack generation
	Constant amplitude fatigue

13. Abstract

Fatigue Technology Inc. (FTI) performed constant amplitude fatigue testing on turbine disks to generate fatigue cracks in the anti-rotational tangs. Testing was performed for Iowa State University (ISU) and Scientific Applications International Corporation (SAIC).

SAIC is developing a non-destructive method of inspecting the disks for cracks at the anti-rotational tangs. In order to evaluate this new method, they required disks with small cracks. These cracks needed to be generated in a controlled manner.

FTI performed testing in two phases. In Phase 1, FTI designed and manufactured the test fixture to mount the disk to the test frame and apply the required loads to the tangs; FTI also generated cracks in a sample disk in order to determine the correct test parameters for testing such as the test frequency and the test stress. In Phase 2, FTI generated cracks at the tangs in five disks using the methods determined from Phase 1.

14. Distribution / Releasability of Report	15. Report Print Date
Customer Proprietary / Non-Releasable	January 8, 2008

16. Responsible Department and Individual	17. Telephone
Engineering Manager	(206) 246-2010

18. Distribution / Releasability of Abstract	19. Total Page Count
Proprietary / Non-Releasable	18 (including cover pages)

Reviewed by: _____   Released by: _____
        Jude Restis   Len Reid
        Engineering Manager   Vice President, Engineering

TABLE OF CONTENTS

SECTION	DESCRIPTION	PAGE

1.0   OBJECTIVE

The objective of this document is for Fatigue Technology Inc. (FTI) to present the methods and results of a test program performed to generate fatigue cracks at the anti-rotational tangs of first stage turbine disks manufactured from IM100 powdered nickel. This test program was performed for Iowa State University (ISU) and Scientific Applications International Corporation (SAIC).

2.0   BACKGROUND

Currently the U.S. Air Force is not able to inspect for the cracks that may occur at the anti-rotation tangs on first stage turbine disks. SAIC is developing a non-destructive method for inspecting and measuring cracks at the anti-rotational tangs on these disks. FTI generated the cracks needed in the disks to be used as crack standards to evaluate the new inspection method and inspection equipment.

3.0   TEST PROGRAM

FTI performed testing in two phases. Phase 1 was performed to develop the test method for generating the cracks. Phase 2 was performed to generate cracks in five disks using the method developed in Phase 1.

3.1   Phase 1

In this Phase FTI designed and manufactured the test fixture as well as determined the test parameters for generating the cracks in the disks.

The disk and fixture setup is shown in Figure 3.1-1.

Figure 3.1-1
Disk and Fixture Setup

The disk stand assembly was mounted to the test frame. The disk was installed between two plates in the fixture and the plates were clamped to prevent the disk from rotating during testing.

The load-bars, with a key that fit in the anti-rotation tang, were gripped in the hydraulic grips of the test frame. During testing the load bars were cycled in the frame thus loading the anti-rotation tang tangentially, similar to the way it was loaded in the actual application. Some Teflon spacers were used in the load-bars to prevent any fretting between the disk and the fixture.

SAIC provided a sample disk to FTI for the first setup of the test fixtures and to perform any preliminary tests. FTI used this disk to determine test loads, crack inspection and measurement method and make any adjustments to the fixture as necessary.

For the first tang in the sample disk, FTI started fatigue testing at a maximum test stress of 100 ksi, R-ratio of +0.10 and frequency of 2 Hz. Testing was performed at ambient temperature and humidity conditions in FTI's lab. Testing was stopped periodically for crack inspections. The tangs were inspected using a Digital Traveling Microscope (DTM) mounted to the test frame (Figure 3.1-2 shows the complete test frame setup with DTM). When no cracks were observed at 40,000 cycles, the stress was increased in increments of 10 ksi (with approval from SAIC). Testing continued in this manner until a crack could be measured to 0.050 inch. After the first tang was tested, a second tang in the sample disk was tested to verify the test methods from the first. Testing of this specimen was started at a maximum test stress of 120 ksi as crack initation in the first tang did not occur until it was tested at this stress. All other parameters were the same. FTI was able to generate and monitor crack growth in this tab at these parameters. SAIC personnel visited FTI's facility to check out the

setup and verify the cracking method after FTI produced the first tang crack. FTI then continued to Phase 2.

Figure 3.1-2
Test Frame Setup

3.2 Phase 2

In this phase, FTI generated cracks in five disks provided by SAIC. On each disk there are four anti-rotation tangs, two symmetric and two asymmetric. SAIC required cracks in the longer portion of the asymmetric tangs. When the disk was oriented such that the asymmetric tangs were at the 3 o'clock and 9 o'clock positions, the longer portion of the tangs were both at the bottom. The tang at the 9 o'clock position was considered Tang A and the tang at the 3 o'clock position was considered Tang B. FTI used this naming convention for all disks.

For tracking and load-calculation purposes FTI measured the dimensions of the tangs to be tested. The width of each tang was measured at the edge of the tang (the section furthest away from the disk surface) and at the base of the tang (the section closest to the disk surface). The average of these two measurements was recorded as the width of the tang. The depth of the tang was measured from the edge of the tang to the bottom of the notch or cutout at each tang. The tang area was calculated by multiplying the width and the depth.

All disks were mounted in the test fixture as described for Phase 1. The disks were tested at various test stresses, R-ratio of +0.10 and frequency of 2 Hz. The stresses were adjusted as necessary to initiate cracks and to control the crack growth. The actual test stresses for each tang are listed in the crack growth reports in the appendix. Testing was completed when the cracks reached the desired crack lengths (SAIC provided a list of desired crack lengths). Because the cracks tended to grow diagonally, FTI measured the horizontal and vertical crack lengths for each crack then used Pythagorean theorem to calculate the actual crack length.

FTI's test frames are load calibrated to one percent or better accuracy following the guidelines of ASTM E4. The test frames are aligned to five percent or better following the guidelines of ASTM E1012. All laboratory test and measurement equipment is regularly calibrated using standards traceable to the National Institute of Standards and Technology.

4.0 TEST RESULTS AND DISCUSSION

The final crack lengths are listed in Table 4.0-1. The crack growth data and other test data are provided in the crack growth reports for each specimen provided in the appendix. The crack growth reports also include digital photos of the cracks at the end of testing. The digital were taken by placing the lens of the digital camera on the eyepiece of the DTM at the frame.

Table 4.0-1
Final Crack Lengths

Disk Number	Tang Identification	Crack Length, inch
1	A	0.040
1	B	0.013
2	A	0.009
2	B	0.016*
3	A	0.021
3	B	0.029
4	A	0.011*
4	B	0.026

Disk Number	Tang Identification	Crack Length, inch
5	A	0.036
5	B	0.017

*Note: Secondary cracks were observed
at Disk 2 Tang B and Disk 4 Tang A.

A secondary crack was observed at Disk 2, Tang B. This secondary crack was 0.012 inch long (horizontal crack length=0.006 inch, vertical crack length=0.011 inch).

A secondary crack was observed at Disk 4, Tang A. This crack was 0.008 inch long (horizontal crack length=0.003 inch, vertical crack length=0.007 inch).

The shorter tab of Tang A of Disk 3 was inadvertently broken off the disk. SAIC was informed of this and testing was continued on the appropriate portion of the tang.

All cracks generated in this test program will be used at SAIC as crack standards for the evaluation and further development of the new inspection method.

Appendix A
Crack Growth Reports

CONSTANT AMPLITUDE TEST REPORT

Customer:	SAIC/ISU	**FTI Project Number:**	SO64875
Disk #, Tang Identification:	Disk 1, Tang A	**Frame:**	15
Specimen Type:	Engine Disk	**Crack Plane Orientation:**	N/A
Material:	Powder Nickel		

TEST CONDITIONS   Tang Dimensions

Testing performed at ambient lab temperature and relative humidity

Temperature (°F):	70	**Notch Depth (inch):**	0.108
Relative Humidity (%):	44	**Width (inch):**	0.080
		Gross Area (inch^2):	0.009

Test Parameters   Final Crack Length

Maximum Gross Stress (ksi):	Various (see notes)	**Targeted Crack Length (inch):**	0.040
R-Ratio: (Min./Max. Stress):	+0.1	**Actual Crack Length (inch):**	0.040
Maximum Load (lb):	Various (see notes)		
Minimum Load (lb)	Various (see notes)		
Test Frequency (Hz):	2		

Notes:
1. Testing was started at a maximum gross stress of 120 ksi or max./min. load of 1030/103 lbs.
2. At 60,490 cycles, no cracks were observed so the stress level was increased to maximum gross stress of 130 ksi or max./min. load of 1116/112 lbs.
3. Crack initiation was observed at 61,112 cycles. The stress level was decreased to the original stress of 120 ksi.
4. At 91,112 cycles, the stress level was increased to 130 ksi because crack growth was not observed.
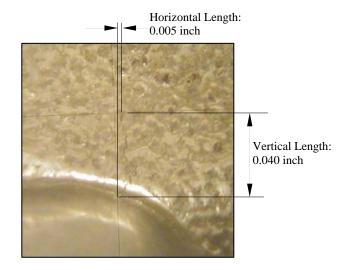
Crack Growth Data

Cycles	Horizontal Crack Length, inch	Vertical Crack Length, inch	Calculated Crack Length, inch
61,112	0.005	0.009	0.010
63,112	0.005	0.010	0.011
69,612	0.005	0.011	0.012
72,112	0.005	0.012	0.013
77,112	0.005	0.013	0.014
79,612	0.005	0.014	0.015
109,612	0.005	0.025	0.025
118,112	0.005	0.029	0.029
124,112	0.005	0.033	0.033
133,112	0.005	0.035	0.035
136,112	0.005	0.040	0.040

Note: FTI visually measured the horizontal and vertical length of the crack using a DTM mounted to the test frame. The actual length of the crack was calculated using the Pythagorean theorem.

CONSTANT AMPLITUDE TEST REPORT

Horizontal Length:
0.005 inch

Vertical Length:
0.040 inch

Customer:	SAIC/ISU	**FTI Project Number:**	SO64875
Disk #, Tang Identification:	Disk 1, Tang B	**Frame:**	15
Specimen Type:	Engine Disk	**Crack Plane Orientation:**	N/A
Material:	Powder Nickel		

TEST CONDITIONS

Testing performed at ambient lab temperature and relative humidity

Temperature (°F):	72
Relative Humidity (%):	40

Test Parameters

Maximum Gross Stress (ksi):	120
R-Ratio: (Min./Max. Stress):	+0.10
Maximum Load (lb):	987
Minimum Load (lb)	99
Test Frequency (Hz):	2

Tang Dimensions

Notch Depth (inch):	0.108
Width (inch):	0.076
Gross Area (inch²):	0.008

Final Crack Length
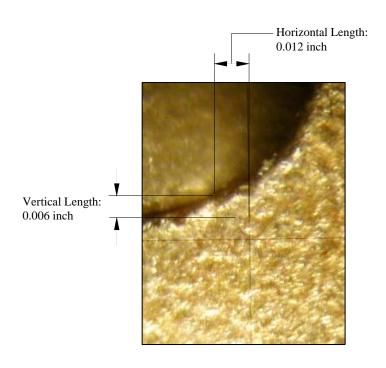
Targeted Crack Length (inch):	0.013
Actual Crack Length (inch):	0.013

Crack Growth Data

Cycles	Horizontal Crack Length, inch	Vertical Crack Length, inch	Calculated Crack Length, inch
28,000	0.006	0.002	0.006
31,500	0.009	0.004	0.010
36,000	0.010	0.005	0.011
38,500	0.012	0.006	0.013

Note: FTI visually measured the horizontal and vertical length of the crack using a DTM mounted to the test frame. The actual length of the crack was calculated using the Pythagorean theorem.

Horizontal Length:
0.012 inch

Vertical Length:
0.006 inch

CONSTANT AMPLITUDE TEST REPORT

Customer:	SAIC/ISU	**FTI Project Number:**	SO64875
Disk #, Tang Identification:	Disk 2, Tang A	**Frame:**	15
Specimen Type:	Engine Disk	**Crack Plane Orientation:**	N/A
Material:	Powder Nickel		

TEST CONDITIONS

Testing performed at ambient lab temperature and relative humidity

Temperature (°F):	72
Relative Humidity (%):	42

Tang Dimensions

Notch Depth (inch):	0.112
Width (inch):	0.073
Gross Area (inch²):	0.008

Test Parameters

Maximum Gross Stress (ksi):	Various (see notes)
R-Ratio: (Min./Max. Stress):	+0.10
Maximum Load (lb):	Various (see notes)
Minimum Load (lb)	Various (see notes)
Test Frequency (Hz):	2

Final Crack Length

Targeted Crack Length (inch):	0.009
Actual Crack Length (inch):	0.009

Notes:
1. Testing of this tang was started at a maximum gross stress of 120 ksi or max./min. load of 959/96 lbs.
2. At 40,000 cycles, the stress was increased to 130 ksi or max./min. load of 1039/104 lbs.

Crack Growth Data

Cycles	Horizontal Crack Length, inch	Vertical Crack Length, inch	Calculated Crack Length, inch
40,871	0.002	0.009	0.009

Note: FTI visually measured the horizontal and vertical length of the crack using a DTM mounted to the test frame. The actual length of the crack was calculated using the Pythagorean theorem.

Horizontal Length: 0.002 inch

Vertical Length: 0.009 inch

CONSTANT AMPLITUDE TEST REPORT

Customer:	SAIC/ISU	**FTI Project Number:**	SO64875
Disk #, Tang Identification:	Disk 2, Tang B	**Frame:**	15
Specimen Type:	Engine Disk	**Crack Plane Orientation:**	N/A
Material:	Powder Nickel		

TEST CONDITIONS

Testing performed at ambient lab temperature and relative humidity

Temperature (°F):	71
Relative Humidity (%):	45

Tang Dimensions

Notch Depth (inch):	0.107
Width (inch):	0.075
Gross Area (inch^2):	0.008

Test Parameters

Maximum Gross Stress (ksi):	Various (see notes)
R-Ratio: (Min./Max. Stress):	+0.10
Maximum Load (lb):	Various (see notes)
Minimum Load (lb)	Various (see notes)
Test Frequency (Hz):	2

Final Crack Length

Targeted Crack Length (inch):	0.015
Actual Crack Length (inch):	0.016

Notes:
1. Testing of this tang was started at a maximum gross stress of 120 ksi or max./min. load of 963/96 lbs.
2. At 40,000 cycles, the stress was increased to 130 ksi or max./min. load of 1043/104 lbs.
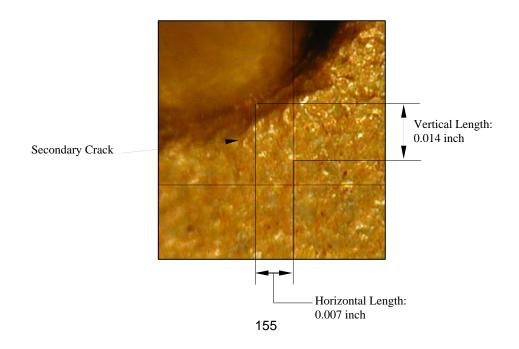
Crack Growth Data

Cycles	Horizontal Crack Length, inch	Vertical Crack Length, inch	Calculated Crack Length, inch
67,635	0.007	0.012	0.014
68,635	0.007	0.013	0.015
71,135	0.007	0.014	0.016

Notes:
1. FTI visually measured the horizontal and vertical length of the crack using a DTM mounted to the test frame. The actual length of the crack was calculated using the Pythagorean theorem.
2. A secondary crack was observed on this tang. This crack was 0.012 inch long (horizontal crack length=0.006 inch, vertical crack length=0.011 inch).

Secondary Crack

Vertical Length: 0.014 inch

Horizontal Length: 0.007 inch

CONSTANT AMPLITUDE TEST REPORT

Customer:	SAIC/ISU	**FTI Project Number:**	SO64875
Disk #, Tang Identification:	Disk 3, Tang A	**Frame:**	15
Specimen Type:	Engine Disk	**Crack Plane Orientation:**	N/A
Material:	Powder Nickel		

TEST CONDITIONS

Testing performed at ambient lab temperature and relative humidity

Temperature (°F):	72
Relative Humidity (%):	41

Tang Dimensions

Notch Depth (inch):	0.112
Width (inch):	0.073
Gross Area (inch^2):	0.008

Test Parameters

Maximum Gross Stress (ksi):	Various (see notes)
R-Ratio: (Min./Max. Stress):	+0.10
Maximum Load (lb):	Various (see notes)
Minimum Load (lb)	Various (see notes)
Test Frequency (Hz):	2

Final Crack Length

Targeted Crack Length (inch):	0.021
Actual Crack Length (inch):	0.021

Notes:
1. Testing of this tang was started at a maximum gross stress of 130 ksi or max./min. load of 1058/106 lbs.
2. At 40,000 cycles, the stress was increased to 140 ksi or max./min. load of 1175/118 lbs.

Crack Growth Data

Cycles	Horizontal Crack Length, inch	Vertical Crack Length, inch	Calculated Crack Length, inch
40,225	0.000	0.021	0.021

Note: FTI visually measured the horizontal and vertical length of the crack using a DTM mounted to the test frame. The actual length of the crack was calculated using the Pythagorean theorem.

Vertical Length: 0.021 inch

CONSTANT AMPLITUDE TEST REPORT

Customer:	SAIC/ISU	**FTI Project Number:**	SO64875
Disk #, Tang Identification:	Disk 3, Tang B	**Frame:**	15
Specimen Type:	Engine Disk	**Crack Plane Orientation:**	N/A
Material:	Powder Nickel		

TEST CONDITIONS

Testing performed at ambient lab temperature and relative humidity

Temperature (°F):	72
Relative Humidity (%):	43

Tang Dimensions

Notch Depth (inch):	0.110
Width (inch):	0.076
Gross Area (inch^2):	0.008

Test Parameters

Maximum Gross Stress (ksi):	130
R-Ratio: (Min./Max. Stress):	+0.10
Maximum Load (lb):	1099
Minimum Load (lb)	110
Test Frequency (Hz):	2

Final Crack Length

Targeted Crack Length (inch):	0.029
Actual Crack Length (inch):	0.029

Crack Growth Data
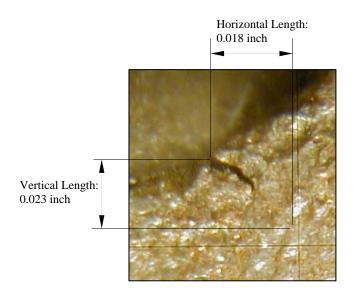
Cycles	Horizontal Crack Length, inch	Vertical Crack Length, inch	Calculated Crack Length, inch
15,985	0.011	0.008	0.014
16,064	0.012	0.008	0.014
27,982	0.013	0.009	0.016
32,900	0.017	0.020	0.026
34,000	0.018	0.023	0.029

Note: FTI visually measured the horizontal and vertical length of the crack using a DTM mounted to the test frame. The actual length of the crack was calculated using the Pythagorean theorem.

Horizontal Length: 0.018 inch

Vertical Length: 0.023 inch

CONSTANT AMPLITUDE TEST REPORT

Customer:	SAIC/ISU	**FTI Project Number:**	SO64875
Disk #, Tang Identification:	Disk 4, Tang A	**Frame:**	15
Specimen Type:	Engine Disk	**Crack Plane Orientation:**	N/A
Material:	Powder Nickel		

TEST CONDITIONS

Testing performed at ambient lab temperature and relative humidity

Temperature (°F):	72
Relative Humidity (%):	40

Tang Dimensions

Notch Depth (inch):	0.104
Width (inch):	0.075
Gross Area (inch^2):	0.008

Test Parameters

Maximum Gross Stress (ksi):	Various (see notes)
R-Ratio: (Min./Max. Stress):	+0.10
Maximum Load (lb):	Various (see notes)
Minimum Load (lb)	Various (see notes)
Test Frequency (Hz):	2

Final Crack Length

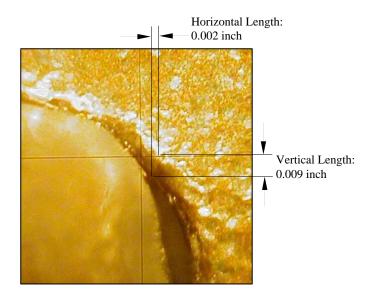|	
Targeted Crack Length (inch):	0.011
Actual Crack Length (inch):	0.011

Notes:
1. Testing was started at a maximum gross stress of 120 ksi or a max./min. load of 936/94 lbs.
2. At 60,000 cycles, the maximum gross stress was increased to 125 ksi (max./min. load of 975/98 lbs.).

Crack Growth Data

Cycles	Horizontal Crack Length, inch	Vertical Crack Length, inch	Calculated Crack Length, inch
89,908	0.003	0.005	0.006
91,023	0.003	0.006	0.007
127,000	0.003	0.007	0.008
152,500	0.005	0.010	0.011

Notes:
1. FTI visually measured the horizontal and vertical length of the crack using a DTM mounted to the test frame. The actual length of the crack was calculated using the Pythagorean theorem.
2. A secondary crack was observed at this tang. This crack was 0.008-inch long (horizontal crack length=0.003 inch, vertical crack length=0.007 inch long).

Horizontal Length: 0.005 inch

Secondary Crack

Vertical Length: 0.010 inch

CONSTANT AMPLITUDE TEST REPORT

Customer:	SAIC/ISU	**FTI Project Number:**	SO64875
Disk #, Tang Identification:	Disk 4, Tang B	**Frame:**	15
Specimen Type:	Engine Disk	**Crack Plane Orientation:**	N/A
Material:	Powder Nickel		

TEST CONDITIONS

Testing performed at ambient lab temperature and relative humidity

Temperature (°F):	70
Relative Humidity (%):	38

Tang Dimensions

Notch Depth (inch):	0.106
Width (inch):	0.076
Gross Area (inch²):	0.008

Test Parameters

Maximum Gross Stress (ksi):	Various (see notes)
R-Ratio: (Min./Max. Stress):	+0.10
Maximum Load (lb):	Various (see notes)
Minimum Load (lb)	Various (see notes)
Test Frequency (Hz):	2

Final Crack Length

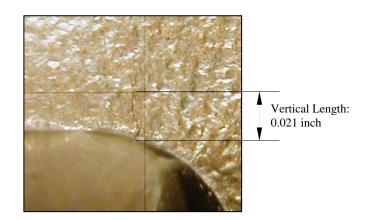|	
Targeted Crack Length (inch):	0.025
Actual Crack Length (inch):	0.026

Notes:
1. Testing was started at a maximum gross stress of 125 ksi or a max./min. load of 1000/100 lbs.
2. At 40,000 cycles, the maximum gross stress was increased to 130 ksi (max./min. load of 1040/104 lbs.).

Crack Growth Data

Cycles	Horizontal Crack Length, inch	Vertical Crack Length, inch	Calculated Crack Length, inch
42,864	0.009	0.009	0.013
44,500	0.010	0.011	0.015
48,500	0.014	0.016	0.021
49,500	0.020	0.017	0.026

Note: FTI visually measured the horizontal and vertical length of the crack using a DTM mounted to the test frame. The actual length of the crack was calculated using the Pythagorean theorem.

Horizontal Length: 0.020 inch

Vertical Length: 0.017 inch

CONSTANT AMPLITUDE TEST REPORT

Customer:	SAIC/ISU	**FTI Project Number:**	SO64875
Disk #, Tang Identification:	Disk 5, Tang A	**Frame:**	15
Specimen Type:	Engine Disk	**Crack Plane Orientation:**	N/A
Material:	Powder Nickel		

TEST CONDITIONS

Testing performed at ambient lab temperature and relative humidity

Temperature (°F):	70
Relative Humidity (%):	41

Tang Dimensions

Notch Depth (inch):	0.106
Width (inch):	0.077
Gross Area (inch^2):	0.008

Test Parameters

Maximum Gross Stress (ksi):	Various (see notes)
R-Ratio: (Min./Max. Stress):	+0.10
Maximum Load (lb):	Various (see notes)
Minimum Load (lb)	Various (see notes)
Test Frequency (Hz):	2

Final Crack Length

Targeted Crack Length (inch):	0.034
Actual Crack Length (inch):	0.036

Notes:
1. Testing was started at a maximum gross stress of 125 ksi or a max./min. load of 1020/102 lbs.
2. At 40,000 cycles, the maximum gross stress was increased to 130 ksi (max./min. load of 1061/106 lbs.).
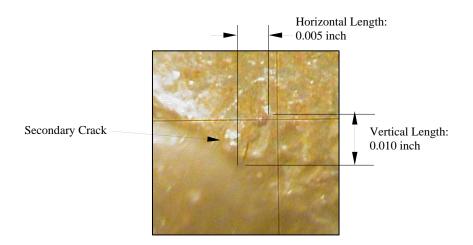
Crack Growth Data

Cycles	Horizontal Crack Length, inch	Vertical Crack Length, inch	Calculated Crack Length, inch
41,000	0.004	0.006	0.007
56,000	0.006	0.009	0.011
77,500	0.007	0.010	0.012
80,000	0.008	0.010	0.013
105,000	0.009	0.010	0.013
112,500	0.013	0.012	0.018
119,000	0.014	0.017	0.022
121,000	0.015	0.017	0.023
123,000	0.019	0.017	0.027
143,000	0.020	0.022	0.030
146,000	0.023	0.025	0.034
147,000	0.023	0.028	0.036

Note: FTI visually measured the horizontal and vertical length of the crack using a DTM mounted to the test frame. The actual length of the crack was calculated using the Pythagorean theorem.

Horizontal Length: 0.023 inch

Vertical Length: 0.028 inch

CONSTANT AMPLITUDE TEST REPORT

Customer:	SAIC/ISU	**FTI Project Number:**	SO64875
Disk #, Tang Identification:	Disk 5, Tang B	**Frame:**	15
Specimen Type:	Engine Disk	**Crack Plane Orientation:**	N/A
Material:	Powder Nickel		

TEST CONDITIONS

Testing performed at ambient lab temperature and relative humidity

Temperature (°F):	70
Relative Humidity (%):	42

Tang Dimensions

Notch Depth (inch):	0.107
Thickness (inch):	0.075
Gross Area (inch^2):	0.008

Test Parameters

Maximum Gross Stress (ksi):	Various (see notes)
R-Ratio: (Min./Max. Stress):	+0.10
Maximum Load (lb):	Various (see notes)
Minimum Load (lb)	Various (see notes)
Test Frequency (Hz):	2

Final Crack Length

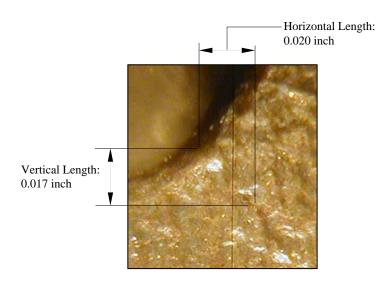|	
Targeted Crack Length (inch):	0.018
Actual Crack Length (inch):	0.017

Notes:
1. Testing was started at a maximum gross stress of 125 ksi or a max./min. load of 1020/102 lbs.
2. At 40,000 cycles, the maximum gross stress was increased to 130 ksi (max./min. load of 1061/106 lbs.).

Crack Growth Data

Cycles	Horizontal Crack Length, inch	Vertical Crack Length, inch	Calculated Crack Length, inch
46,087	0.008	0.015	0.017

Note: FTI visually measured the horizontal and vertical length of the crack using a DTM mounted to the test frame. The actual length of the crack was calculated using the Pythagorean theorem.

Vertical Length: 0.015 inch

Horizontal Length: 0.008 inch

Appendix C
Crack Length Measurements in TF33 Blades
(Note: All figures are included at the end of this report.
Figure 13 shows the terminology used for the crack length measurements. This figure is not
referenced in the report, but was added later for clarification.)

MML LOG NO.:	*12038*
PART NAME:	*Turbine Blade*
PART ID NO.:	*Blades 1 - 7*
PART S/N:	*N/A*
CUSTOMER PO:	*4400136017*
DATE:	*11/24/2006*

REQUESTED BY:	*Donna Mayton* *SAIC* *16701 West Bernardo Drive* *San Diego, California 92127*
COPIES TO:	*N/A*
WORK REQUESTED:	*See SAIC scope of work below.*
REPORTED BY:	*M. Poormon*
TESTED/ANALYZED BY:	*M. Poormon*

SUMMARY:

- See matrix below for comprehensive crack measurement data.

BACKGROUND:

Seven rejected jet engine turbine blades were sent to Martin MetLabs for crack length
documentation (see **Figure 1**). The cracked blades are to be used for the development of Sonic
IR test procedures. Crack locations (10 total) were pre-marked on each blade by SAIC. Close-
up macro photographs were captured of cracked regions (pressure and suction sides) on all
blades (see **Figure 2**). The SAIC scope of work was requested as follows.

- Replicate all pre-marked crack locations.
- Measure and record crack lengths from replications.
- Provide written report of all crack documentation.

RESULTS:

Cellulose acetate replications were taken from each of the pre-marked airfoil crack regions. Sequential 50X annotated microphotographs were captured of each crack in dark field mode and documented in the following figures.

- Blade #1   **Figure 3**
- Blade #2   **Figure 4**
- Blade #3   **Figure 5**
- Blade #4A   **Figure 6**
- Blade #4B   **Figure 7**
- Blade #5   **Figure 8**
- Blade #6   **Figure 9**
- Blade #7A   **Figure 10**
- Blade #7B   **Figure 11**
- Blade #7C   **Figure 12**

Crack measurements were subsequently performed using image analysis software and recorded in the following data matrix.

BLADE CRACK MEASUREMENTS				
Blade ID	*Crack ID*	*Crack Length Measurements (inches)*		
		PS (apparent)	LE / TE (apparent)	SS (apparent)
Blade #1	#1-LE	0.0400	0.0108	0.0000
Blade #2	#2-LE	0.1058	0.0588	0.0304
Blade #3	#3-TE	0.2903	0.0288	0.2280
Blade #4	#4A-TE	0.0793	0.0483	0.1875
	#4B-TE	0.2907	0.0000	0.0000
Blade #5	#5-TE	0.0935	0.0285	0.1129
Blade #6	#5-TE	0.0000	0.0139	0.0718
Blade #7	#7A-TE	0.2781	0.0289	0.2449
	#7B-TE	0.0962	0.0233	0.1321
	#7C-TE	0.1039	0.0280	0.0503

NOTE 1:   All measurements taken along transverse blade chord.

NOTE 2:   LE /TE crack measurements span approximately from PS radius tangent to SS radius tangent.

NOTE 3:   All PS and SS crack length measurements are apparent measurements (include LE / TE radius).
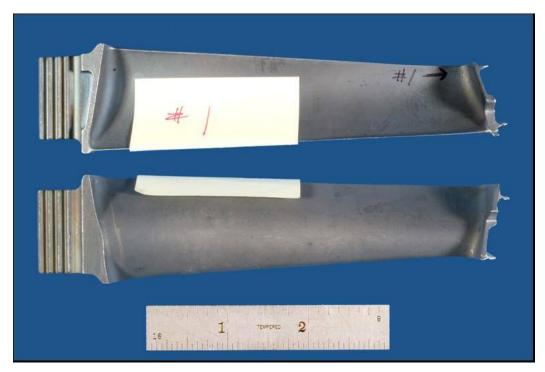
FIGURE 1a. Composite macro photograph of Turbine Blade #1 as received.

FIGURE 1b. Composite macro photograph of Turbine Blade #2 as received.
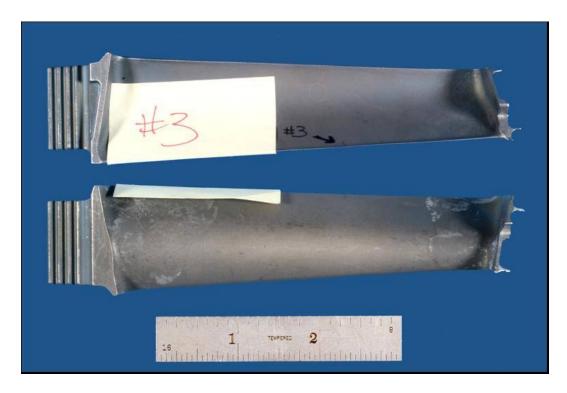
FIGURE 1c. Composite macro photograph of Turbine Blade #3 as received.
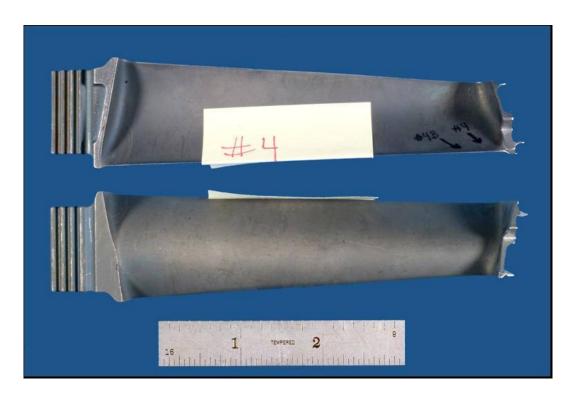
FIGURE 1d. Composite macro photograph of Turbine Blade #4 as received.

FIGURE 1e. Composite macro photograph of Turbine Blade #5 as received.
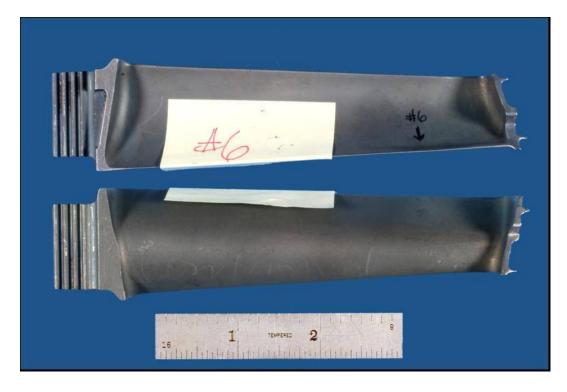
FIGURE 1f. Composite macro photograph of Turbine Blade #6 as received.
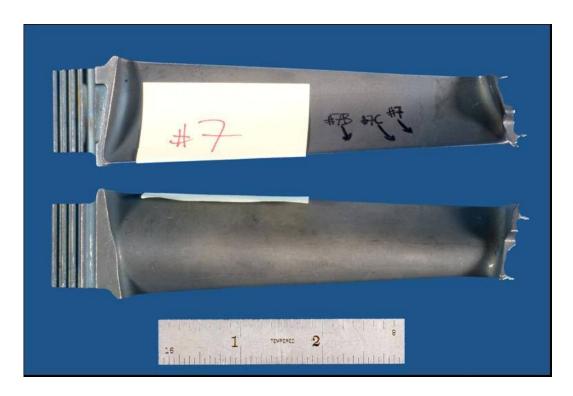
FIGURE 1g. Composite macro photograph of Turbine Blade #7 as received.
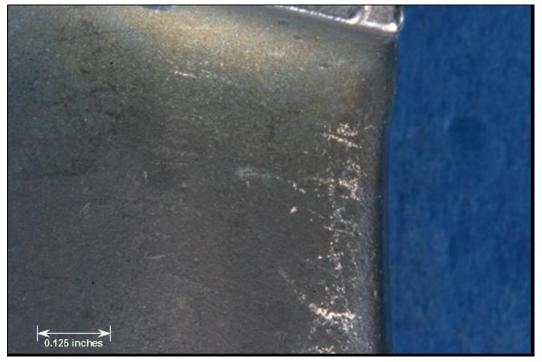
FIGURE 2a. *TOP:* Close-up macro photograph of Blade #1 (leading edge, pressure side) showing cracked airfoil location. *BOTTOM:* Close-up macro photograph of Blade #1 (leading edge, suction side) at same cracked vicinity.
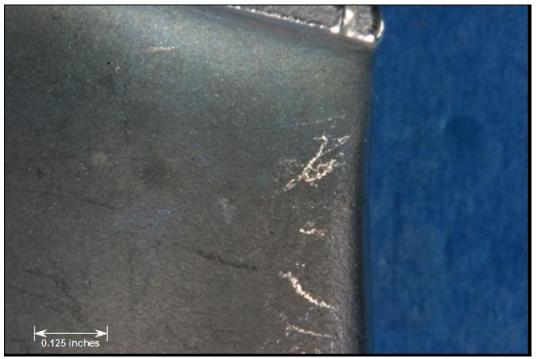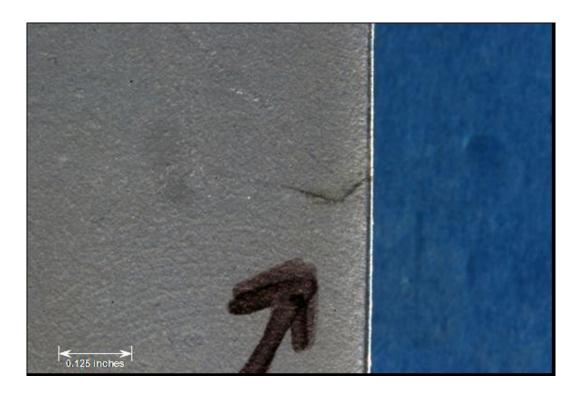
FIGURE 2b. *TOP:* Close-up macro photograph of Blade #2 (leading edge, pressure side) showing cracked airfoil location. *BOTTOM:* Close-up macro photograph of Blade #2 (leading edge, suction side) at same cracked vicinity.
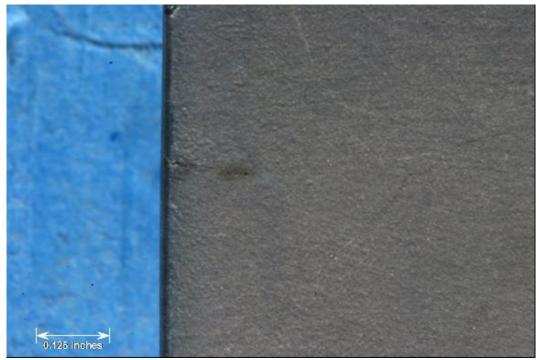
FIGURE 2c. *TOP:* Close-up macro photograph of Blade #3 (trailing edge, pressure side) showing cracked airfoil location. *BOTTOM:* Close-up macro photograph of Blade #3 (trailing edge, suction side) at same cracked vicinity.

FIGURE 2d. *TOP:* Close-up macro photograph of Blade #4 (trailing edge, pressure side) showingcracked airfoil location. *BOTTOM:* Close-up macro photograph of Blade #4 (trailing edge, suction side) at same cracked vicinity.
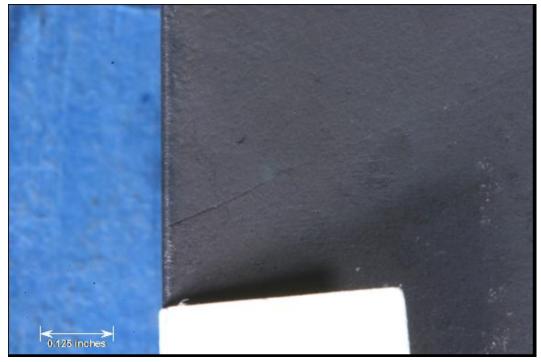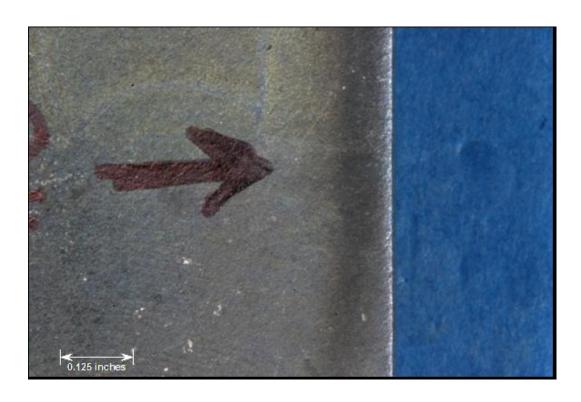
FIGURE 2e. *TOP:* Close-up macro photograph of Blade #5 (trailing edge, pressure side) showing cracked airfoil location. *BOTTOM:* Close-up macro photograph of Blade #5 (trailing edge, suction side) at same cracked vicinity.
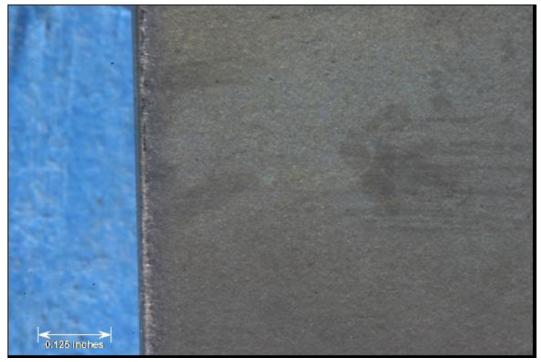
FIGURE 2f. *TOP:* Close-up macro photograph of Blade #6 (trailing edge, pressure side) showing cracked airfoil location. *BOTTOM:* Close-up macro photograph of Blade #6 (trailing edge, suction side) at same cracked vicinity.
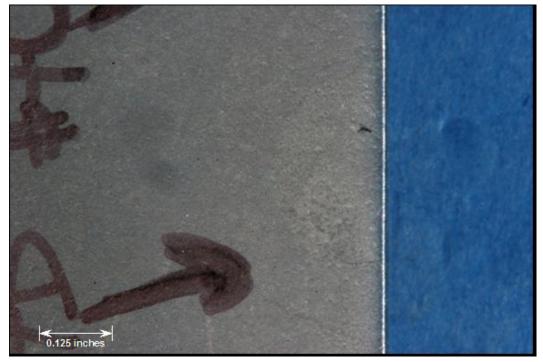
FIGURE 2g. *TOP:* Close-up macro photograph of Blade #7 (trailing edge, pressure side) showing cracked airfoil location. *BOTTOM:* Close-up macro photograph of Blade #7 (trailing edge, pressure side) showing cracked airfoil location.
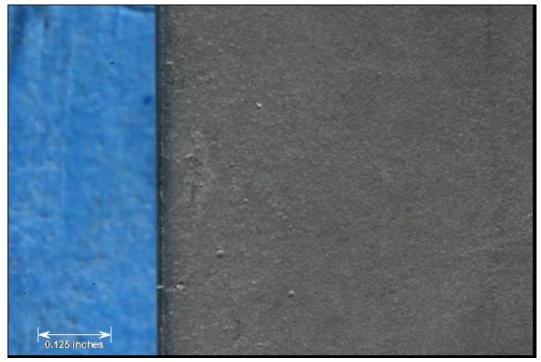
FIGURE 2h. *TOP:* Close-up macro photograph of Blade #7 (trailing edge, suction side) showing cracked airfoil location. *BOTTOM:* Close-up macro photograph of Blade #7 (trailing edge, suction side) showing cracked airfoil location.
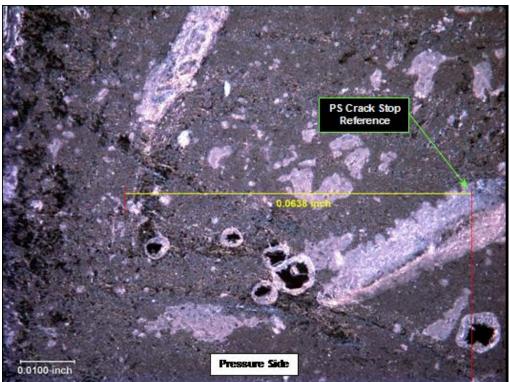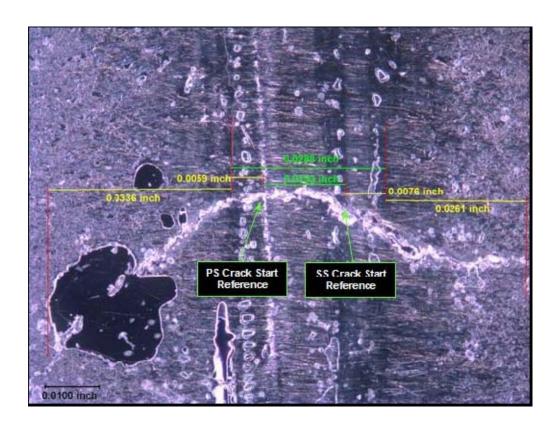
FIGURE 3. *TOP:* 50X microphotograph of Turbine Blade #1 replica (LE). *BOTTOM:* 50X microphotograph of Turbine Blade #1 replica (PS).

FIGURE 4. *TOP:* 50X microphotograph of Turbine Blade #2 replica (LE).
BOTTOM: 50X microphotograph of Turbine Blade #2 replica (PS).
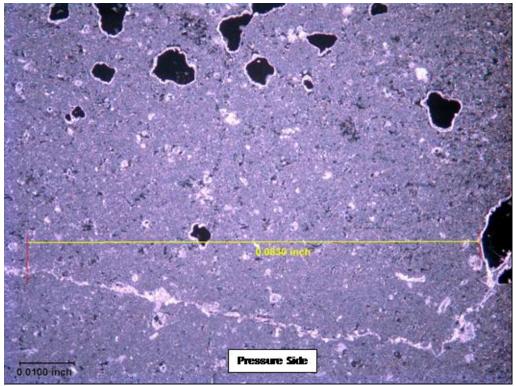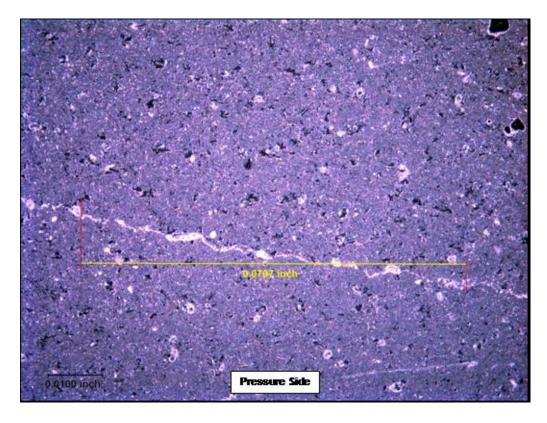
FIGURE 5a. *TOP:* 50X microphotograph of Turbine Blade #3 replica (TE). *BOTTOM:* 50X microphotograph of Turbine Blade #3 replica (PS, FOV 1).
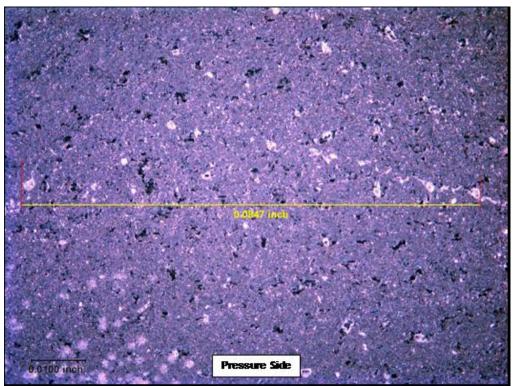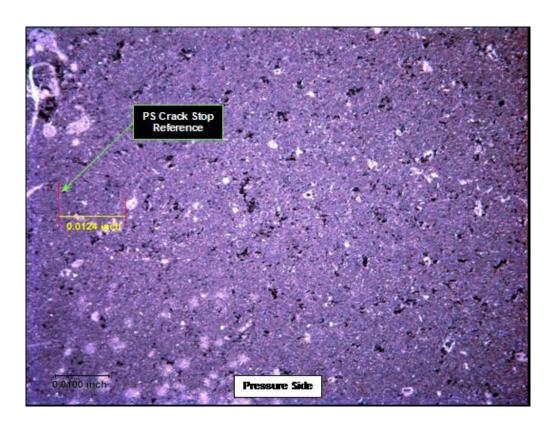
FIGURE 5b. *TOP:* 50X microphotograph of Turbine Blade #3 replica (PS, FOV 2). *BOTTOM:* 50X microphotograph of Turbine Blade #3 replica (PS, FOV 3).
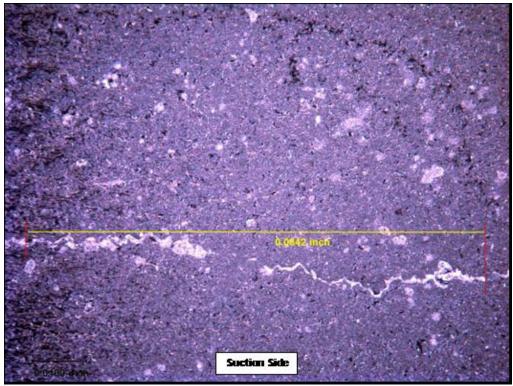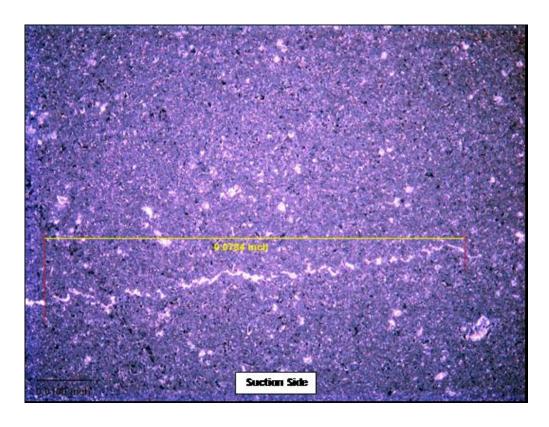
FIGURE 5c. *TOP:* 50X microphotograph of Turbine Blade #3 replica (PS, FOV 4). *BOTTOM:* 50X microphotograph of Turbine Blade #3 replica (SS, FOV 1).
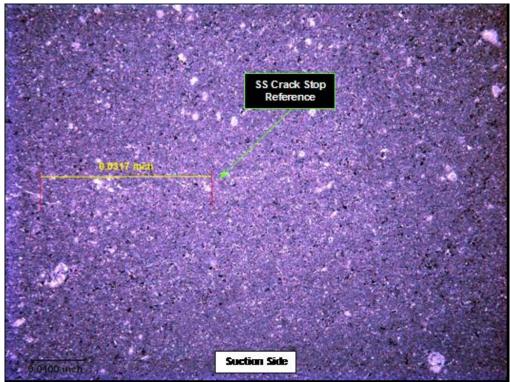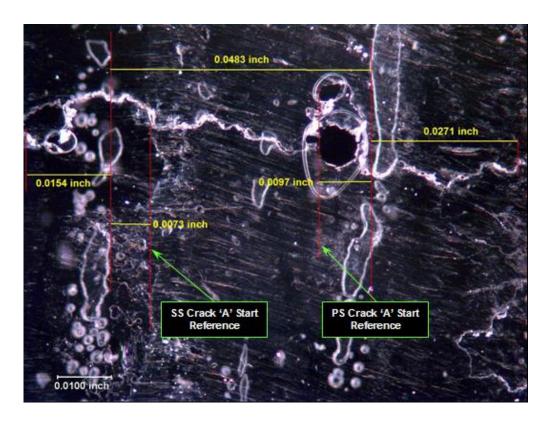
FIGURE 5d. *TOP:* 50X microphotograph of Turbine Blade #3 replica (SS, FOV 2). *BOTTOM:* 50X microphotograph of Turbine Blade #3 replica (SS, FOV 3).
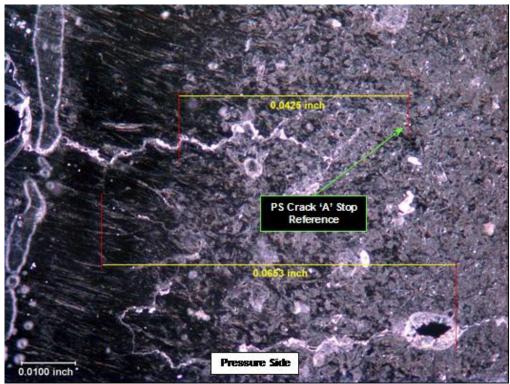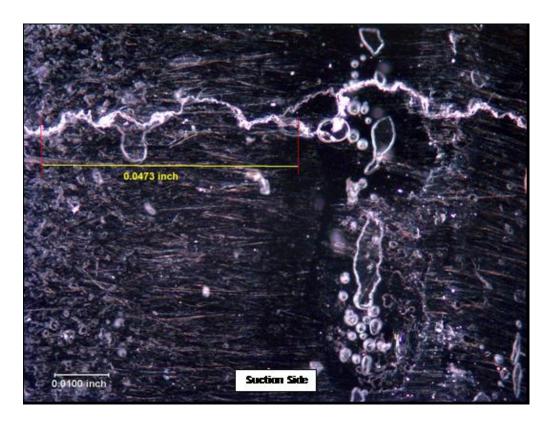
FIGURE 6a. *TOP:* 50X microphotograph of Turbine Blade #4A replica (TE).
BOTTOM: 50X microphotograph of Turbine Blade #4A replica (PS).
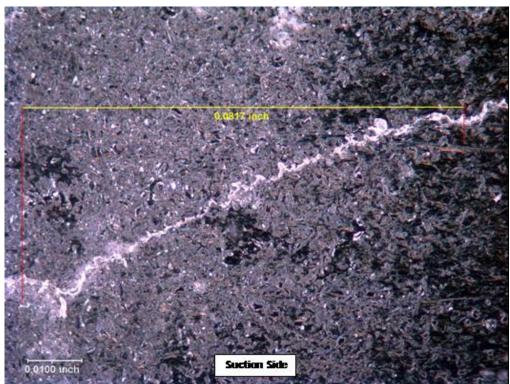
FIGURE 6b. *TOP:* 50X microphotograph of Turbine Blade #4A replica (SS, FOV 1). *BOTTOM:* 50X microphotograph of Turbine Blade #4A replica (SS, FOV 2).
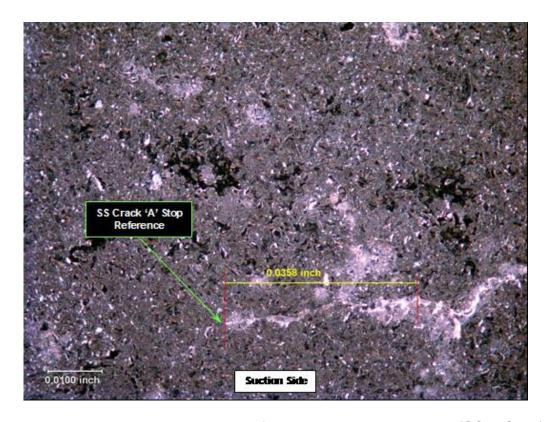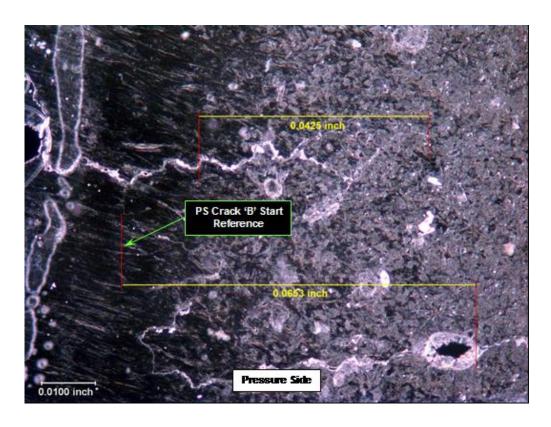
FIGURE 6c. 50X microphotograph of Turbine Blade #4A replica (SS, FOV 3).
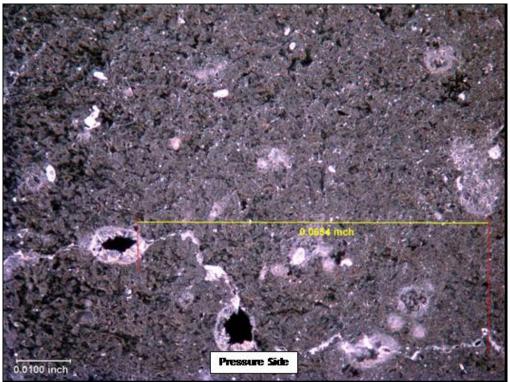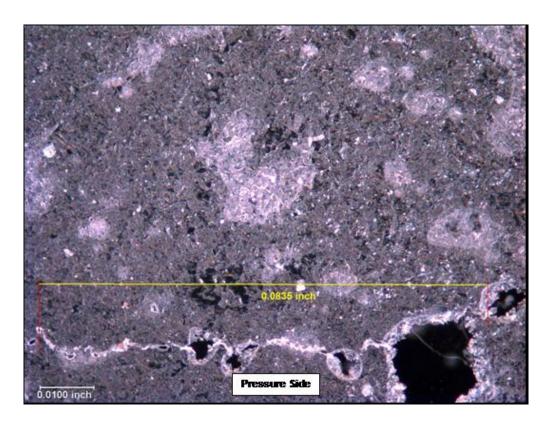
FIGURE 7a. *TOP:* 50X microphotograph of Turbine Blade #4B replica (PS, FOV 1). *BOTTOM:* 50X microphotograph of Turbine Blade #4B replica (PS, FOV 2).
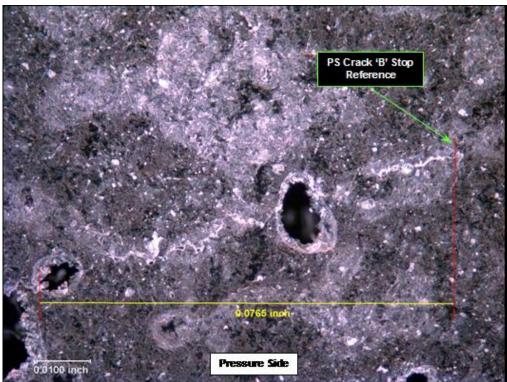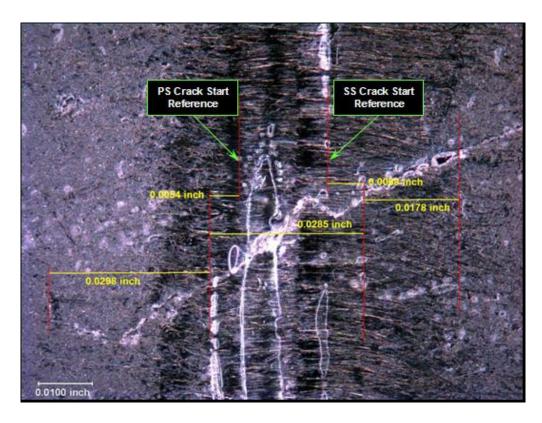
FIGURE 7b. *TOP:* 50X microphotograph of Turbine Blade #4B replica (PS, FOV 3). *BOTTOM:* 50X microphotograph of Turbine Blade #4B replica (PS, FOV 4).
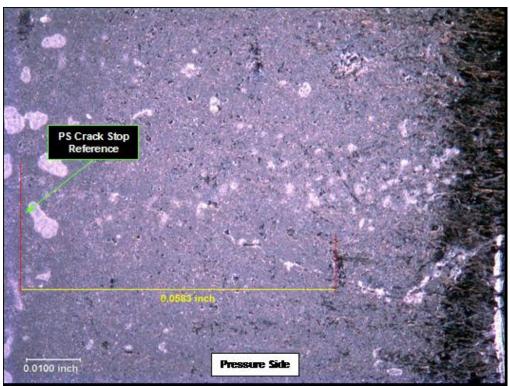
FIGURE 8a. *TOP:* 50X microphotograph of Turbine Blade #5 replica (TE).
BOTTOM: 50X microphotograph of Turbine Blade #5 replica (PS).
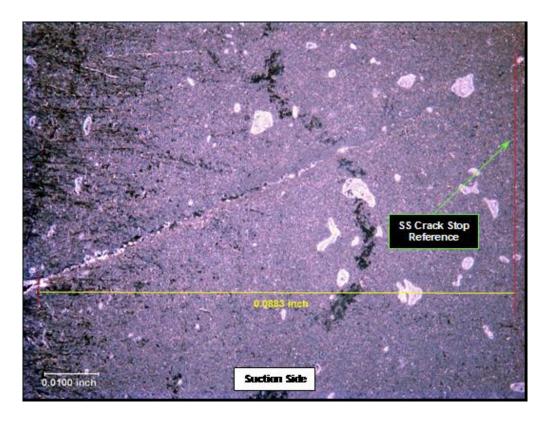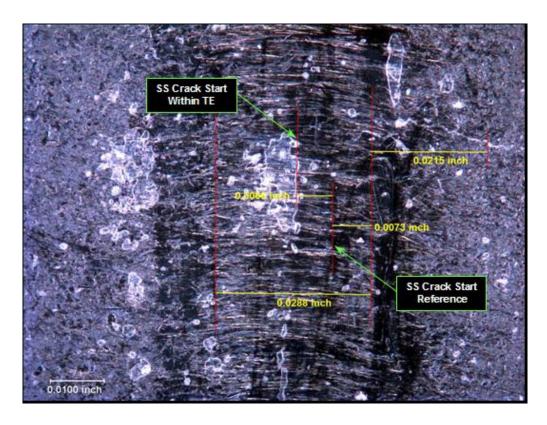
FIGURE 8b. 50X microphotograph of Turbine Blade #5 replica (SS).
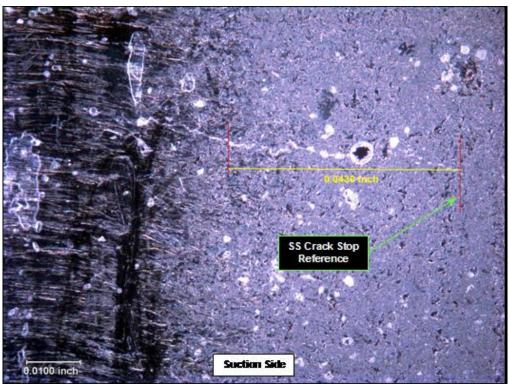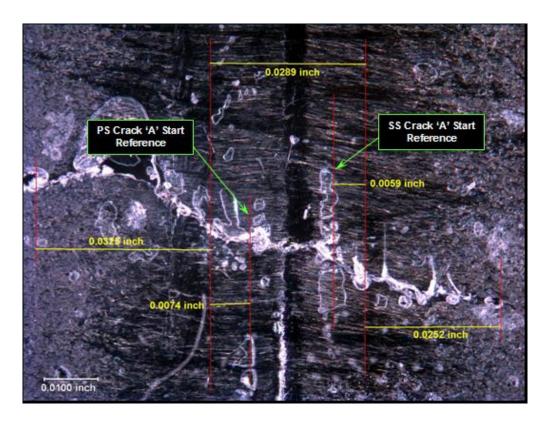
FIGURE 9. *TOP:* 50X microphotograph of Turbine Blade #6 replica (TE).
BOTTOM: 50X microphotograph of Turbine Blade #6 replica (SS).
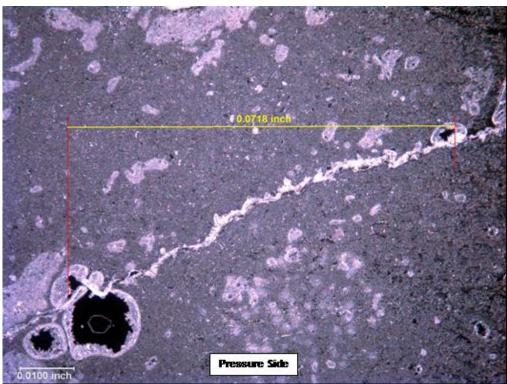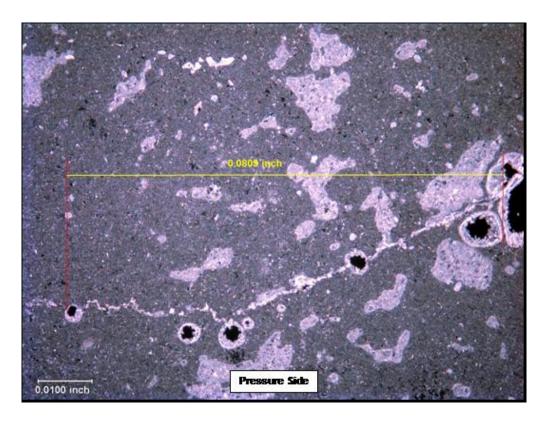
FIGURE 10a. *TOP:* 50X microphotograph of Turbine Blade #7A replica (TE). *BOTTOM:* 50X microphotograph of Turbine Blade #7A replica (PS, FOV 1).
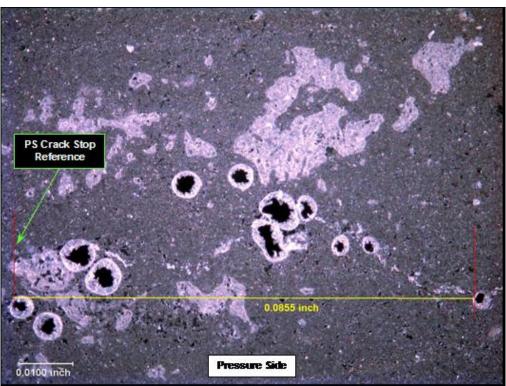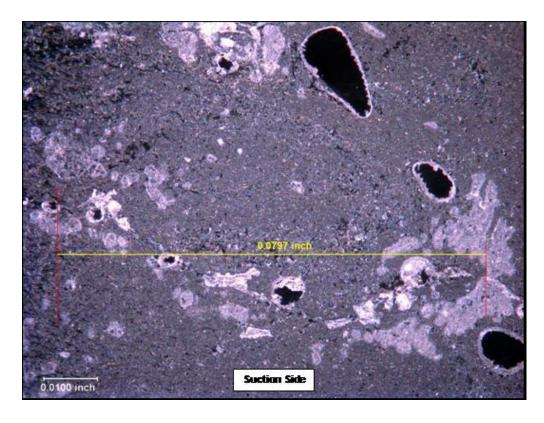
FIGURE 10b. *TOP:* 50X microphotograph of Turbine Blade #7A replica (PS, FOV 2). *BOTTOM:* 50X microphotograph of Turbine Blade #7A replica (PS, FOV 3).
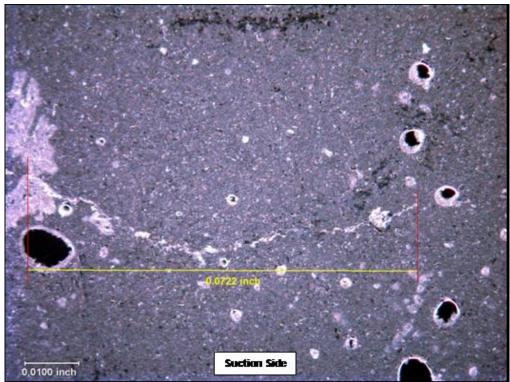
FIGURE 10c. *TOP:* 50X microphotograph of Turbine Blade #7A replica (SS, FOV 1). *BOTTOM:* 50X microphotograph of Turbine Blade #7A replica (SS, FOV 2).
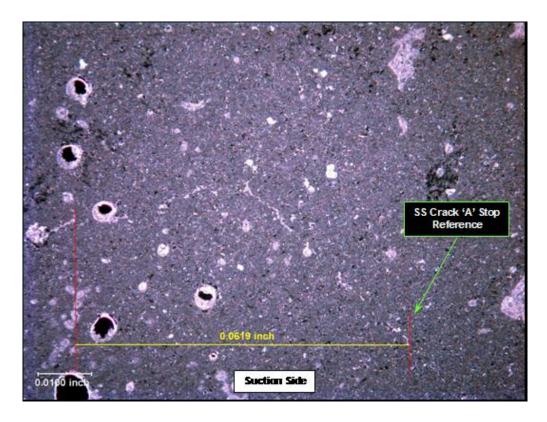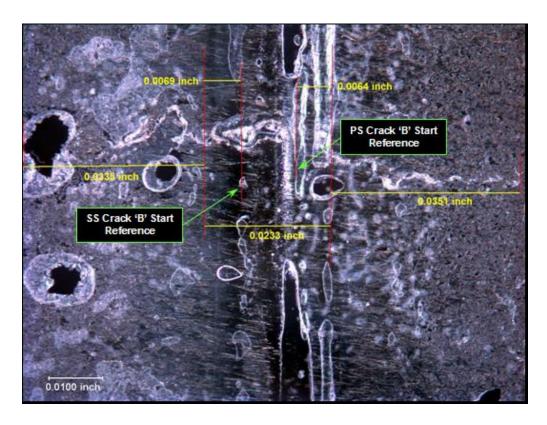
FIGURE 10d. 50X microphotograph of Turbine Blade #7A replica (SS, FOV 3).
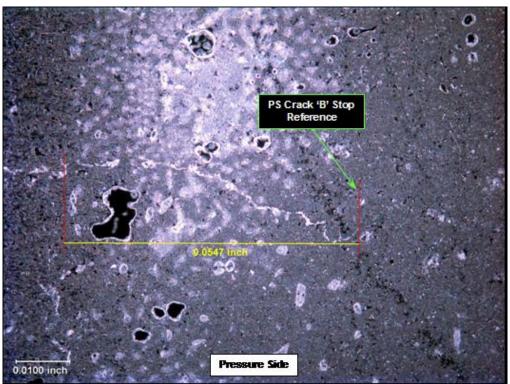
FIGURE 11a. *TOP:* 50X microphotograph of Turbine Blade #7B replica (TE).
BOTTOM: 50X microphotograph of Turbine Blade #7B replica (PS).
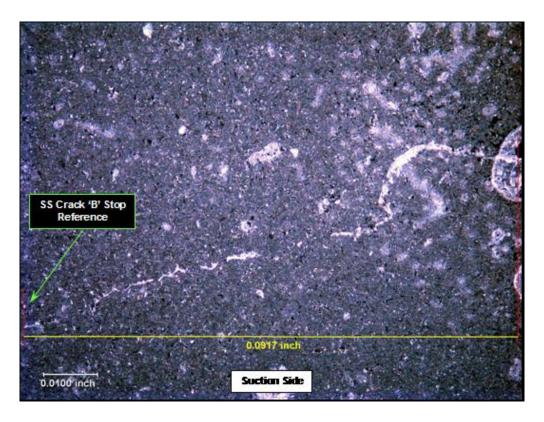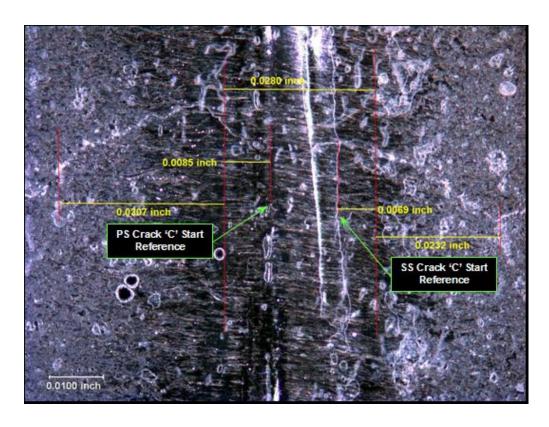
FIGURE 11b. 50X microphotograph of Turbine Blade #7B replica (SS).
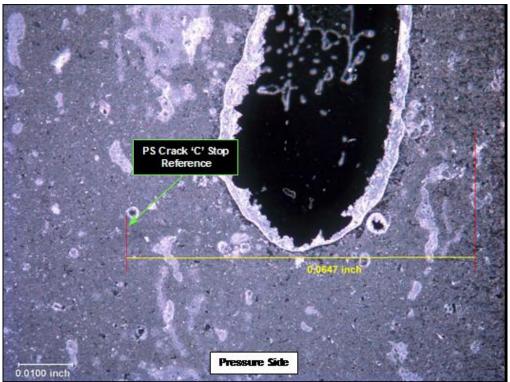
FIGURE 12a. *TOP:* 50X microphotograph of Turbine Blade #7C replica (TE).
BOTTOM: 50X microphotograph of Turbine Blade #7C replica (PS).
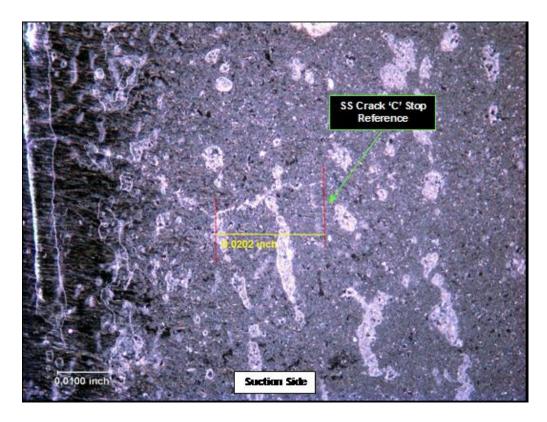
FIGURE 12b. 50X microphotograph of Turbine Blade #7C replica (SS).
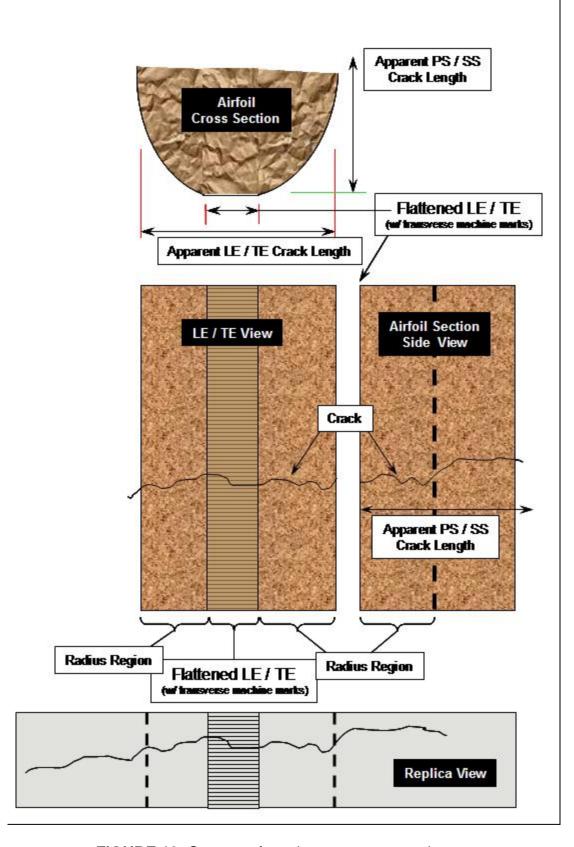
FIGURE 13. Cartoon of crack measurement scheme.

Appendix D
Preparation and Crack Development of Aluminum and Inco-718 Notched Plates

**Preparation and Crack Development of
Aluminum and Inco-718 EDM Notched Plates**

**Science Applications International Corporation (S.A.I.C)
16701 W. Bernado Drive
San Diego, CA 92127**

Attention: Donna Mayton

Purchase Order No.: 4400125566

Metcut Project No.: 4232-83041-1

JULY 24, 2006

<div style="border-top: 1px solid black;"></div>

Thomas E. Arnold, Manager	**Guy R. Johns**
Engineering	Test Engineer

J:\83041\35\reports\83041-1
Krh

Table of Contents

Project

At the request of Ms. Donna Mayton, Metcut Research, Inc. was contracted to perform machining operations and generate cracks in NDE Plate specimens of Inco-718 and 7056-T6 aluminum. The plate blanks were provided to Metcut. Metcut prepared the plate specimens as described in the statement of work and generated cracks to target lengths as required. A total of 28 plates were prepared and 24 were cracked.

The Inco-718 blanks were provided to Metcut in an annealed state so it was decided by Metcut and S.A.I.C. to solution treat and age the material in order to optimize the material characteristics for crack propagation behavior. Metcut performed this heat treatment in house following standard accepted procedures.

Specimen Preparation

Metcut prepared a total of 28 plate specimens, 14 of Inco-718 and 14 of 7075-T6 aluminum as directed by S.A.I.C. Two plates of each material were machined as spares. Each plate contained a single EDM starter notch precisely positioned at the location assigned by S.A.I.C. The majority of the EDM starter notches were placed on one flat surface of each specimen, and a few were placed onto the corners of the specimens. The corner notches were made by plunging an electrode into the corner of the plates such that the resulting surface length would be roughly .010 inches long and the depth of the notch would be roughly .010 inches deep. The surface notches were either .020" long x 0.10" deep or .010" long x .005" deep, depending on the assigned crack length target. All of the notches were oriented such that cracks would propagate from the notches parallel with the 2.0" dimension of the specimens. After fatigue cracks were developed onto the surfaces of the specimens, the notches were ground off the specimens using low stress grinding techniques, leaving only natural fatigue cracks in the plates.

Fatigue Crack Development

The crack development was performed using an MTS servo-hydraulic test frame in a 3-point bend mode of fatigue. The notched area of the plates was oriented directly under the load fulcrum such that the tensile moment would propagate the cracks as a function of elapsed cycles.

The span of the fixturing was held constant at 3.50 inches. The maximum stress used to initiate the cracks was held constant at 80 - 100 ksi for the Inco-718 plates and 30.0 – 40.0 ksi for the aluminum plates. The plates were cycled at a frequency of 10 Hz using a sinusoidal waveshape. The load ratio for cycling was held constant at $R = 0.10$.

Metcut cycled the specimens for prescribed cycle blocks based on the test operator's judgment. The crack length was measured after each cycle block using a linearly traveling Gaertner microscope. After the cracks were initiated from the EDM notches to their assigned target length or conservative lengths, the plates were sent to the shop to have the notches removed by low stress grinding. Many of the plates were completed at this point and no further crack development was necessary. Others had to have the crack extended by 3-point bend fatigue. Some of the plates had to be sent to the shop to have additional material removed in order to remove some of the starter notch that still remained in the plates.

Project Completion

All of the final crack lengths provided within this report are based on surface measurements only. Metcut can make no estimates or measurements of the crack depths for any specimen. The individual data sheets for each specimen are included in this report.
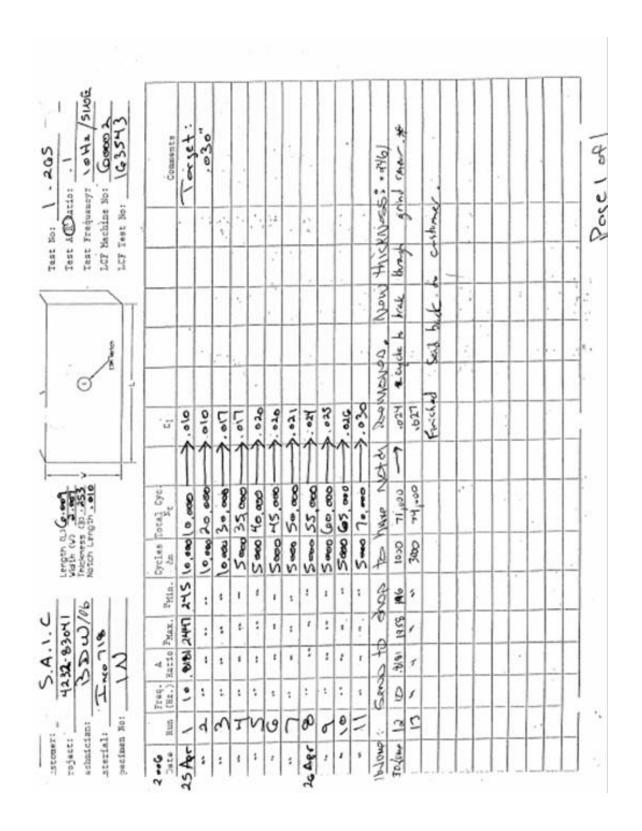
FINAL CRACK LENGTH SUMMARY

FOR INCO 718 PLATES
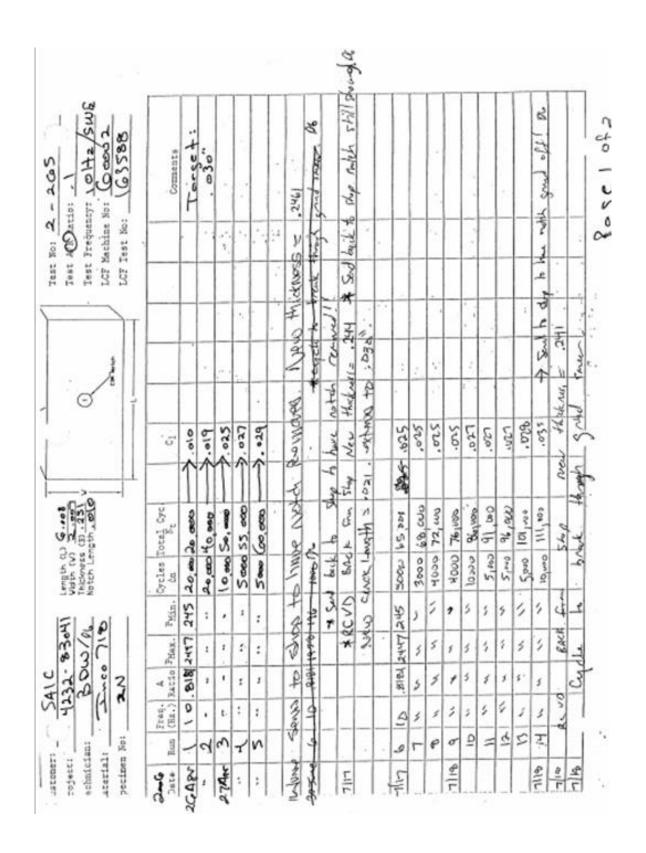
Max. Stress: 90 – 100 ksi			Load Ratio (R): 0.10	
Frequency: 10 Hz			Fixture Span: 3.50 inches	
Waveshape: Sinusoidal			Test Temperature: 75°F	
Specimen	Crack **Type**	**Total Fatigue Cycles**	**Final Crack Length (inches)**	
1N	Surface	74,000	.027	
2N	Surface	113,000	.036	
3N	Surface	100,000	.029	
4N	Surface	106,000	.029	
5N	Surface	104,400	.258	
6N	Surface	105,500	.249	
7N	Surface	129,400	.249	
8N	Surface	120,500	.248	
9N	Corner	192,600	.027	
10N	Corner	161,723	.027	
11N	Corner	170,500	.029	
12N	Corner	203,500	.028	
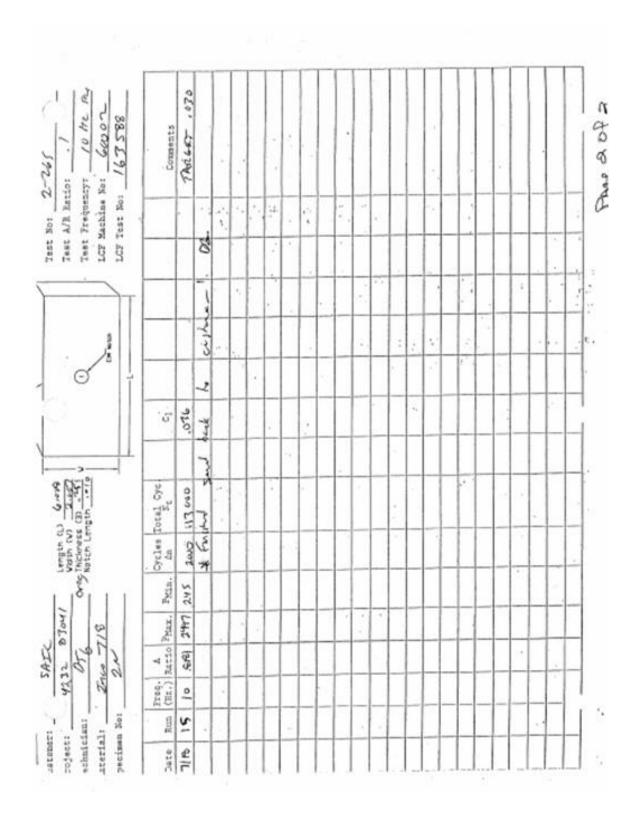
FINAL CRACK LENGTH SUMMARY

FOR 7075-T6 ALUMINUM PLATES
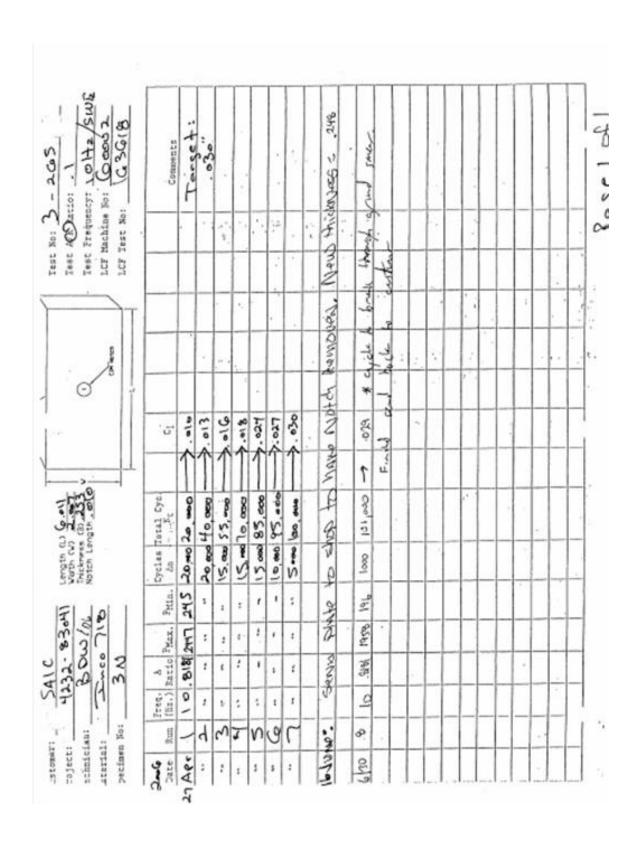
Max. Stress: 30 – 40 ksi			Load Ratio (R): 0.10
Frequency: 10 Hz			*Fixture Span: 3.50 inches*
Waveshape: Sinusoidal			*Test Temperature: 75°F*
Specimen	Crack **Type**	**Total Fatigue Cycles**	**Final Crack Length (inches)**
1A	Surface	32,250	.027
2A	Surface	33,750	.028
3A	Surface	28,000	.030
4A	Surface	25,250	.028
5A	Surface	25,250	.295
6A	Surface	23,850	.247
7A	Surface	26,600	.249
8A	Surface	25,350	.249
9A	Corner	85,200	.029
10A	Corner	56,400	.028
11A	Corner	129,200	.029
12A	Corner	88,400	.037
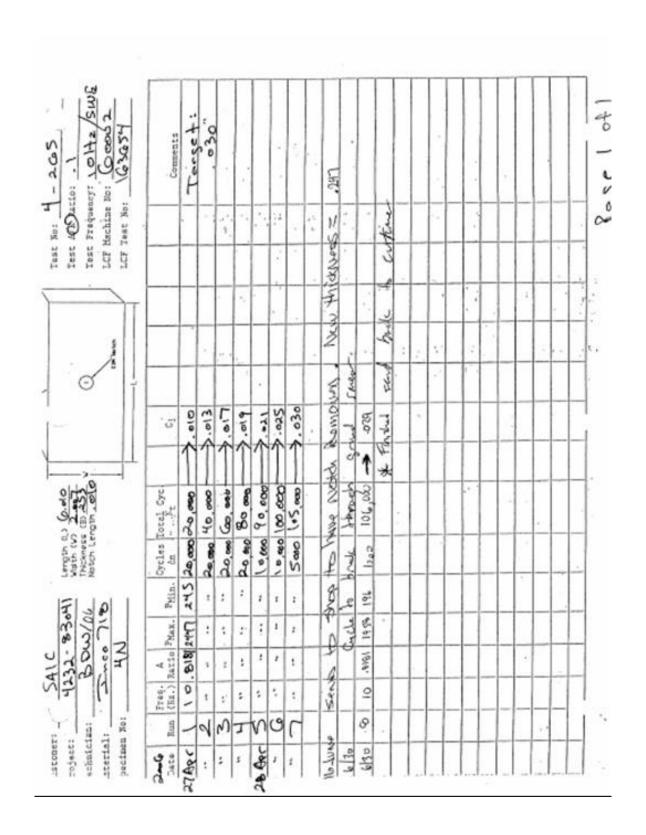
Appendix A
RAW DATA SHEETS

Customer: S.A.I.C

Project: 4232-83041

Technician: 3DW/lb

Material: Inco 718

Specimen No: ___

Test No: 1-205

Test A/B ratio: .1

Test Frequency: 10 Hz / 5 ksi

LCF Machine No: Good 2

LCF Test No: 1G3543

Length (L): 6.00
Width (W): 1.00
Thickness (B): .253
Notch Length: .010

Target: .030"

2006 Date	Run	Freq. (Hz.)	A Ratio	Pmax.	Pmin.	Cycles Δn	Total Cyc Σc	c_i	Comments
25 Apr	1	10	.0181	2447	245	10,000	10,000	.010	
"	2	"	"	"	"	10,000	20,000	.010	
"	3	"	"	"	"	10,000	30,000	.017	
"	4	"	"	"	"	5,000	35,000	.017	
"	5	"	"	"	"	5,000	40,000	.020	
"	6	"	"	"	"	5,000	45,000	.020	
"	7	"	"	"	"	5,000	50,000	.021	
26 Apr	8	"	"	"	"	5,000	55,000	.024	
"	9	"	"	"	"	5,000	60,000	.025	
"	10	"	"	"	"	5,000	65,000	.026	
"	11	"	"	"	"	5,000	70,000	.030	Removed, New thickness: .246
1b/ow Today	12	10	.9/91	1355	146	1020	71,000	.024	# cycle to break through grind over #
	13	"	"	"	"	300	74,000	.027	Finished Sent back to customer.

Page 1 of 1

Tester: —
Project: 4232-8304
Technician: BDW/RG
Material: Inco 718
Specimen No: 2N

Length (L) 6 ref
Width (W) 2 _
Thickness (B) .25?
Notch Length .010

Test No: 2 - 205
Test Ratio: -1
Test Frequency: 10 Hz/SWE
LCF Machine No: Good 2
LCF Test No: (63588)

Date	Run	Freq. (Hz.)	A Ratio	Pmax.	Pmin.	Cycles on	Total Cyc P_t	c_i	Comments
26 Apr	1	10	.818	2447	245	20,000	20,000	→.010	Target: .030"
"	2	"	"	"	"	20,000	40,000	→.019	
27 Apr	3	"	"	"	"	10,000	50,000	→.025	
"	4	"	"	"	"	5,000	55,000	→.027	
"	5	"	"	"	"	5,000	60,000	→.029	
Where som to stop to		to	larger notch Romans						New thickness = .246
6 10									length to break thay gund nodes %
			✱ Sul back to	stop h have notch crew!!					
7/17		✱ RCVD				Back Fan Thy New thickness = .244			✱ Sul back to stop notch still though a
		Now crack length = .021							within to .038"
7/17	6	10	.818	2447	245	5000	65,304	.625	
	7	5	5	5	2	3000	68,000	.025	
	8	5	5	5	"	4000	72,000	.025	
7/18	9	5	5	5	✱	4000	76,000	.015	
	10	5	5	5	5	10,000	86,000	.027	
	11	5	5	5	5	5,000	91,000	.007	
	12	5	5	5	5	5,000	96,000	.020	
	13	5	5	5	"	5,000	101,000	.028	
7/18	14	As no	5	5	5	10,000	111,000	.035	→ Sul h dry h h w with grind off! R
7/18		Back from				stop		new thickness = .241	
7/18		Cyclic	h			back though		Sched Remove	

Page 1 of 2

Customer: _____

Project: 4232 BJ041
Technician: 056
Material: Zhao 7/8
Specimen No: 2~

Length (L) 6.058
Width (W) 2.060
Orig Thickness (B) .251
Notch Length .018

Test No: 2-245
Test A/R Ratio: 1
Test Frequency: 10 Hz Py
LCF Machine No: 66002
LCF Test No: 163588

Date	Run	Freq. (Hz.)	A Ratio	Pmax	Pmin	Cycles Δn	Total Cyc ΣN	c_i	Comments
7/10	15	10	.881	2447	245	2005	113,040	.076	Project .070
						* Finished		to center	0~
						saw back			

Customer: SAIC
Project: 4232-8304
Technician: BDW/DW
Material: Inco 718
Specimen No: 3N

Test No: 3-205
Test A/N Ratio: .1
Test Frequency: 1.0 Hz/SWE
LCF Machine No: Good 2
LCF Test No: G3G18

Length (L): 6.01
Width (W): 2.533
Thickness (B): .233
Notch Length: .010

Date	Run	Freq. (Hz.)	& Ratio	Pmax.	Pmin.	Cycles Δn	Total Cyc ΣPc	c_i	Comments
27 Apr	1	1.0	.818	2447	245	20,000	20,000	→ .010	Target: .030"
"	2	"	"	"	"	20,000	40,000	→ .013	
"	3	"	"	"	"	15,000	55,000	→ .016	
"	4	"	"	"	"	15,000	70,000	→ .018	
"	5	"	"	"	"	15,000	85,000	→ .021	
"	6	"	"	"	"	10,000	95,000	→ .027	
"	7	"	"	"	"	5,000	100,000	→ .030	
6/30/06:			Servo Plate to shop to have Notch removed. New thickness = .248						
6/30	9	12	.591	1958	196	1000	131,000	→ .029 Final	# cycle to break through grind marks. cut hole to center

Page 1 of 1

Customer: SAIC
Project: 1232-83041
Technician: BDW/DL
Material: Inco 718
Specimen No: 4N

Length (L): 6.040
Width (W): 2.483
Thickness (B): .253
Notch Length: .010

Test No: 4-265
Test A@Ratio: .1
Test Frequency: 10Hz/SWE
LCF Machine No: Groove 2
LCF Test No: 163054

Date	Run Num	Freq. (Hz.)	A Ratio	P Max.	P Min.	Cycles dn	Total Cyc ...t	c_i	Comments
27 Apr	1	10	0.818	2447	245	20,000	20,000	→ .010	Target: .030"
"	2	:	:	:	:	20,000	40,000	→ .013	
"	3	:	:	:	:	20,000	60,000	→ .017	
"	4	:	:	:	:	20,000	80,000	→ .019	
28 Apr	5	:	:	:	:	10,000	90,000	→ .21	
"	6	:	:	:	:	10,000	100,000	→ .025	
"	7	:	:	:	:	5,000	105,000	→ .030	
No lunge 6/30							Send to Drop to Wire Notch Removal, New Thickness = .247 Cycle to back through actual stress			
6/30	0	10	.848	1458	191	1,212	106,000 → .089		
							※ Finish and hole to continue		

212

Customer: _____ SAIC

Project: 4232-8304

Technician: BDW/PL

Material: Inco 718

Specimen No: SN

Length (L): 6.016
Width (W): 2.003
Thickness (B): .251
Notch Length: .020

Test No: S-205

Test A Ratio: -1

Test Frequency: 10 Hz / SWG

LCF Machine No: G00012

LCF Test No: 163656

Date	Run	Freq (Hz)	A Ratio	Pmax	Pmin	Cycles dn	Total Cyc ΣN_i	c_i	Comments
28 Apr	1	10	0.818	2447	245	20,000	20,000	→ .026	Target: 250
"	2	"	"	"	"	20,000	40,000	→ .035	
"	3	"	"	"	"	10,000	50,000	→ .044	
"	4	"	"	"	"	10,000	60,000	→ .057	
"	5	"	"	"	"	10,000	70,000	→ .07	
"	6	"	"	"	"	5000	75,000	→ .091	
"	7	"	"	"	"	5000	80,000	→ .111	
"	8	"	"	"	"	5000	85,000	→ .132	
"	9	"	"	"	"	5000	90,000	→ .156	
"	10	"	"	"	"	5000	95,000	→ .188	
"	11	"	"	"	"	5000	100,000	→ .222	
"	12	"	"	"	"	1000	101,000	→ .230	
"	13	"	"	"	"	800	101,800	→ .238	
"	14	"	"	"	"	600	102,400	→ .245	
"	15	"	"	"	"	400	102,800	→ .245	
"	16	"	"	"	"	400	103,200	→ .246	
"	17	"	"	"	"	200	103,400	→ .248	

Unable Sent to stop to have notch removed. New thickness = .243

* Cycle to break through ground surface

| 6/10 | 18 | 10 | 601 | 1956 | 196 | 1000 | 104,400 | → .250 | Finished Run 1 to contract .Pt. |

Page 1

Requestor: –
Project: –
Technician: SAIC 4232-83041 / B.Dw/06 / Inco 718
Material:
Specimen No: GN

Length (L): 6 in
Width (W): .024
Thickness (B): .251
Notch Length: .010

Test No: 6-205
Test A@Ratio: -1
Test Frequency: 10 Hz /SWE
LCF Machine No: G0002 /2
LCF Test No: G3705

Date	Run	Freq. (Hz)	A Ratio	Pmax	Pmin	Cycles On	Total Cyc $\sum n_t$	c_i	Comments
28 Apr / 1 May	1	10	.818	2447	245	20,000	20,000	.020	Target: .250"
"	2	"	"	"	"	20,000	40,000	.035	
"	3	"	"	"	"	20,000	60,000	.053	
"	4	"	"	"	"	10,000	70,000	.075	
"	5	"	"	"	"	10,000	80,000	.104	
"	6	"	"	"	"	5,000	85,000	.128	
"	7	"	"	"	"	5,000	90,000	.150	
"	8	"	"	"	"	5,000	95,000	.179	
"	9	"	"	"	"	5,000	100,000	.211	
"	10	"	"	"	"	1,000	101,000	.218	
"	11	"	"	"	"	1,000	102,000	.227	
"	12	"	"	"	"	1,000	103,000	.238	
"	13	"	"	"	"	500	103,500	.237	
"	14	"	"	"	"	500	104,000	.242	
"	15	"	"	"	"	500	104,500	.248	
16 Jun		Bent to GND to have NOTCH Removed. New thickness = .244						→ .249	*cycle to break through grind smear. End to failure
6/30	16	10	.384	1458	196	1000	105,500	* Finished	

Page 1 of 1

Customer: SAIC
Project: 4232-8304l
Technician: B Dw/?
Material: Inco 718
Specimen No: 72

Length (L): 6.011
Width (W): 2.005
Thickness (B): .256
Notch Length: .020

Date	Run	Freq. (Hz.)	A Ratio	Pmax.	Pmin.	Cycles (n)	Total Cyc. (...Rt)	c_i	Comments
1 May	1	1	0.818	2417	245	3,000	30,000 →	.029	Target: .250"
"	2	"	"	"	"	30,000	60,000 →	.049	
2 May	3	"	"	"	"	20,000	80,000 →	.045	
(done)			Began Spike to stop #/cycle to break through grind & stone #				Very Notch Removal. New thickness = .244		
7/3	4	10	.881	1959	196	1000	81,000 →	.09?	
	5	10	.892	1959	196	5000	86,000 →	.104	
	6	10	.891	1450	196	10,000	96,000 →	.123	
	7	10	.891	1959	196	10,000	106,000 →	.149	
	8	10	.891	1959	196	12,000	118,000 →	.195	
7/5	9	10	.891	1959	196	6000	124,000 →	.223	
	10	10	.891	1959	196	3500	127,500 →	.240	
	11	10	.901	1998	196	1000	128,500 →	.244	
	12	10	.891	1908	196	900	129,400 →	.244	
						✳ Finished test	back to customer. #s		

215

Customer: ___

Project: ___ SAIC 4232-83041

Technician: 2000 b756 Inco 718

Material: BN

Specimen No: ___

Test No: 08 - 265
Test A/R Ratio: 1
Test Frequency: 10 Hz/sine
LCF Machine No: 60062
LCF Test No: 164562

Length (L): 6.004
Width (W): 2.383
Thickness (B): .251
Notch Length: .020

2006 Date	Run	Freq. (Hz.)	A Ratio	Pmax.	Pmin.	Cycles On	Total Cyc	c_i	Comments
5/31	0	10	0.818	2447	245	0	0	→ .020 notch	Target: .250"
5/31	1	10	.818	2447	245	10,000	10,000	.020	
	2	10	.818	2447	245	10,000	20,000	.020	
	3	"	"	"	"	10,000	30,000	.027	
	4	"	"	"	"	10,000	40,000	.039	
	5	"	"	"	"	20,000	60,000	.070	
6/1	6	"	"	"	"	10,000	70,000	.099	
					1 cycle to break	Stop & SENT & done to have notch good off 11. New thickness .243 good through bream
7/5	7	10	.840	1950	196	1000	71,000	→ .096	
7/5	8	10	.840	1950	196	10,000	81,000	→ .110	
	9	10	.840	1950	196	15,000	96,000	.146	
	10	10	.840	1950	196	15,000	111,000	.202	
	11	10	.840	1950	196	5,000	116,000	.225	
7/6	12	10	.840	1950	196	2500	118,500	.229	
	13	10	.840	1950	196	1000	119,500	.241	
	14	10	"	—	"	1000	120,500	.248	* Finished send back to customer/QA

Customer: -
Project: SAIC 4232-8304
Technician: Brow M16
Material: Inco 718
Specimen No: 9N

Length (L) 6.008
Width (W) 1.0005
Thickness (B) .25x
Notch Length .040

Test No: 9-205
Test 4(#) Ratio: -1
Test Frequency: 10 Hz/SWE
LCF Machine No: 0002
LCF Test No: 164768

Date	Run	Freq (Hz)	Ratio	A	Pmax	Pmin	Cycles Δn	Total Cyc Σn=ΣΔn	c_i	Comments
6/1	0	1	0	.818	2447	245	0	0	→.040 .009	Target: .030" (.015 ±.05)
	1	10	.910	.910	2447	245	10,000	10,000	.009	
	2	10	.910	.910	2447	245	5000	15,000	.008	
	3	10	.910	.910	2447	245	5000	20,000	.006	
6/2	4	10	.910	.910	2447	245	5000	25,000	.008	
	5	10	.910	.910	2447	245	5000	30,000	.008	
	6	10	.910	.910	2447	245	5000	35,000	.007	
	7	10	.910	.910	2447	245	5005	40,005	.008	
	8	10	.910	.910	2447	245	5000	45,005	.008	
	9	10	.910	.910	2447	245	5000	50,005	.008	
6/3	10	10	.910	.910	2447	245	2000	52,005	.008	※ Specimen fell off grip, no teeth, no damage!
	11	10	.910	.910	2447	245	5000	57,005	.008	
	12	10	.910	.910	2447	245	5000	62,100	.008	
	13	10	.910	.910	2447	245	5000	67,100	.008	
	14	10	.910	.910	2447	245	5000	72,100	.008	
6/5	15	10	.910	.910	2447	245	10,000	82,100	.010	
	16	10	.910	.910	2447	245	10,000	92,100	.010	
	17	10	.910	.910	2447	245	10,000	102,100	.010	
	18	10	.910	.910	2447	245	10,000	112,100	.013	
	19	10	.910	.910	2447	245	5005	122,100	.014 .014	
9/9	20	4	.910	.910	2447	245	5005	127,100	.010	
	21	10	.910	.910	2447	245	10,000	177,100	.014	
	22	10	.910	.910	2447	245	10,500	187,600	.010	

Customer:
Project:
Technician:
Material: Inco 718
Specimen No: 9N

CA-C
4272 - 67041
056
Inco 718
9N

Length (L) 6.028
Width (V) 2.035
Thickness (B) .234
Notch Length n/a

Test No: 9-265
Test A@ Ratio: 1
Test Frequency: 10 hz/sec
LCF Machine No: 60023
LCF Test No: 164766

Date	Run	Freq. (Hz.)	A Ratio	Pmax.	Pmin.	Cycles Δn	Total Cyc. Σ_t	c_i	Comments
6/6	23	10	.8181	2047	245	10,000	157,100	.017	
	24	10	.8181	2047	245	10,000	167,100	.020	
	25	10	.8181	2047	245	10,000	177,100	.024	
	26	10	.8181	2047	245	5,000	182,100	.025	
6/7	27	10	.8181	2047	245	10,000	192,100	.030	No loose # seal to chip b two notch grind off. New thickness = .249
7/6		*		Cycle to break					through grind screw .021
7/6	28	10	.8181	1498	146	500	192,600		* Forgot Rsu back to customer - No

DADE 2 of 2

Customer: -
Project: SAIC
            4232-83041
Technician: 3800 DS6
Material: Inco 718
Specimen No: (●N)

Length (L) 6.005
Width (W) 2.005
Thickness (B) .25N
Notch Length .10

Date	Run	Freq. (Hz.)	A Ratio	Pmax.	Pmin.	Cycles Δn	Total Cyc $n = N_2$	c_i		Comments
6/7	8	1	0.818	2447	245	0	0	→ .010		Target: .030 (.015+.015)
	1	10	.9191	2447	245	25000	25,000	.010		
	2	10	.9191	2447	245	25000	50,000	.016		
6/8	3	10	.9191	2447	245	25000	75,000	.010→ .010		
	4	10	.9191	2447	245	25000	100,000	.010		
6/9	5	10	.9191	2447	245	6227	106,227	.015		*specimen felt off post *No damage to specimen
	6	10	.9191	2447	245	10,000	116,227	.017		
	7	10	.9191	2447	245	15,000	131,227	.018		
	8	10	.9191	2447	245	20,000	151,227	.034		
	9	10	.9191	2447	245	10,000	161,227	.035		
						16 June	* Sw'd to stop to have notch spad off for the z = .249			
7/6						* Cycle to break through grind sample			
2/6	10	10	.9191	2447	246	500	161,727	.027		* Specimen very separated threaded crack * finished and back to system ... A

Engineer: ___
Project: SAIC 4232-8304
Technician: 2-000-072
Material: Inco 718
Specimen No: 112

Length (L) 6 in/a
Width (w)
Thickness (t)
Notch Length .010

Test No: 11-205
Test A(R)atio: -1
Test Frequency: 10 Hz/SWG
LCF Machine No: C-00-2
LCF Test No: 164 924

Date	Run	Freq. (Hz.)	A Ratio	Pmax.	Pmin.	Cycles Δn	Total Cyc Σt	c_i	Comments
6/9	1	10	0.818	2447	245	0	0	→.010	Target: .030 (.015 ±.015)
6/12	1	10	.818	2447	245	25000	25000	.010	
	2	10	.818	2447	245	25000	50,000	.010	
6/13	3	10	.818	2447	243	20,000	70,000	.011	
	4	10	.818	2447	245	20,000	90,000	.012	
	5	10	.818	2447	245	20,000	110,000	.016	
	6	10	.818	2447	245	20,000	130,000	.018	
6/14	7	10	.818	2447	245	20,000	150,000	.022	
	8	10	.818	2447	245	20,000	170,000	.033	
7/6						16 JUNE			Cycle to break through grind flaw
7/6	9	10	.818	1858	186	5...	170,500	.029	

220

Customer: SAIC
Project: 4232-83041
Technician: (illegible)
Material: Inco 718
Specimen No: 12N

Test No: 12-205
Test Ratio: 1
Test Frequency: 10 Hz / SWG
LCF Machine No: Good 2
LCF Test No: 16504

Length (L): 6.009
Width (W): 3.002
Thickness (B): .354
Notch Length: .008

Date	Run	Freq (Hz.)	A Ratio	Pmax	Pmin	Cycles dn	Total Cyc	c_i	Comments
6/14	0	10	.818	2447	245	-0-	-0-	→.008	Target: .030 (.015±.005)
	1	10	.4151	2447	245	50,000	50,000	.008	
	2	10	.818	2447	245	20,000	70,000	.012	
5/17	3	10	.8181	2447	245	20,000	90,000	.012	
	4	10	.818	2447	245	20,000	110,000	.014	
	5	10	.818	2447	245	25,000	135,000	L10:	
	6	12	.818	2447	245	25,000	160,000	.021	
	7	10	.818	2447	245	20,000	150,000	-.030	to have had to stop to break through spread off new holes = .249
7/6						1b store * send			
7/6	8	10	.817	1959	196	500	180,500	.024	cycle
	9	10	..	..	..	500	181,000	.024	
	10	10	..	..	..	500	181,500	.056	
	11	10	..	..	..	1000	182,500	.520°	
	12	10	..	..	..	1000	183,500	.520°	
	13	10	..	..	..	2000	185,590	.520°	
	14	10	..	..	..	3000	188,500	.520°	
7/7	15	10	.818	1948	196	2000	190,500	.520°	
	16	10	..	..	..	2000	192,500	.020	
	17	10	..	..	..	3000	195,500	.027	
	18	10	..	..	..	2000	197,500	.027	
	19	..	..	..	..	2000	199,500	.027	
	20	..	..	..	..	2000	201,500	.027	

Customer: _____
Project: 4172 - 6309
Technician: DJ6
Material: Inco 718
Specimen No: 12 N

Length (L) 6.008
Width (W) .257
Thickness (B) .257
Notch Length

Test No: 12-345
Test A/R Ratio: .1
Test Frequency: 10 Hz / 5m
LCF Machine No: 60002
LCF Test No: 165047

Test Date	Run	Freq. (Hz.)	A Ratio	Pmax.	Pmin.	Cycles dn	Total Cyc Nt	c_i	Comments
7/7	2.1	10	.6861	1898	196	2000	20750 2015-	→ .028 *Finished	Steel bent in columns Do

Customer: SAIC

Project: 4272-9304|

Technician: DSG

Material: 7075-T6 Aluminum

Specimen No: 1A

Length (L): 6.002
Width (W): 1.57
Thickness (B): .011
Notch Length: .011

Test No: 13 -265
Test A Ratio: .10
Test Frequency: 10 Hz, Sine
LCF Machine No: 60002
LCF Test No: 16S177

Date	Run	Freq. (Hz.)	A Ratio	P_{max}	P_{min}	Cycles (n)	Total Cyc (N_t)	C_i	Comments
15Jun	0	10	.0043	983	98	0	0	.011	σ_{max} = 40.0 ksi
	1	10	.0081	983	98	10,000	10,000	.011	span = 5.50 volts
	2	10	.0081	983	98	10,000	20,000	.016 cab	TRESET .070
16Jun	3	10	.0081	983	98	10,000	30,000	.026	2 cracks growing apart but 1 took w 1 on the side
	4	10	.0091	987	98	2,000	32,000	.070	On the ht side with 2 cracks I cut your longer
						* Cycle to break	* tried to stop to have nitch signal = .off 11 show		.249
7/7							through good scan		
7/7	5	10	.819	786	78	250	32,250	.098	I than L that E = sea nitch then ver by 06
7/11		RCVD	Bode Frm Shop				* Send back to stop to have nitch signal off. 06		
7/11							new thickness = .246	New crack length = .027	
7/11							Finished	Send back to customer	

Engineer:
Project: 4272-8304(1)
Technician: DSL
Material: 7075-T6 Aluminum
Specimen No: 2A

SAIC
Length (L): 6.000
Width (W): 2.002
Thickness (B): .259 .260
Notch Length: .210

Test No: 14-265
Test A/R Ratio: .10
Test Frequency: 10 Hz Sine
LCF Machine No: 60002
LCF Test No: 165153

Date	Run	Freq. (Hz.)	A Ratio	Pmax.	Pmin.	Cycles dn	Total Cyc.	c_i	Comments
4 Jul	0	10	.5191	903	99	0	0	.010	TARGET= .030
	1	10	.841	903	96	10,000	10,000	.014	
	2	10	.841	903	99	10,000	20,000	.019	
	3	10	.841	903	99	9,000	29,000	.078	
									* Send to shop to have notch ground off '' new photos 2, 240
7/10						Cycle to break through good times			
7/10	4	10	.941	786	76	250	29,250	.026	
	5	"	"	"	"	500	29,750	.026	
	6	"	"	"	"	1000	30,750	.026	
	7	"	"	"	"	1000	31,750	.027	
	8	"	"	"	"	1000	32,750	.027	
	9	"	"	"	"	1000	33,750	.028	
						* Finished		pull back to continue /b	

Account: __SAIC__

Project: __4272-8304l__

Technician: __DSC__

Material: __7075-T6 Aluminum__

Specimen No: __7A__

Length (L) 6.002
Width (W) 2.007
Thickness (B) .255
Notch Length .010

Date	Run	Freq. (Hz)	A Ratio	Pmax.	Pmin.	Cycles dn	Total Cyc	c_i	Comments
16 Jun	0	10	.001	983	98	0	0	.010	TARGET = .070
	1	10	.001	983	98	10,000	10,000	.014	
17 Jun	2	10	.001	983	98	10,000	20,000	.021	
	3	10	.001	983	98	8,000	28,000	.036	
7/17	Recvd	Gave Stop	New Thickness = .246					* Scan to have notch spaced off!! Po
7/10								New A= .030
7/10					Sent back to Customer! Po

Customer: SAIC
Project: 4272 - 83041
Technician: DSG
Material: 7075 - T6 Aluminum
Specimen No: 4A

Length (L) 6.002
Width (w) 1.003
Thickness (B) .250
Notch Length .010

Test No: 16 -265
Test A/R Ratio: .10
Test Frequency: 10 Hz Sine
LCF Machine No: 60002
LCF Test No: 165175

Date	Run	Freq. (Hz.)	A Ratio	Pmax.	Pmin.	Cycles Δn	Total Cyc n...Σt	c_i	Comments
6/17	0	10	.814	997	996	0	0	.010	TARGET = .030
	1	10	.814	987	98	10,000	10,000	.015	
	2	"	"	"	"	10,100	20,000	.021	
	3	"	"	"	"	5,000	25,000	.029	* send to shop to have notch special off! New height=
4 July						Cycle to break through small piece	.248
7/10								.046	small piece
7/10	4	13	.811	796	70	250	25,250	* finished and put in cabinet

Customer: _____
Project: 4232 - 6304
Technician: DTG
Material: 7075-T6 Aluminum
Specimen No: 5A

Length (L) 6.00
Width (W) 3.00
Thickness (B) .25
Notch Length .720

Test No: 17-265
Test A/B Ratio: .10
Test Frequency: 10 HZ Sine
LCF Machine No: 60002
LCF Test No: 165/92

Date	Run	Freq. (Hz.)	A Ratio	Pmax.	Pmin.	Cycles/in	Total Cyc	c_i	Comments
6/7	0	10	.101	963	98	0	0	.010	TARGET = .250
	1	"	"	"	"	25,000	25,000	.7080	
				Cycle to break		* Seal to stop to have notch ground off. New thickness .243			
7/9				break		* break through grind smear			
7/10	2	10	.980	786	70	250	25,250	.295	* OVERSHOT target.

Customer: SAIC
Project: 4272-85041
Technician: DSL
Material: 7075-T6 Aluminum
Specimen No: 64

Length (L) 6.002
Width (w) .295
Thickness (B) .252
Notch Length

Test No: 18-265
Test A/R Ratio: .10
Test Frequency: 10 Hz Sine
LCF Machine No: 60002
LCF Test No: 165/97

Date	Run	Freq. (Hz.)	A Ratio	Pmax.	Pmin.	Cycles dn	Total Cyc N_t	c_i	Comments
6/19	0	10	.9181	943	98	0	0	.021	Thickness = .250
	1					10,000	10,000	.041	
	2					10,000	20,000	.171	
	3					2,000	22,000	.233	
	4					500			* Sand to shop to have notch ground .01" slow thickness = .242
7/10					cycle to break	during sand store			
7/10	4		2	.8181	78¢	78	250	22,250	.228
	5		10	.9181	78¢	78	500	22,750	.231
	6					500	23,250	.239	
	7					250	23,500	.242	
	8					250	23,750	.246	
	9					100	23,850	.247	
						* Finished Send bulk to contract R_0			

Page 1 of 1

Customer: SAIC
Project: 4272-83041
Technician: DSTL
Material: 7075-T6 Aluminum
Specimen No: 7A

Length (L) 6.000
Width (W) 2.025
Thickness (B) .254
Notch Length .011

Test No: 19 - 265
Test A/R Ratio: .10
Test Frequency: 10 Hz Sine
LCF Machine No: 60002
LCF Test No: 165200

Date	Run	Freq (Hz.)	A Ratio	Pmax.	Pmin.	Cycles (in)	Total Cyc N_f	c_i	Comments
6/19	0	10	.6/11	.983	.92	0	0	.021	TARGET ~ .250
	1		3	"	"	10,000	10,000	.030	
	2			"	"	10,000	20,000	.111	
	3			"	"	3,000	23,000	.196	
	4			"	"	2,000	25,000	.22A	
						# Cycle to break through		★ Seal to stop to hr. notch crack DPII flow thickness .243	
7/10	5			746	90	250	25,250	.232	smeared
7/10	6			746	90	250	25,500	.277	
	7	10	.810	746	90	250	25,750	.239	
	8		1	"	"	250	26,000	.241	
	9		"	"	"	250	26,250	.244	
	10		3	"	"	250	26,500	.247	
	11		3	3	"	100	26,600	.249	family Seal break to customer flex.

Engineer: SAIC
Project: 4272-03041
Technician: DSC
Material: 7075-T6 Aluminum
Specimen No: 8A

Length (L): 6.00
Width (W): 1.023
Thickness (B): .254
Notch Length: .036

Test No: 20 -265
Test A/R Ratio: .10
Test Frequency: 10 Hz Sine
LCF Machine No: 60002
LCF Test No: 165207

Date	Run	Freq. (Hz.)	A Ratio	&	Pmax.	Pmin.	Cycles Δn	Total Cyc n	c_i	Comments
6/9	0	10	.2081		987	98	0	0	.020	THRUST .250
	1						10,000	10,000	.033	
	2						10,000	20,000	.150	
	3						2,000	22,000	.190	
	4						1,000	23,100	.216	
6/10	5						200	23,200	.221	
										* Seal to shut so has not thought off New
7/11							* Cycle to break through seal spacer			thickness: .242
7/11	6	10	.2081		786	79	250	23,450	.225	
	7						250	23,700	.229	
	8						250	23,950	.271	
	9						300	24,250	.236	
	10						300	24,550	.242	
	11						300	24,850	.244	
	12						300	25,150	.247	
	13						200	25,350	.249	
							* Ended fail to cut through to custom .05			

Page 1 of 1

Customer: ____
Project: ____
Technician: ____
Material: 7075-T6 Aluminum
Specimen No: 9A

Length (L): 6.001
Width (W): 2.005
Thickness (B): .252
Notch Length: .008

SAIC
4232 - 83041
DSTL

Test No: 21 -265
Test A/R Ratio: .10
Test Frequency: 10 Hz Sine
LCF Machine No: 60002
LCF Test No: 16521

Date	Run	Freq. (Hz.)	A Ratio	Pmax.	Pmin.	Cycles dn	Total Cyc	C;	Comments
6/20	0	10	.9194	987	98	0	0	.008	THREE: .078
	1					10,000	10,000	.010	CORNER
	2					10,000	20,000	.010	
	3					10,000	30,000	.010	
	4					10,000	40,000	.010	
	5					10,000	50,000	.010	
	6					10,000	60,000	.014	
	7					10,000	70,000	.019	
	8					10,000	80,000	.024	
	9					5,000	85,000	.035	* tried to stop 2 then notch opened off
7/11				NEW	thickness		.247		* Cycle to break through sidewall
7/11	10	-	.9921	786	79	200	85,200	.039	Send back to distr. - No.
						* finished			

Pg 1 of 1

SAIC
4232-93.04\
DTG

Length (L) 6.000
Width (W) 2.083
Thickness (D) .125
Notch Length .018

Test No: 22 -265
Test A/R Ratio: .10
Test Frequency: 10 Hz Sine
LCF Machine No: 6000 2
LCF Test No: 165290

Date	Run	Freq. (Hz.)	A Ratio	Pmax.	Pmin.	Cycles Δa	Total Cyc. a...Σ	c_i	Comments
4/31	0	10	.1141	985	99	θ	θ	.010	TR[?]sT = .070
	1	'	''	''	''	25,000	25,000	.012	corner
	2	''	''	''	''	20,000	45,000	.018	
	3	''	''	''	''	2,000	47,000	.020	
				*		cycle to best though		※ Seal to stay to have cath speed off 11 thickness .215	
7/10	4	90	.1181	796	70	200	47,200	.023	3-dot smear
	5	10	.9181	796	76	200	47,400	.027	
	6	10	.9082	796	76	300	47,700	.073	
	7	10	.1181	786	76	505	48,200	.520	
	8	''	''	''	''	505	48,700	.520	
	9	''	''	''	''	505	49,200	.720	
	10	''	''	''	''	505	49,700	.720	
	11	''	''	''	''	510	50,200	.920	
	12	''	''	''	''	505	50,700	.920	
	13	''	''	''	''	500	51,200	.920	
	14	''	''	''	''	700	51,900	.920	
	16	''	''	''	''	1000	52,900	.920	
	17	''	''	''	''	1000	53,900	.920	
	18	''	''	''	''	1000	54,900	.920	
	19	''	''	''	''	1000	55,900	.920	
	20	''	''	''	''	1000	56,900	.020	
			*		Finished				

Pac 1.1.1

Customer: SAIC
Project: 4272 - 8304l
Technician: DSL
Material: 7075-T6 Aluminum
Specimen No: 11A

Length (L): 6.000
Width (W): 2.00
Thickness (B): .234
Notch Length: .205

Test No: 23 -265
Test A Ratio: .10
Test Frequency: 10 HZ Sine
LCF Machine No: 6000 2
LCF Test No: 165296

Date	Run	Freq. (Hz.)	A Ratio	Pmax	Pmin	Cycles Δa	Total Cyc ΣT	c_i	Comments
6/14	0	10	.0991	993	98	0	0	.005	TARGET: .90
	1					25,000	25,...	.005	
	2					20,000	45,000	.005	
	3					10,000	55,000	.006	
	4					5,000	60,000	.006	
	5					5,000	65,000	.009	
	6					5,000	70,000	.009	
	7					8,000	78,000	.008	
	8					8,000	86,000	.009	
	9					8,000	94,000	.009	
	10					8,000	106,000	.013	
	11					5,000	111,000	.013	
6/14	12					8,000	119,000	.018	
	13					8,000	129,000	.031	
						✳ Send it to break through spml shear			
7/11	14	10	.591	786	79	200	129,200	.079	✳ Cycle to break through spml shear
7/11						finished	Bad Bad to cushion / Dig.		optl. dia. fracture = .248 had high notch spml

page 1 of 1

Customer: SAIC
Project: 4272 - 93041
Technician: DTC
Material: 7075 - T6 Aluminum
Specimen No: 12 A

Length (L): 5.001
Width (W): 2.995
Thickness (B): .244
Notch Length: .007

Test No: 24 - 265
Test A/B Ratio: .10
Test Frequency: 10 Hz Sine
LCF Machine No: 60002
LCF Test No: 165772

Date	Run	Freq. (Hz.)	A Ratio	Pmax	Pmin	Cycles Δn	Total Cyc n = Σ	c_i	Comments
4/1	0	10	.6091	993	98	0	0	.007	TARGET= .090
	1	"	"	"	"	25000	25,000	.007	Gages
	2	"	"	"	"	25000	50,000	.011	
	3	"	"	"	"	10000	60,000	.014	
4/3	4	"	"	"	"	10,000	70,000	.020	
	5	"	"	"	"	10,900	80,000	.026	
					*	Cycle to break	* Send to shop to have both gold screw	
7/11	6	10	.8091	776	78	200	81,200	.022	through gold screw
7/11	7	9	"	"	—	200	80,400	.022	
	8	10	"	"	"	505	80,900	.022	
	9	"	"	"	"	1000	81,900	.023	
	10	"	"	"	"	1500	82,900	.024	
	11	"	"	"	"	1000	83,900	.024	
	12	"	"	"	"	1500	85,400	.024	
	13	"	"	"	"	1500	86,900	.025	
	14	"	"	"	"	1500	88,400	.037	
					*	Finished	Finished test hit to break		

Page 1 of 1

APPENDIX B
PURCHASE ORDER/CUSTOMER'S INSTRUCTIONS

OMITTED: Contains Financial Information

APPENDIX C
SPECIMEN DRAWING/QUALITY CONTROL INSPECTION

METCUT RESEARCH INC.
QUALITY INSPECTION SUMMARY

Specimen Number	Before Test		After Cracked		
	Gage Thick	Gage Width	Gage Width	Gage Thick	amount removed
1N	0.2526	2.0081		0.2461	0.0065
2N	0.2529	2.0080		0.2461	0.0068
3N	0.2534	2.0090		0.2477	0.0057
4N	0.2533	2.0080		0.2474	0.0059
5N	0.2542	2.0080		0.2431	0.0111
6N	0.2542	2.0081		0.2435	0.0107
7N	0.2542	2.0082		0.2436	0.0106
8N	0.2540	2.0080		0.2428	0.0112
9N	0.2542	2.0080	2.0020	0.2491	0.0051
10N	0.2542	2.0080	2.0020	0.2492	0.0050
11N	0.2538	2.0080	2.0020	0.2478	0.0060
12N	0.2536	2.0080	2.0010	0.2487	0.0049

237

METCUT RESEARCH INC.
QUALITY INSPECTION SUMMARY

Job No.:	4232-83041-199-01-02
Form No.:	65-00-05
Lot:	14
Date:	8-Apr-06
Inspector:	D. BECKSTEDT
Test Eng.:	GRJ
Material:	AL

Specimen Number	Before Test Gage Thick	Before Test Gage Width		After Test Gage Thick	After Test Gage Width	Removed After Test
1A	0.2549	2.0050		0.2487		0.0062
2A	0.2544	2.0050		0.2476		0.0068
3A	0.2546	2.0050		0.2488		0.0058
4A	0.2540	2.0050		0.2477		0.0063
5A	0.2545	2.0050		0.2433		0.0112
6A	0.2531	2.0050		0.2417		0.0114
7A	0.2539	2.0050		0.2422		0.0117
8A	0.2540	2.0050		0.2422		0.0118
9A	0.2533	2.0050		0.2470	1.9990	0.0063
10A	0.2510	2.0050		0.2453	1.9990	0.0057
11A	0.2539	2.0050		0.2475	1.9990	0.0064
12A	0.2519	2.0050		0.2457	1.9990	0.0062
13A	0.2502	2.0050				
14A	0.2535	2.0050				

Metcut Research Inc. - 3980 Rosslyn Drive - Cincinnati, OH 45209-1196
Tel (513) 271-5100 - Fax (513) 271-9511

Revised : 04/04/07

Appendix E
Crack Extension of Aluminum and Inco-718 Plates Prepared on Previous
Program

**Crack Extension of Aluminum and Inco-718
Plates Prepared on Previous Program**

**Science Applications International Corporation (S.A.I.C)
16701 W. Bernado Drive
San Diego, CA 92127**

Attention: Donna Mayton

Purchase Order No.: 4400134452

Metcut Project No.: 4232-84162-1

NOVEMBER 27, 2006

_____

_____
    Thomas E. Arnold, Manager   **Guy R. Johns**
Engineering   Test Engineer

J:\84162\35\reports\84162-1
krh

Project

At the request of Ms. Donna Mayton, Metcut Research, Inc. was contracted to extend

existing cracks in Aluminum and Inco-718 plates which were prepared and cracked on a

previous Metcut project. The cracks were extended by 3-point bend fatigue similar to the

methods used on the initial projects.

The final crack lengths are as follows:

Specimen	Test Number	Total Cycles	Final Crack Length (in.)
1N	1-265	199,551	.058
2N	2-265	138,000	.059
3N	3-265	153,694	.060
4N	4-265	215,000	.060
1A	5-265	73,750	.183
2A	6-265	76,550	.188
3A	7-265	57,750	.182
4A	8-265	64,250	.177
9A	9-265	129,900	.121
10A	10-265	99,900	.122
11A	11-265	176,772	.118
12A	12-265	145,900	.118

Data sheets attached.

Date	Run	Freq. (Hz.)	A Ratio	Pmax.	Pmin.	Cycles Δn	Total Cyc. Σ_i	c_i	Comments
28 Jan	13	10	.981	1958	196	300	74,000	.017	TARGET = .060
9/27			RCVD		Back From SAIC to Elongate crack.				$Span = 3.5$ $P_{max} = 84.63$
9/28 Ocbr		10	.951	1958	196	0	74,000	.027	
9/28	14	10	.981	1916	196	18,000	84,000	.027	
9/28	15	12	.981	1958	196		95,231	.027	* Specimen stopped out of fixture.
	16					11,000	95,231	.027	
10/2	17					824	96,055	.027	* Specimen slipped out fixture. Replace by fixture pin.
10/3	18					793	96,848	.027	
	19					1017	97,864	.027	
	20					4261	102,152	.027	* Specimen walking? Repkd lower fixture.
	21					11,000	112,152	.028	
	22					10,000	122,152	.029	
	23					11,000	132,152	.024	
10/4	24	10	.9181	2154	215	2349	134,551	.009	* 10% Pmax! in last due to no growth + Pked elevation
	25					10,000	144,551	.033	
	26					10,000	155,551	.037	
	27					10,000	165,551	.038	
	28					10,000	165,551	.041	
10/5	29					10,000	184,551	.045	$c_i = 7 \times 10^{-7}$
	30					10,000	194,551	.054	$c_i = 6 \times 10^{-7}$
	31					5,000	199,551	.059	$c_i = 9 \times 10^{-7}$ 10/5/06
10/5		* E-drill From E-drill				SEND Back to customer as they are to rework to .060 → 1 final reading to @ .060 .06			

241

NDI FLAT PL 'S SAIC

ustomer: _____
oject: 4232 - 84162
chnician: DDC
terial: INCO
eclmen No: 2N

Length (L) 6.005
Width (V) 2.227
Thickness (B) .341
Notch Length .236

Test No: 10-265
Test A/B Ratio: .6191
Test Frequency: 10 Hz
LCF Machine No: 68002
LCF Test No: 169694

Date	Run	Freq. (Hz.)	A Ratio	Pmax.	Pmin.	Cycles on	Total Cyc Nt	c_i	Comments
7/8	15	10	.6191	2447	245	2000	113000	.036	TAR6ETP.060 STA/=7.5
	⊕	#	RCVD	BACK	From	cithur - cchry vs b elonget	crcks to .060		
8/16	16	10	.6191	215	/	0	113000	.036	
8/16	16	"	"	"	"	5000	118000	.036	
	17	"	"	"	/	5000	123000	.042	
	18	"	"	"	"	6000	129000	.047	
	19	"	"	"	4	5000	134000	.054	
	20	"	"	"	"	3000	137000	.056	
	21	"	"	"	"	1000	137100	.056	
	22	"	"	"	»	1000	138000	.059	Back Jr custom Pt 10/10/06
						Completed	End		

NDE FLAT P:

Customer: SAIC

Object: 4232 ~ 84(162)

Technician: DTb

Material: IN60

Specimen No: 3N

Length (L) 6.011
Width (W) 2.002
Thickness (B) .446
Notch Length .14

FORM NO. 21-860205-1B

Test No: 11-245
Test A/R Ratio: .0181
Test Frequency: 10 Hz
LCF Machine No: 64002
LCF Test No: 168700

Date	Run	Freq. (Hz.)	A Ratio	PMax.	PMin.	Cycles Δn	Total Cyc n_t	c_i	Comments
6/30	8	10	.6181	198	196	1000	101,003	.074	TIMES 7=.060~1
10/10	9	10	.6181	2153.4	215	0	101,120	.024	SPPW = 7.5
	9	1	4	4	14	500	106,100	.029	ashty into ultrasonic crack to .60
	10	5	7	2	2	5000	111,100	.029	
	11	5	5	5	1	740	118,100	.030	
	12	5	5	5	5	5000	127,120 123,000	.070	
10/10	13	5	5	5	5	5000 1000	128,110	.070	
	14	5	5	5	5	1000	129,141	.035	Specimen making !
	15	5	5	5	5	5000	134181	.830	
	16	5	5	5	5	5000	139131	1.40	
	17	5	5	5	5	1000	141,941	750	
	18	5	5	5	5	2000	141,641	750	
	19	5	5	5	5	2000	148151	650	
	20	5	5	5	5	2500	153141	.060	Specimen broke to fracture pl. 10/21/06
					Completed				

NDE FLAT P1

Customer: SBFC
Project: 4272-6411/12
Technician: .072
Material: In600
Specimen No: 4N

Length (L) 6.010
Width (W) 2.02
Thickness (B) .251
Notch Length .020

FORM NO. 21-860205-18
Test No: 12-245
Test A/R Ratio: .9191
Test Frequency: 10 Hz
LCF Machine No: 60002
LCF Test No: 168729

Date	Run	Freq. (Hz.)	A Ratio	Pmax	Pmin	Cycles Δn	Total Cyc. Nt	ci	Comments
8/24	8	10	.9191	1499	196	1000	106,200	.029	Accept = .090
			2.010	2199	BRK	from	Customer	.029 using ut it change the crack b .090 n/	GAGE 3.5
8/24	9	10	.9191		211		106,000	.029	
8/25	9					3000	109,000	.029	
	10					8000	117,000	.029	
	11					8000	125,000	.029	
	12					8000	133,000	.072	
8/26	13					5000	138,000	.057	
	14					5000	143,000	.057	
	15					7000	150,000	.071	
	16					10,000	160,000	.042	
	17					5000	165,000	.042	
	18					8,000	173,000	.042	
	19					10,000	183,000	.042	
	20					6000	189,000	.045	
	21					6000	195,000	.050	
	22					5000	200,000	.050	
	23					5000	205,000	.051	
	24					5000	210,000	.055	
	25					2500	212,500	.050	
	26					2500	215,000	.040	
						Computed	final	back to curtain in no	

244

Customer: SAIC
Project: 4232-84162
Technician: DTB
Material: Aluminum
Specimen No: 1A

Test No: 2-245
Test A/R Ratio: .961
Test Frequency: 10 Hz
LCF Machine No: 60002
LCF Test No: 165249

Length (L) 6.003
Width (W) 2.005
Thickness (B) .249
Notch Length .027

Date	Run	Freq. (Hz.)	A Ratio	Pmax.	Pmin.	Cycles ΔN	Total Cyc Nt	c_i	Comments
7/7	5	10	.961	78b	78	250	72,250	.026	* Front brk & stop & hr with seal off
								.027	SPAN = 3.5
9/27		From SAIC					TB		THICK T = .060
10/5	1	10	.9141	75b	78	0	32,250	.027	crack elongate crack to 120 h.
	6	2	3	3	"	3000	35,250	.030	
	7	4	5	5	3	4000	38,250	.031	
	8	4	4	4	"	3000	41,250	.037	
	9	5	5	5	4	5000	46,250	.033	
	10	3	4	2	1½	5000	51,250	.042	
	11	3	4	4	½	5000	56,250	.054	
	12	2	"	"	"	2000	58,250	.040	
					Seal back to customer 11				
14/5		Customer sealing	back	's/specimen		*E-mail from customer exited to 120 nl			
10/16	13	5	"	3	"	4000	61,250	.085	
14	14	5	4	"	3	5000	68,250	.110	
		* completed				* Ashby to customer by - 10/16/11			
11/7		* Rc up BACK	.9141	78b	78		add elongate crack to .100 nl		
5 Nov	15	10	.9141	78b	78	2500	70,750	.154	Extend to .125
16	16					1000	71,750	.162	
9 nov	17					1000	72,750	.171	
8 nov	18					1000	73,750	.183	sent back to customer for inspection

245

Customer: -
Project: 4232 - 84162
Technician: bJG
Material: Aluminum
Specimen No: 2A

Length (L) 6.000
Width (W) 2.120
Thickness (B) .124
Notch Length .048

Test No: 4-26 S
Test A/R Ratio: .8V8 1
Test Frequency: 10 Hz
LCF Machine No: 6 0002
LCF Test No: 168462

Date	Run	Freq. (Hz.)	A Ratio	Pmax.	Pmin.	Cycles Δa	Total Cyc. Σa	c_i	Comments
7/10	9	10	.981	786	70	1200	33750	.026	
		RCVD	Back	From	Customer	to	ENLARGE	CRACK to .120 b/s.	TARGET=.120 SPAN=3.5
10/13	0	10	.981	786	76	0	33750	.026	
10/15	10	"	"	"	"	2000	35750	.028	
	11	"	"	"	"	4200	39756	.092	
	12	"	"	"	"	6000	44750	.040	CR= 8x10⁻⁷
	13	"	"	"	"	10000	59750	.055	da = 1.5x10⁻⁶
	14	"	"	"	"	10800	69750	.111	da = 5.6x10⁻⁶
	15	"	"	"	"	200	69950	.112	
	16	"	"	"	"	400	70350	.116	
	17	"	"	"	"	200	70550	.118	
				* Completed Cul back to custom... pb 10/17/06					crack life ... b .190
10/17	18	10	* RCVD	RCVD	70	2000	72550	.138	
10/17	19	10	.981	786	78	2000	74550	.144	
	20	10	.981	786	78	2000	76550	.188	SEND BACK TO CUSTOMER

Page 1 of

Test No: 5-265
Test A/R Ratio: .9/91
Test Frequency: 10 Hz
LCF Machine No: 60002
LCF Test No: 46475

Customer: SAIC
Project: 4282-04/62
Technician: D50
Material: Aluminum
Specimen No: 3A

Length (L) 6.001
Width (V) 2.002
Thickness (B) .256
Notch Length .50

Date	Run	Freq. (Hz.)	A Ratio	P max.	P min.	Cycles to	Total Cyc. P_t	c_i	Comments
6/17	3	10	.891	.005	.98	8000	28,000	.030	TAROEF .120
				RCV0 Back	From	28,000	.070	STR ~ 3.5
6/17	0	10	.9890	.987	.98	0	28,006	.070	Entry crack to .120 in
	7					10000	38,000	.0980	
	5					10000	48,000	.0916	
10/16	6					800	48,800	.102	
	7					500	49,300	.103	
	8					600	49,900	.111	
	9					300	50,200	.114	
	10					300	50,500	.114	
	11					300	50,800	.116	
	12					200	51,000	.116	
	13					300		.118	Self had to center .120 in 10/16/06
				# Adv0	Black	Completed Oo 10/16/06 is to elongate Einals to .130 in
11/7						Back hiking			
11/13	14	10	.891	.983	.94	3000	54,100	.155	
	15	10	.883	.983	.98	1000	55,100	.155	
	16	10	.891	.983	.99	1000	56,100	.162	
	17	10	.891	.913	.98	1000	57,100	.171	
	18	10	.891	.983	.88	650	57,750	.182	SEND BACK TO CUSTOMER

Customer: SAEC
Project: 9232-94162
Technician: DJ6
Material: Aluminum
Specimen No: 4A

Length (L) 6.002
Width (W) 2.005
Thickness (B) .249
Notch Length .013

Test No: 6-265
Test A/R Ratio: .9181
Test Frequency: 10 Hz
LCF Machine No: 60002
LCF Test No: 165546

Date	Run	Freq. (Hz.)	A Ratio	Pmax.	Pmin.	Cycles Δn	Total Cyc. Σc	c_i	Comments
7/10	4	10	.9181	796	78	250	25,250	.028	SAWN ~ 7.5
		RCVD BACK FROM customer to evaluate crack to .120 ml.							
10/16	1	10	.9181	796	78	—	25,250	.026	THR165 ~ .120 ml.
10/16	5	10	.9181	796	78	5000	30,250	.028	
	6					10000	40,250	.039	
	7	10				10000	50,250	.054	
10/17	8					10000	60,250	.131	← overshot to will Al - 0% dirgles
		# Completed Back Arbing — Send back to customer? chlogin to Ng/nfc crack to .100 ml.							
H17		# RCVD							
11/18	9					1000	61,250	.140	
	10					1500	62,750	.158	
	11					1500	64,250	.177	SEND BACK TO CUSTOMER

Customer: ___
Project: 4232 - 84162
Technician: DTI
Material: Aluminum
Specimen No: 9A

Test No: 3
Test A/R Ratio: .0181
Test Frequency: 10 Hz
LCF Machine No: 60002
LCF Test No: 168269

Length (L) 6.0
Width (W) 2.0
Thickness (D) .247
Notch Length .029

Date	Run	Freq. (Hz.)	A Ratio	Pmax.	Pmin.	Cycles Δn	Total Cyc Σc	c_i	Comments
7/11	10	10	.0181	786	79	200	85,200	.029	
9/27			At v0	Back	from	SATC			Corner to #length crack
10/5	1	10	AM	786	78	8000	85,200	.029	TARGET = .060
	11	4	4	4	4	1000	86,200	.032	sta/= 2.5
	12	4	4	4	4	3000	91,200	.033	
...ton									
10/6	13	4	4	4	4	5000	96,200	.039	NEW TARGET .120 AL
	14	4	4	4	1	5000	101,200	.045	
	15	4	4	4	4	5000	106,200	.050	
	16	4	4	4	4	3500	109,700	.054	
	17	4	4	4	4	15m	110200	.057	
	18	4	4	4	4	500	110,700	.050	
10/11		Custom cooling back				* Sed back to customer DTi 10/11/06			
10/12		* note that when read				Specimen back + E-mil from customer to request cracks to .180 al.			
						Specimen back that the site opposite the (X) had a little damage			
10/12	19	10	.0181	786	79	5100	115,700	.066	X
	20	4	4	4	4	5000	120,700	.065	
	21	4	4	4	4	1000	121,700	.068	
	22	4	4	4	4	1200	122,900	.092	
	23	4	4	4	4	1100	124,100	.098	
	24	4	4	4	4	1200	125,300	.100	
	25	4	*	4	4	800	126,100	.106	
	26	4	4	4	4	1200	127,700	.112	

Page 1 of 2

Customer: —
Project: 4252 - 04/07
Technician: 676
Material: Aluminum
Specimen No: 9A

Length (L) 6.001
Width (W) 2.25
Thickness (B) .257
Notch Length .25

Test No: 3-265
Test A/R Ratio: .918
Test Frequency: 10 Hz
LCF Machine No: 600??
LCF Test No: 168269

Date	Run	Freq. (Hz.)	A Ratio	Pmax.	Pmin.	Cycles /in	Total Cyc S_t	c_i	Comments
10/16	27	10	.941	746	76	1600	128700	.117	Center
	28	"	"	"	"	400	129,100	.117	Three s-1 fine!
	29	"	"	"	"	400	129,500	.117	Fails 9.5
	30	"	"	"	"	400	129,900	.121	
						* Completed test but to continue			JM 10/16/06

250

FORM NO. 21-860205-18

Test No: 7-265
Test A/R Ratio: .3/.9
Test Frequency: 10 Hz
LCF Machine No: 6000?
LCF Test No: 16675

Customer: SAIC
Project: 9272 - Brier
Technician: 056
Material: Aluminum
Specimen No: 10 A

Length (L) 6.000
Width (W) 2.001
Thickness (B) .125
Notch Length .028

t.i/date	Run	Freq. (Hz.)	A Ratio	Pmax.	Pmin.	Cycles dn	Total Cyc. N_z	c_1	Comments
7/11	20	10	.9/.3	.786	.3/.9	1000	56,400	.026	saw
			* cntnw	Sent		tick	specimen	% elongate cracks	through ≤ .120
M/D	0	10	.9/.3	.786	.75	6	56,400	.028	spec = 7.5
	21					10,000	66,400	.034	
	22					5,000	71,400	.040	
	23					5,000	76,400	.049	
	24					5,000	81,400	.057	
	25					5,000	86,400	.067	
	27					5,000	91,400	.084	
	28					2,000	93,400	.098	
	29					2,000	95,400	.101	
	30					1,000	96,400	.106	
	31					1,000	97,400	.113	
	32					500	97,900	.113	
	33					500	98,400	.116	
	34					500	98,900	.117	
	35					500	99,400	.117	
	34					500	99,900	.172	
						* Complete. Sent back to customer. 26 lb 17/06			

251

NDE FLAT P1 ... SAIC

Customer: SAIC
Project: 4232-84/62
Technician: 05T6
Material: Aluminum
Specimen No: 11 A

Length (L): 6.600
Width (W): ____
Thickness (B): 05T6
Notch Length: .024

Test No: B-265
Test A/R Ratio: .0191
Test Frequency: 10 Hz
LCF Machine No: 68002
LCF Test No: 166504

Date	Run	Freq. (Hz)	A Ratio	Pmax.	Pmin.	Cycles On	Total Cyc. N_t	c_i	Comments
7/?	14	10	.0191	786	79	200	124,780	.029	Coire
		*	RCVO	back	from	customer	requesting that we enlarge the crack to .120 ml		THRGPS .120
10/17	◌	10	.0191	786	79	-0-	124,780	.029	Span 7.5
	15	5	5	5	5	500	134,280	.070	
	16	5	5	5	5	5000	139,280	.030	
10/18	17	5	5	5	5	5000	146,572	.040	* stopped specimen walking
	18	5	5	5	5	5000	151,572	.040	
	19	5	5	5	5	5000	156,572	.050	
	20	5	5	5	5	5000	161,572	.062	
	21	5	5	5	5	5000	166,572	.070	
	22	5	5	5	5	5000	171,572	.080	
	23	5	5	5	5	300	174,572	.101	
	24	5	5	5	5	200	175,944	.111	
	25	5	5	5	5	80	176,772	.118	
				* completed test but no contact					02 10/18/06

NDE FLAT P1 'S

Customer: SAIC
Project: 4252 - 04112
Technician: OJL
Material: Aluminum
Specimen No: 12A

Length (L) 6.000
Width (W) 2.005
Thickness (B) .246
Notch Length .037

Date	Run	Freq. (Hz.)	A Ratio	Pmax	Pmin	Cycles dn	Total Cyc N_t	c_i	Comments
7/11	19	10	.818)	78k	78	1565	864000	.037	Curr
				RCVD	Specimen		buck from Customer. Capacity but no change the Crocks id 120n)		Spen 3.5
10/11	0	10	.841	78k	7k	ϕ	88400	.037	TARGET 120n)
	51					500	43400	.037	
	11					500	98400	.037	
	41					500	103400	.037	
	18					5000	108400	.037	
	W					6000	114400	.042	
	Q					005	121400	.048	
	15					5000	126400	.050	
	22					6000	132400	.070	
	23					5500	138400	.090	
	24					2500	140900	.098	
	25					951	141851	.101	
	26					1000	143400	.110	
	27					600	145000	.111	
	28					600	145600	.116	
	29					300	145900	.118	
10/2							specimen back to customer, No 10/24/06		

Appendix F
Contamination for Crack Contamination Study
Note: All figures are included at the end of this report.

MML LOG NO.:	*12067A*
PART NAME:	*Crack Contamination Specimens*
PART ID NO.:	*See Below*
PART S/N:	*N/A*
CUSTOMER PO:	*4400136017*
DATE:	*12/02/2006*

REQUESTED BY:	*Donna Mayton* *SAIC* *16701 W. Bernardo Drive* *San Diego, California 92127*
COPIES TO:	*N/A*
WORK REQUESTED:	*See comprehensive SAIC scope of work below.*
REPORTED BY:	*M. Poormon*
TESTED/ANALYZED BY:	*M. Poormon*
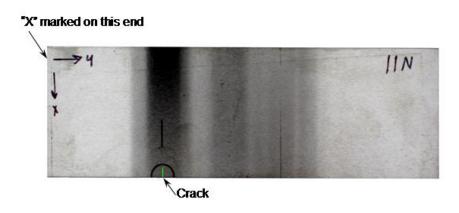
SUMMARY:

- This laboratory report provides initial sample crack length measurements and associated macro/micro photographic documentation as well as contamination process information.
- See comprehensive data matrix below for comprehensive specimen crack locations, contamination used, and before/after crack length measurements.

BACKGROUND:

Fifteen fatigue crack contamination specimens were sent to Martin MetLabs for crack length documentation and contaminant processing. These specimens were to be used in a study to review the effects of specific contaminants on the performance of Sonic IR testing of engine components. The specimens were comprised of nine Inconel 718 and six 7075-T6 aluminum plates that had dimensions of 2.00 inches X 6.00 inches X 9.20 inches.

Ten of the specimens contained surface cracks and the remaining five had corner cracks. The crack positions were referenced by a coordinate system devised by SAIC. An example of this position measurement system was illustrated on the specimen image below.

"X" marked on this end

4

x

Crack

IIN

The specimens were pre-identified by SAIC as follows.

1N (surface crack)	5N (surface crack)	9N (corner crack)
2N (surface crack)	6N (surface crack)	12N (corner crack)
2A (surface crack)	6A (surface crack)	10A (corner crack)
3N (surface crack)	7N (surface crack)	11N (corner crack)
3A (surface crack)	7A (surface crack)	11A (corner crack)

Note that the alpha-suffix denotes material type: N = nickel alloy, A = aluminum alloy.

The SAIC scope of work was requested as follows.

- Measure each specimen crack length. Provide length measurements for each of two faces on corner cracks.
- Apply SAIC specified contaminants to samples by 'winking' (3-point bend loading several times). Contaminant should cover approximately one inch square area but excess can be wiped off after loading cycles.
- For Inco 718 specimens – bake sample at $800^{o}F$ for 4 hours, remove and let cool to < $200^{o}F$, repeat this process 3 times.
- Thoroughly document the process and return samples to SAIC.
- Provide written laboratory report of data.

RESULTS:

Crack locations were identified using the SAIC coordinate key. **Figure 1** depicted 'as received' condition of each sample following crack location identification. Optical microscopy and image analysis software was employed to perform actual crack measurements. Several specimens (i.e., 2A, 3N and, 5N) had cracks that were very faint or not resolved at all. Permission was given to cycle these specimens at a reduced load (approximately 50% of initial precrack load) in order to

resolve cracks. **Figure 17** depicted test machine and related fixturing set-up. Cycling test parameters for each of these specimens were as follows.

- *Specimen #2A*   Pmax = 300 lbs (Initial Precrack Pmax = 786 lbs)

  R = 0.1

  Frequency = 5 Hz

  Total Cycles = 5,000

- *Specimen #3N*   Pmax = 1,000 lbs (Initial Precrack Pmax = 2,154 lbs)

  R = 0.1

  Frequency = 5 Hz

  Total Cycles = 4,000

- *Specimen #5N*   Pmax = 1,000 lbs (Initial Precrack Pmax = 1,958 lbs)

  R = 0.1

  Frequency = 5 Hz

  Total Cycles = 2,000

Annotated 200X sequential fields of view were captured of all specimen cracks as received. The following figures correspond to respective crack imagery.

Specimen 1N	**Figure 2**	Specimen 7N	**Figure 10**
Specimen 2N	**Figure 3**	Specimen 7A	**Figure 11**
Specimen 2A	**Figure 4**	Specimen 9N	**Figure 12**
Specimen 3N	**Figure 5**	Specimen 10A	**Figure 13**
Specimen 3A	**Figure 6**	Specimen 11N	**Figure 14**
Specimen 5N	**Figure 7**	Specimen 11A	**Figure 15**
Specimen 6N	**Figure 8**	Specimen 12N	**Figure 16**
Specimen 6A	**Figure 9**		

All as-received crack measurements were recorded in the data matrix below.

Contamination Specimen Data				
Sample ID	Crack Position		Contaminant Used	Initial Crack Measurements (inches)
	X Coord. (in)	Y Coord. (in)		
1N [3]	1.00	1.75	Fuel	0.0457
2N [3]	1.00	1.75	WD-40	0.0550
2A	1.00	1.75	WD-40	0.1682
3N [3]	1.00	1.75	Anti-gallant	0.0467
3A	1.00	1.75	CPC	0.1811
5N [3]	1.00	1.75	Fuel	0.2513
6N [3]	1.00	1.75	WD-40	0.2520
6A	1.00	1.75	WD-40	0.2449
7N [3]	1.00	1.75	Anti-gallant	0.2483
7A	1.00	1.75	CPC	0.2501
9N [3]	2.00	1.75	Fuel	0.0241 [1]
				0.0229 [2]
12N [3]	2.00	1.75	WD-40	0.0232 [1]
				0.0227 [2]
10A	2.00	1.75	WD-40	0.1165 [1]
				0.0874 [2]
11N [3]	2.00	1.75	Anti-gallant	0.0271 [1]
				0.0220 [2]
11A	2.00	1.75	CPC	0.1128 [1]
				0.0838 [2]

Note 1: Corner Crack Surface Measurement

Note 2: Corner Crack Edge Measurement

Note 3: Nickel specimens were baked at 800°F for 4 hours (process repeated 3X)

All specimens were individually set-up on a fatigue machine with three-point bend fixturing in preparation for a 'winking' contamination procedure. The contaminants selected by SAIC were as follows.
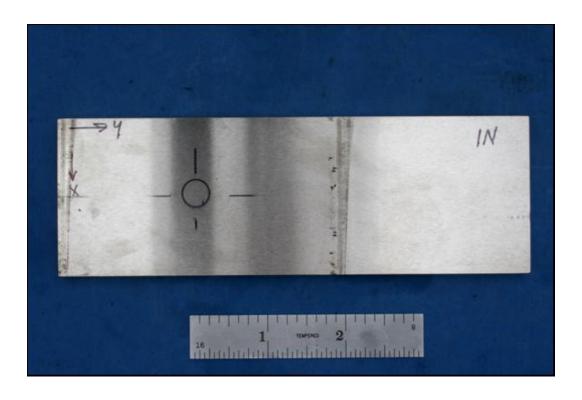
- Jet Fuel (i.e., JP-4)
- WD-40® lubricant
- Corban® 35 Corrosion Preventative Compound (CPC)
- Permatex® High Temperature Anti-Seize Lubricant (#80078)

Specified contaminants (listed above) were applied to the localized crack region of each specimen; approximately one inch square area. Each specimen was subsequently loaded in

three-point bending for several cycles. Specific contaminant-to-specimen application was also summarized in the data matrix above (*see page 4*).   Test machine and related three-point-bend fixturing set-up was illustrated in **Figure 17.**

Following the contamination process, the nickel specimens were run through a baking cycle. This process involved a 4 hour exposure at 800°F and then allowed to cool to less than 200°F. This contamination and baking cycle was repeated 3 times for nickel samples only.

All samples were then returned to SAIC for Sonic IR testing.
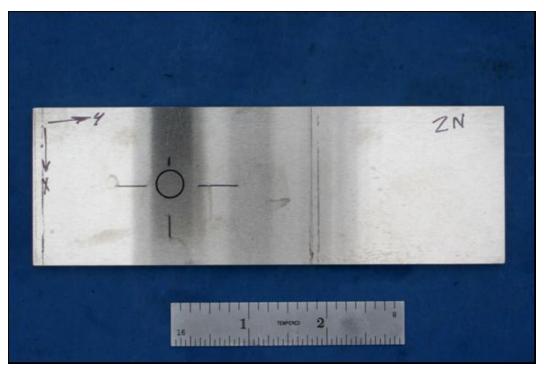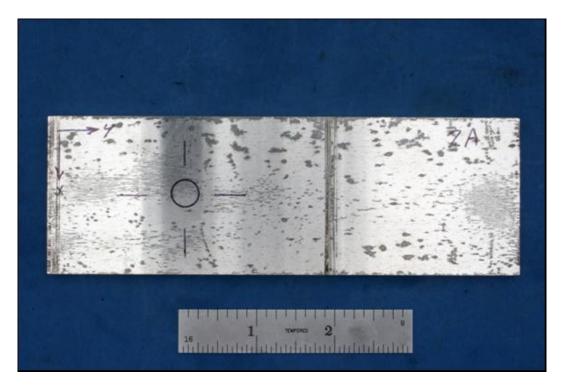
FIGURE 1a. *TOP:* Close-up macro photograph of Contamination Specimen 1N as received with marked location of crack. *BOTTOM:* Close-up macro photograph of Contamination Specimen 2N as received with marked location of crack.
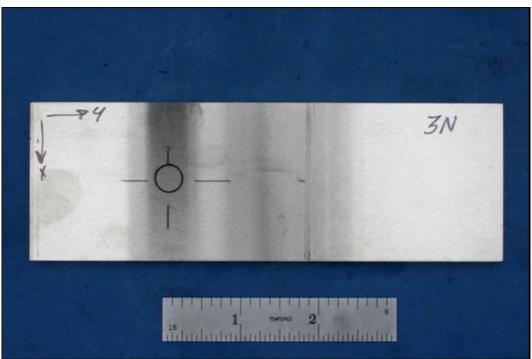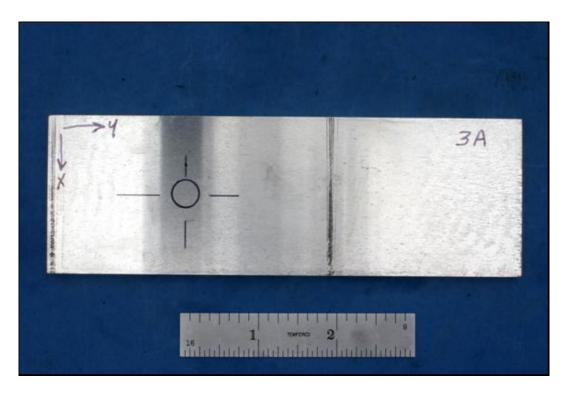
FIGURE 1b. *TOP:* Close-up macro photograph of Contamination Specimen 2A as received with marked location of crack. *BOTTOM:* Close-up macro photograph of Contamination Specimen 3N as received with marked location of crack.
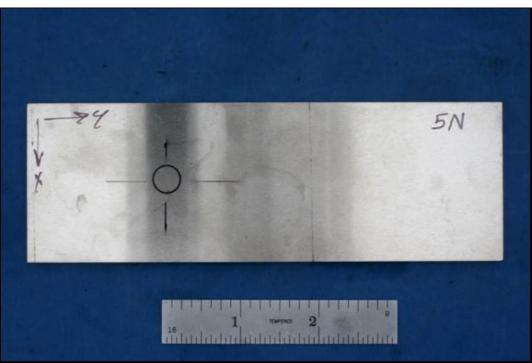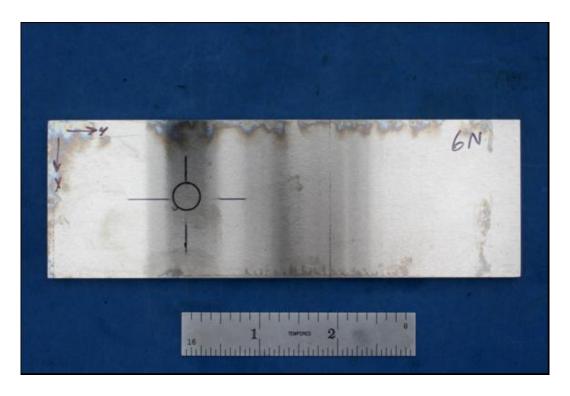
FIGURE 1c. *TOP:* Close-up macro photograph of Contamination Specimen 3A as received with marked location of crack. *BOTTOM:* Close-up macro photograph of Contamination Specimen 5N as received with marked location of crack.
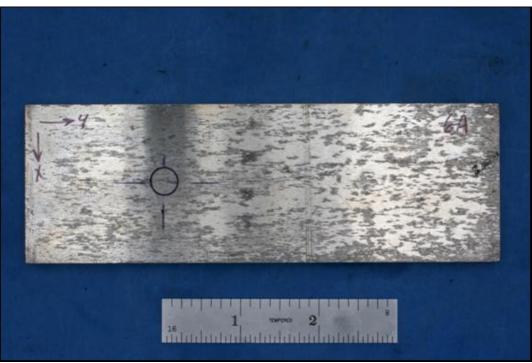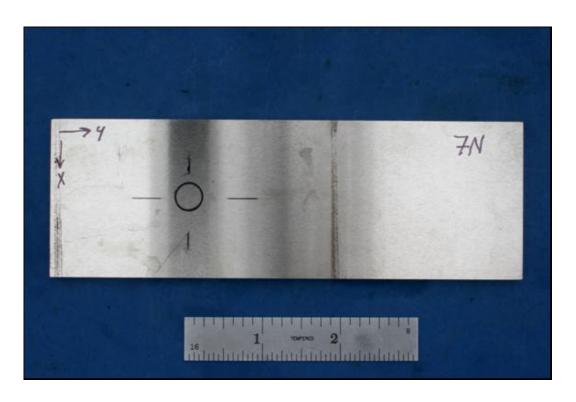
FIGURE 1d. *TOP:* Close-up macro photograph of Contamination Specimen 6N as received with marked location of crack. *BOTTOM:* Close-up macro photograph of Contamination Specimen 6A as received with marked location of crack.
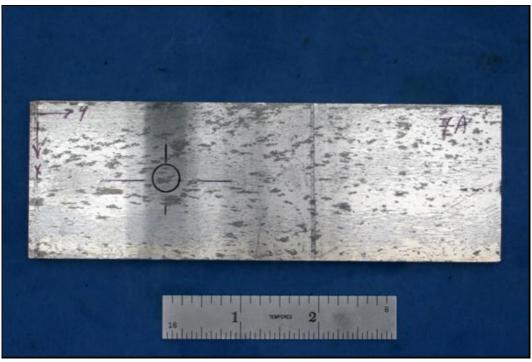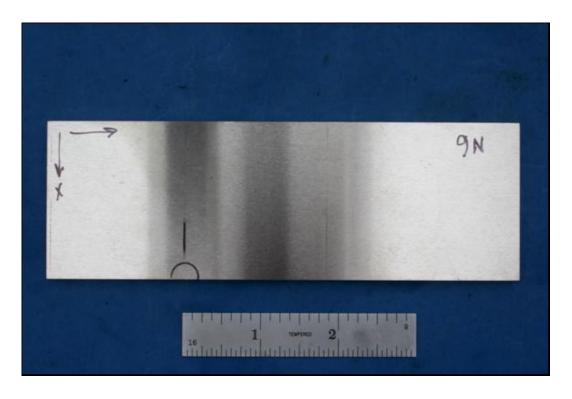
FIGURE 1e. *TOP:* Close-up macro photograph of Contamination Specimen 7N as received with marked location of crack. *BOTTOM:* Close-up macro photograph of Contamination Specimen 7A as received with marked location of crack.
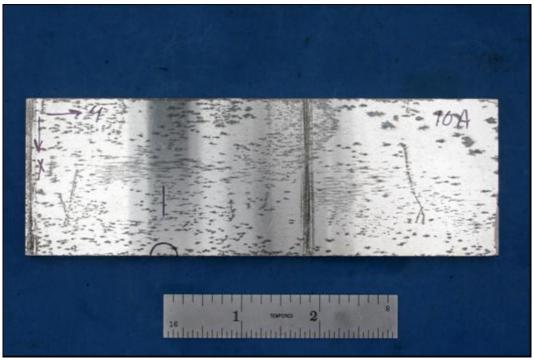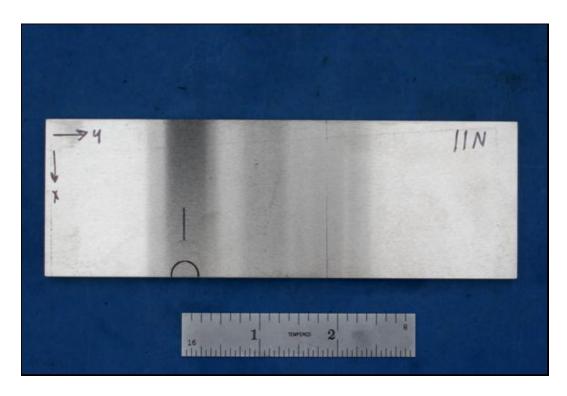
FIGURE 1f. *TOP:* Close-up macro photograph of Contamination Specimen 9N as received with marked location of crack. *BOTTOM:* Close-up macro photograph of Contamination Specimen 10A as received with marked location of crack.
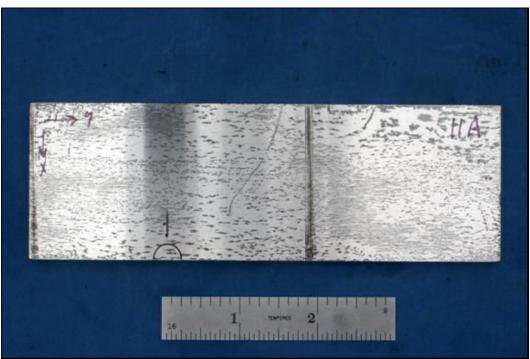
FIGURE 1g. *TOP:* Close-up macro photograph of Contamination Specimen 11N as received with marked location of crack. *BOTTOM:* Close-up macro photograph of Contamination Specimen 11A as received with marked location of crack.
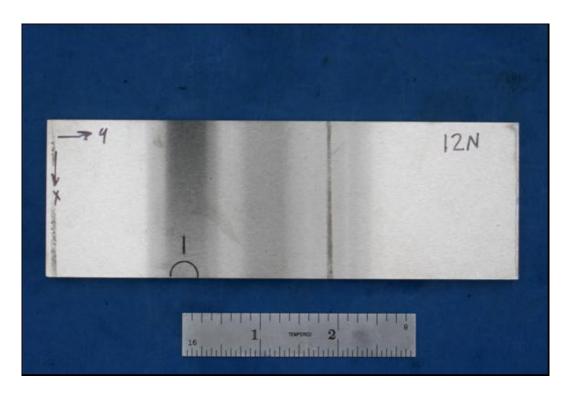
FIGURE 1h. Close-up macro photograph of Contamination Specimen 12N as received with marked location of crack.

Specimen #1N Surface Crack
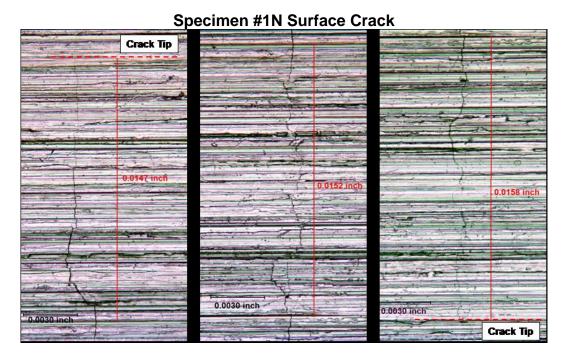
FIGURE 2. 200X sequential FOV of Specimen #1N surface crack (length = 0.0457 inches).

Specimen #2N Surface Crack
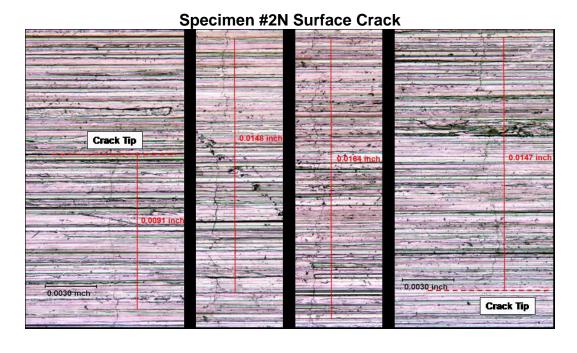
FIGURE 3. 200X sequential FOV of Specimen #2N surface crack (length = 0.0550 inches).

Specimen #2A Surface Crack
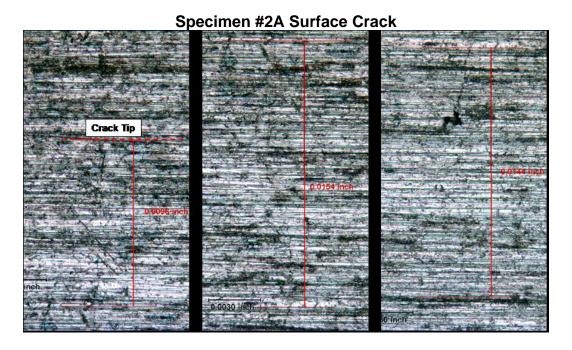
FIGURE 4a. 200X sequential FOV of Specimen #2A surface crack (length = 0.1682 inches).). Specimen required additional cycling to resolve crack. (Pmax = 300 lbs, R = 0.1, Freq. = 5 Hz, Total Cycles = 5,000)
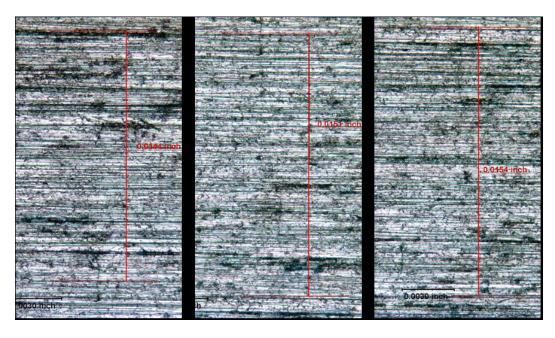
FIGURE 4b. 200X sequential FOV of Specimen #2A surface crack (length = 0.1682 inches).
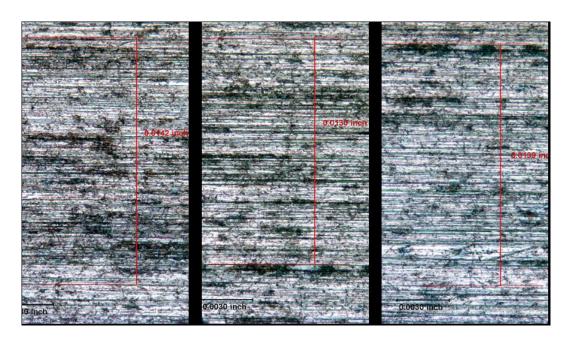
**FIGURE 4c.** 200X sequential FOV of Specimen #2A surface crack (length = 0.1682 inches).
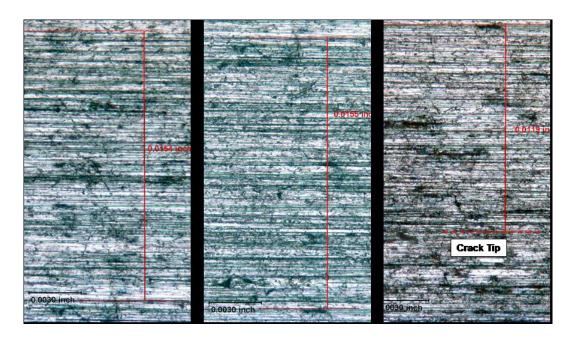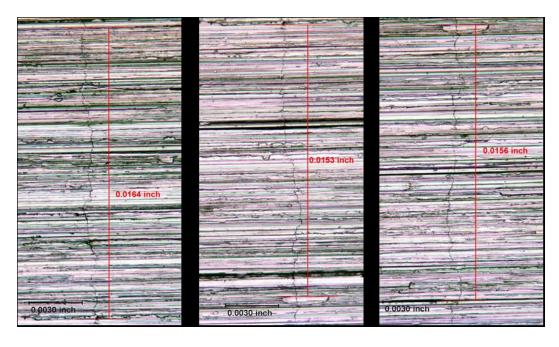

FIGURE 4d. 200X sequential FOV of Specimen #2A surface crack (length = 0.1682 inches).

Specimen #3N Surface Crack
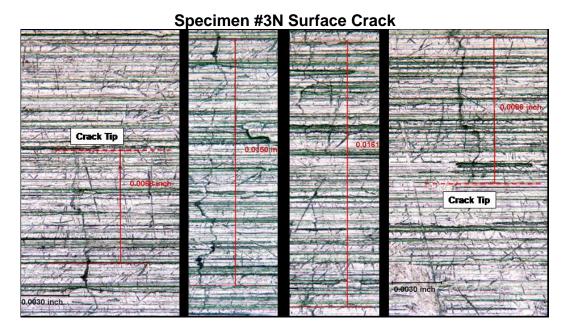
FIGURE 5. 200X sequential FOV of Specimen #3N surface crack (length = 0.0467 inches). Specimen required additional cycling to resolve crack. (Pmax = 1,000 lbs, R = 0.1, Freq. = 5 Hz, Total Cycles = 4,000)

Specimen #3A Surface Crack
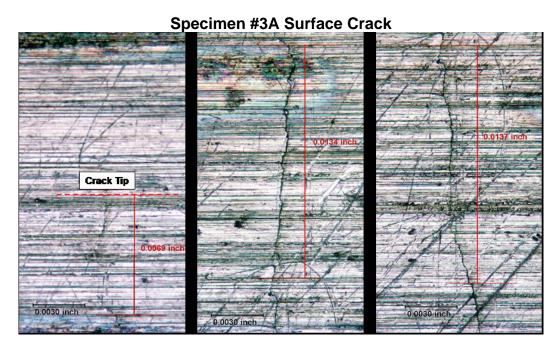
FIGURE 6a. 200X sequential FOV of Specimen #3A surface crack (length = 0.1811 inches).
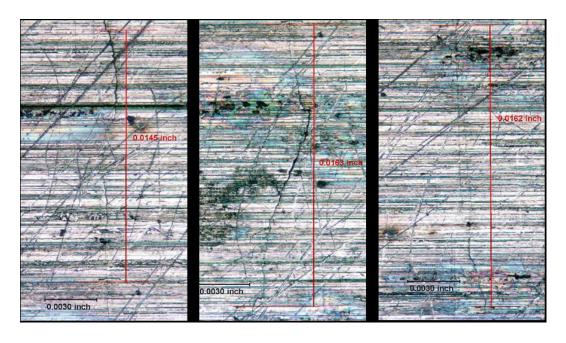
FIGURE 6b. 200X sequential FOV of Specimen #3A surface crack (length = 0.1811 inches).
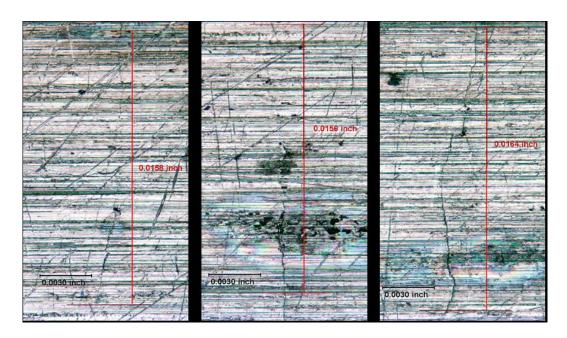
FIGURE 6c. 200X sequential FOV of Specimen #3A surface crack (length = 0.1811 inches).
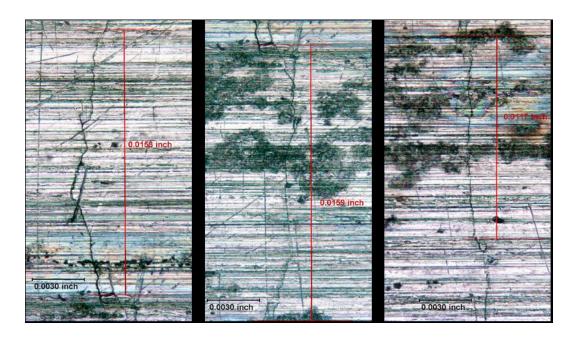
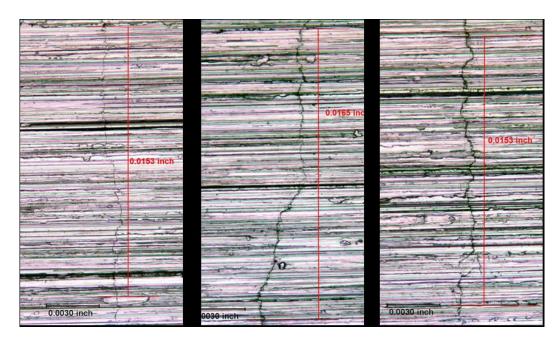**FIGURE 6d.** 200X sequential FOV of Specimen #3A surface crack (length = 0.1811 inches).
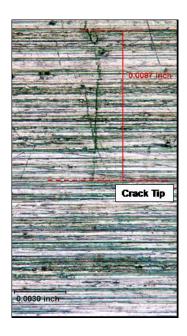
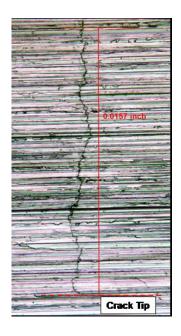**FIGURE 6e.** 200X sequential FOV of Specimen #3A surface crack (length = 0.1811 inches).

Specimen #5N Surface Crack
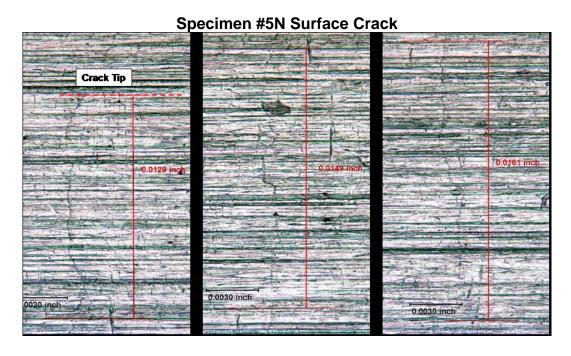
FIGURE 7a. 200X sequential FOV of Specimen #5N surface crack (length = 0.2513 inches). Specimen required additional cycling to resolve crack. (Pmax = 1,000 lbs, R = 0.1, Freq. = 5 Hz, Total Cycles = 2,000)


FIGURE 7b. 200X sequential FOV of Specimen #5N surface crack (length = 0.2513 inches).
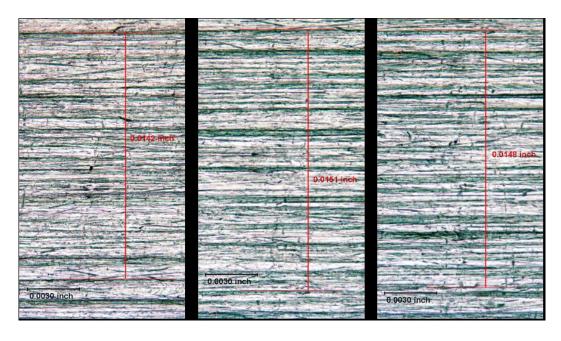
**FIGURE 7c.** 200X sequential FOV of Specimen #5N surface crack (length = 0.2513 inches).
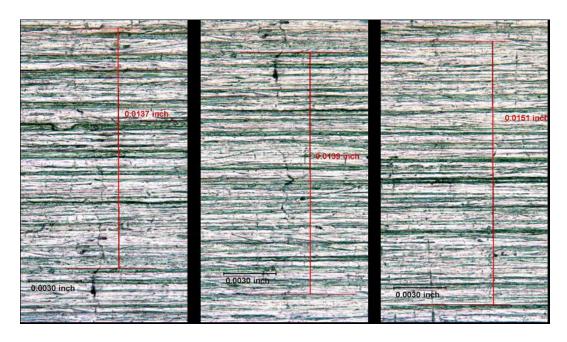
FIGURE 7d. 200X sequential FOV of Specimen #5N surface crack (length = 0.2513 inches).
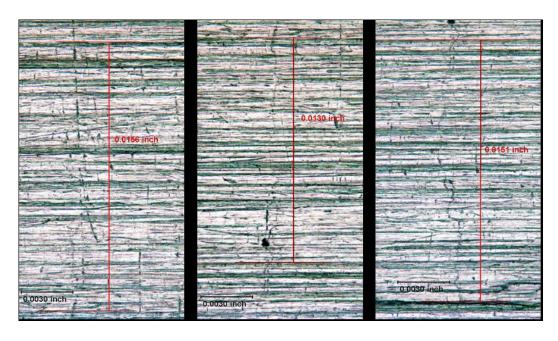
FIGURE 7e. 200X sequential FOV of Specimen #5N surface crack (length = 0.2513 inches).
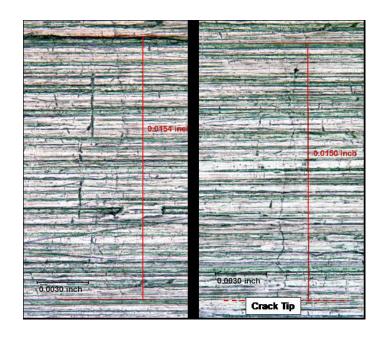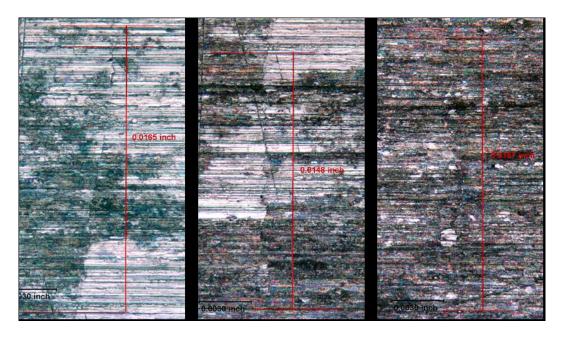

FIGURE 7a. 200X sequential FOV of Specimen #5N surface crack (length = 0.2513 inches).

Specimen #8A Surface Crack
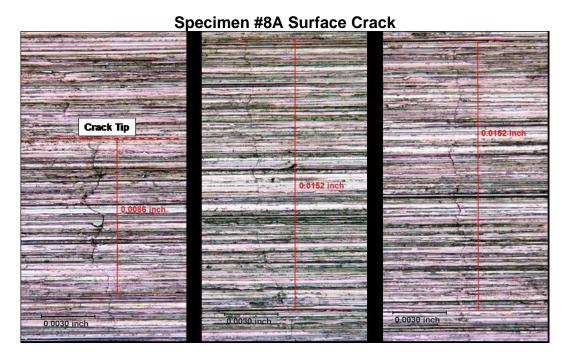
FIGURE 8a. 200X sequential FOV of Specimen #6N surface crack (length = 0.2520 inches).
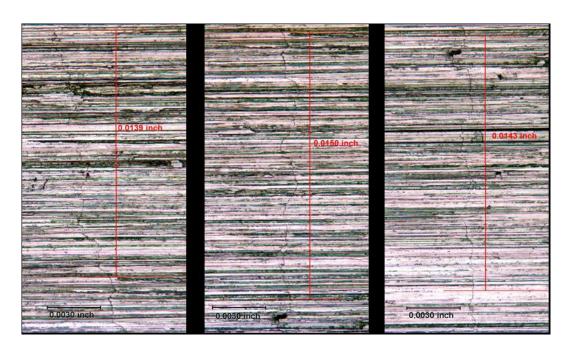
FIGURE 8b. 200X sequential FOV of Specimen #6N surface crack (length = 0.2520 inches).
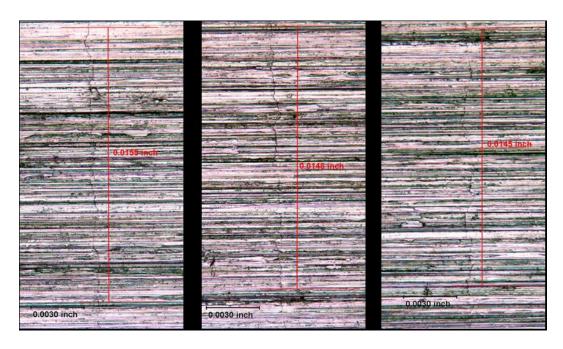
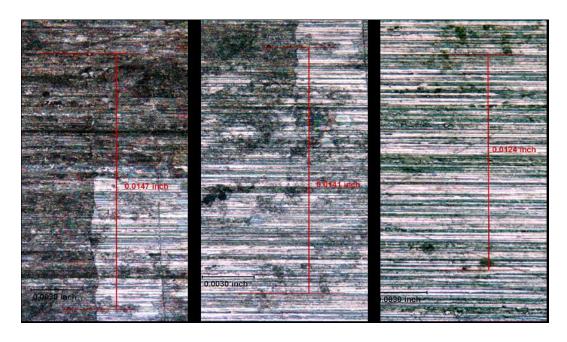**FIGURE 8c.** 200X sequential FOV of Specimen #6N surface crack (length = 0.2520 inches).
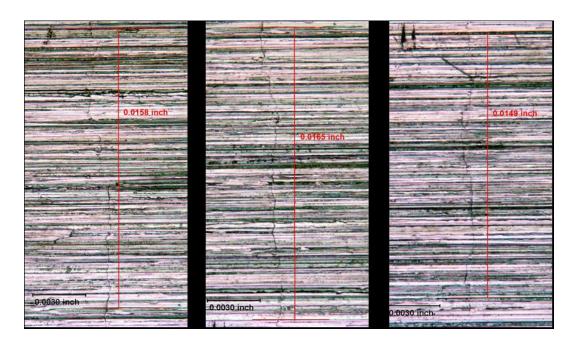
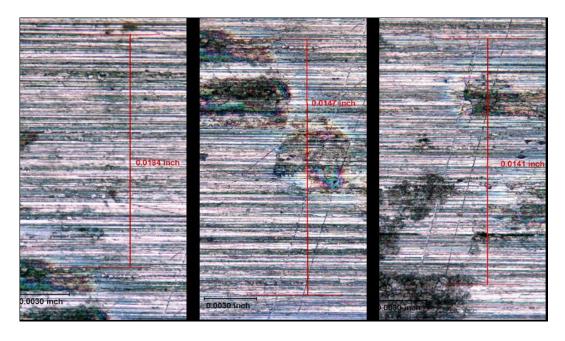**FIGURE 8d.** 200X sequential FOV of Specimen #6N surface crack (length = 0.2520 inches).
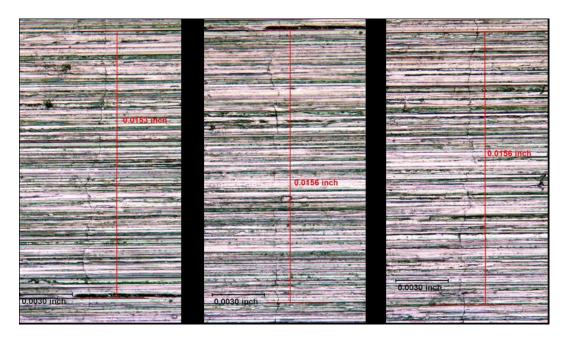
FIGURE 8e. 200X sequential FOV of Specimen #6N surface crack (length = 0.2520 inches).
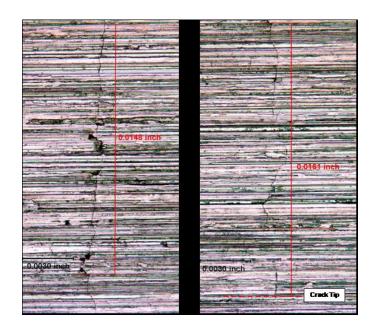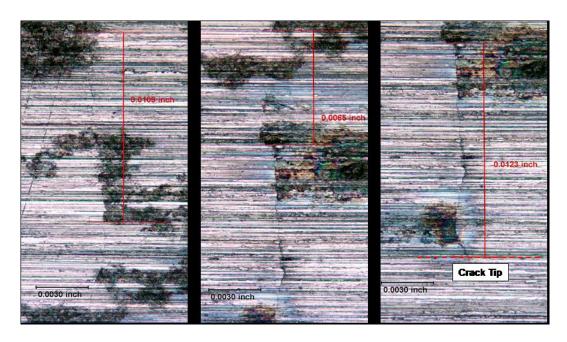

FIGURE 8f. 200X sequential FOV of Specimen #6N surface crack (length = 0.2520 inches).

Specimen #6A Surface Crack
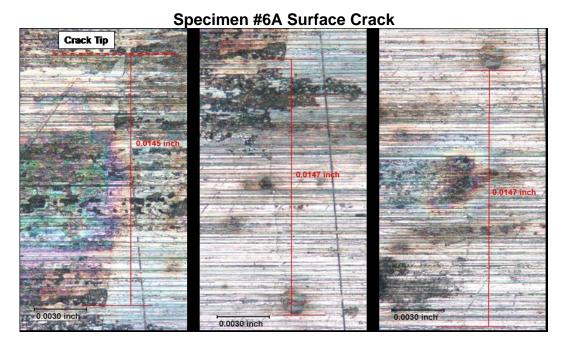
FIGURE 9a. 200X sequential FOV of Specimen #6A surface crack (length = 0.2449 inches).
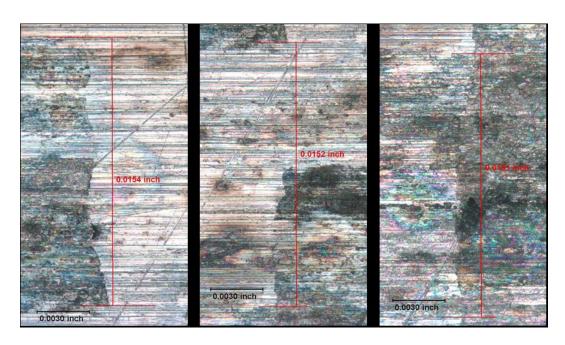
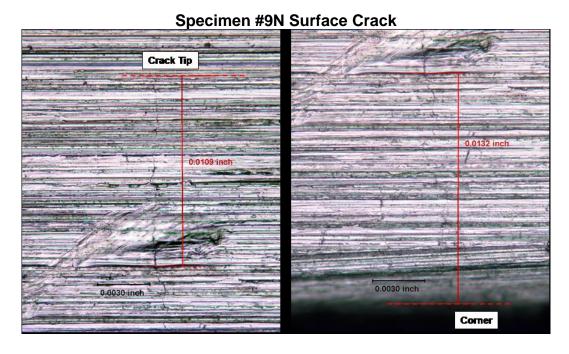**FIGURE 9b.** 200X sequential FOV of Specimen #6A surface crack (length = 0.2449 inches).

FIGURE 9c. 200X sequential FOV of Specimen #6A surface crack (length = 0.2449 inches).
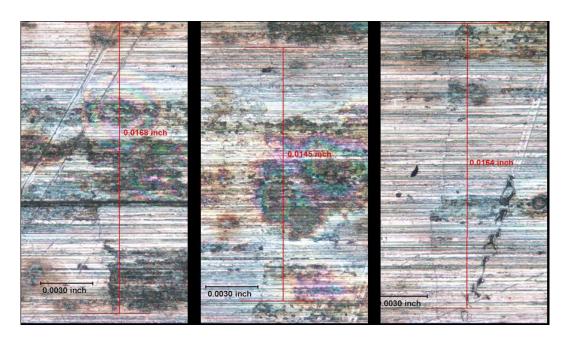
FIGURE 9d. 200X sequential FOV of Specimen #6A surface crack (length = 0.2449 inches).
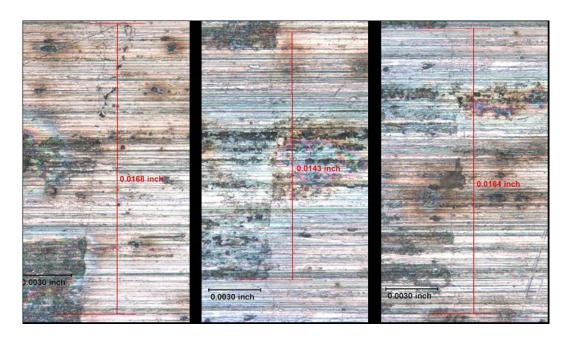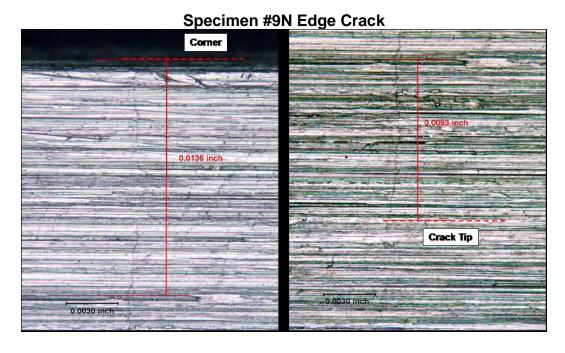
FIGURE 9e. 200X sequential FOV of Specimen #6A surface crack (length = 0.2449 inches).
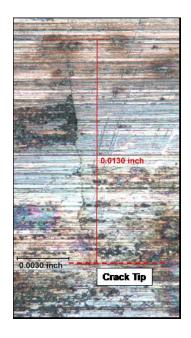
FIGURE 9f. 200X sequential FOV of Specimen #6A surface crack (length = 0.2449 inches).
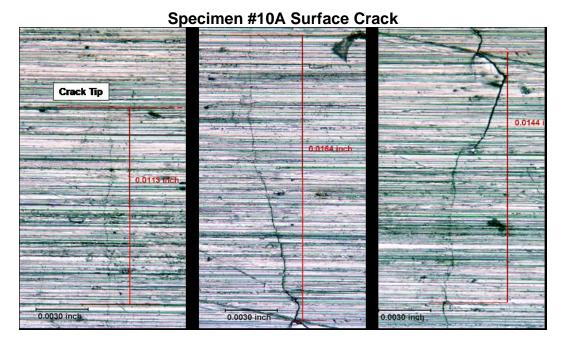
Specimen #7N Surface Crack
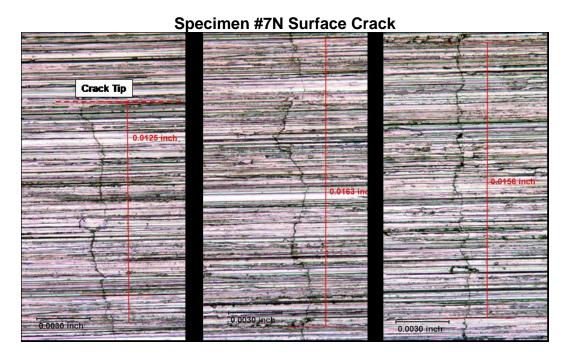
FIGURE 10a. 200X sequential FOV of Specimen #7N surface crack (length = 0.2483 inches).
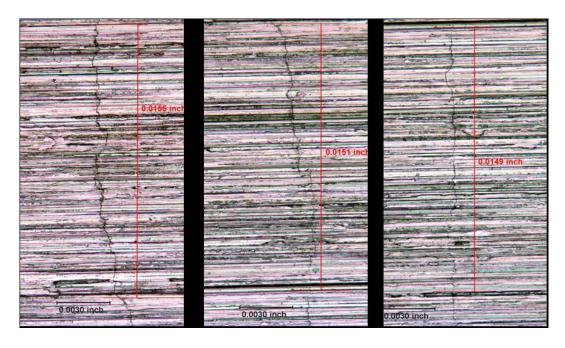
FIGURE 10b. 200X sequential FOV of Specimen #7N surface crack (length = 0.2483 inches).
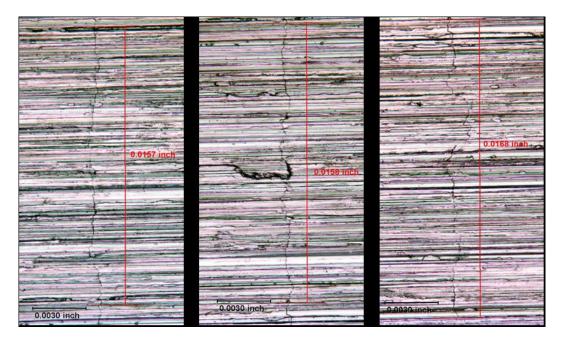
FIGURE 10c. 200X sequential FOV of Specimen #7N surface crack (length = 0.2483 inches).
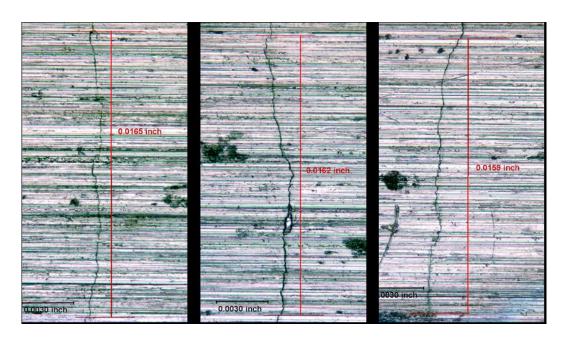

FIGURE 10d. 200X sequential FOV of Specimen #7N surface crack (length = 0.2483 inches).

FIGURE 10e. 200X sequential FOV of Specimen #7N surface crack (length = 0.2483 inches).

FIGURE 10f. 200X sequential FOV of Specimen #7N surface crack (length = 0.2483 inches).

Specimen #7A Surface Crack
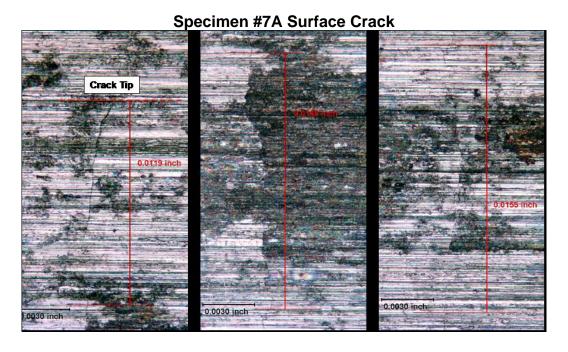
FIGURE 11a. 200X sequential FOV of Specimen #7A surface crack (length = 0.2501 inches).
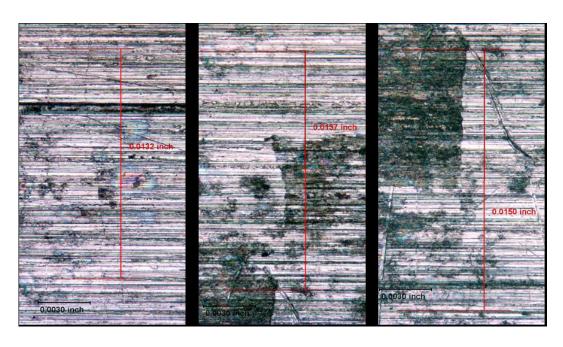
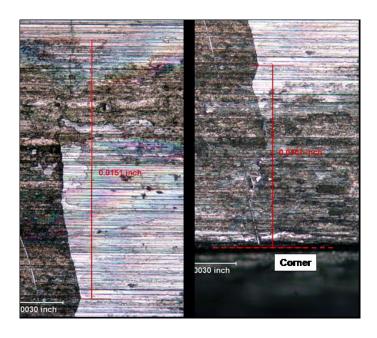**FIGURE 11b.** 200X sequential FOV of Specimen #7A surface crack (length = 0.2501 inches).

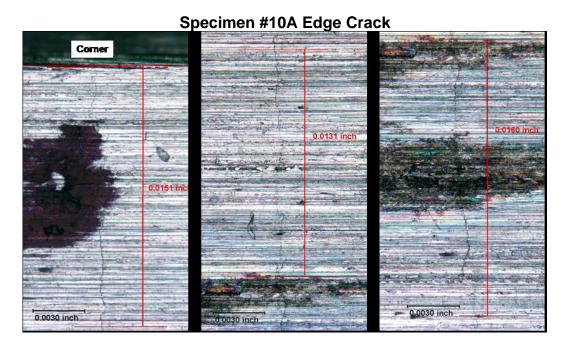**FIGURE 11c.** 200X sequential FOV of Specimen #7A surface crack (length = 0.2501 inches).

FIGURE 11d. 200X sequential FOV of Specimen #7A surface crack (length = 0.2501 inches).

FIGURE 11e. 200X sequential FOV of Specimen #7A surface crack (length = 0.2501 inches).

FIGURE 11f. 200X sequential FOV of Specimen #7A surface crack (length = 0.2501 inches).

Specimen #9N Surface Crack

FIGURE 12a. 200X sequential FOV of Specimen #9N surface crack (length = 0.0241 inches).

Specimen #9N Edge Crack

FIGURE 12b. 200X sequential FOV of Specimen #9N edge crack (length = 0.0229 inches).
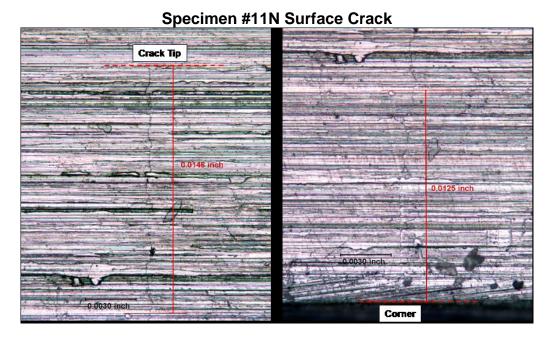
Specimen #10A Surface Crack

FIGURE 13a. 200X sequential FOV of Specimen #10A surface crack (length = 0.1165 inches).

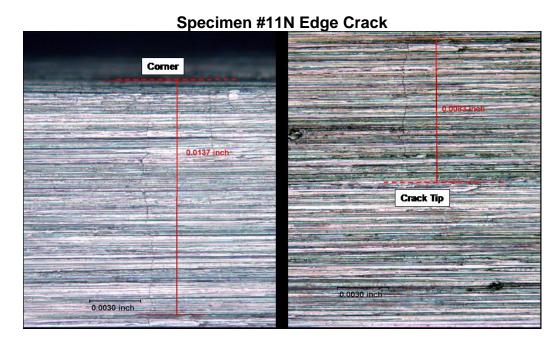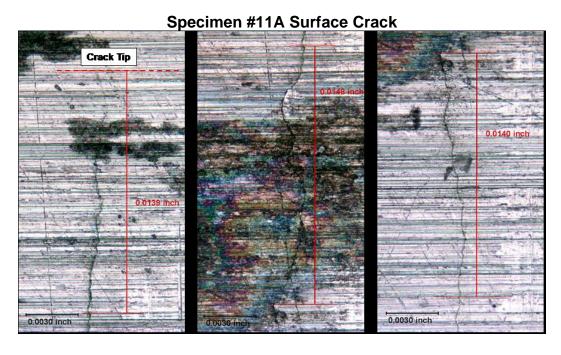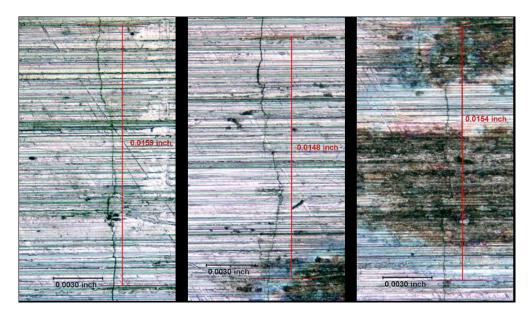**FIGURE 13b.** 200X sequential FOV of Specimen #10A surface crack (length = 0.1165 inches).

FIGURE 13c. 200X sequential FOV of Specimen #10A surface crack (length = 0.1165 inches).

Specimen #10A Edge Crack

FIGURE 13d. 200X sequential FOV of Specimen #10A edge crack (length = 0.0874 inches).
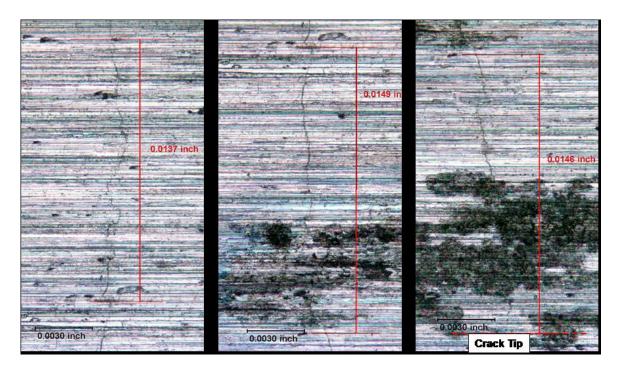
FIGURE 13e. 200X sequential FOV of Specimen #10A edge crack (length = 0.0874 inches).

Specimen #11N Surface Crack

FIGURE 14a. 200X sequential FOV of Specimen #11N surface crack (length = 0.0271 inches).

Specimen #11N Edge Crack

FIGURE 14b. 200X sequential FOV of Specimen #11N edge crack (length = 0.0220 inches).

Specimen #11A Surface Crack

FIGURE 15a. 200X sequential FOV of Specimen #11A surface crack (length = 0.1128 inches).

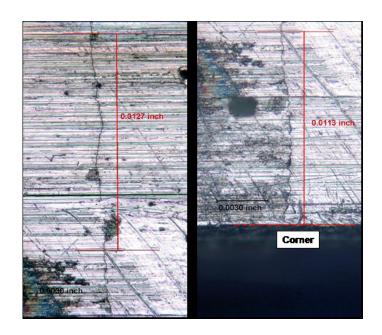**FIGURE 15b.** 200X sequential FOV of Specimen #11A surface crack (length = 0.1128 inches).

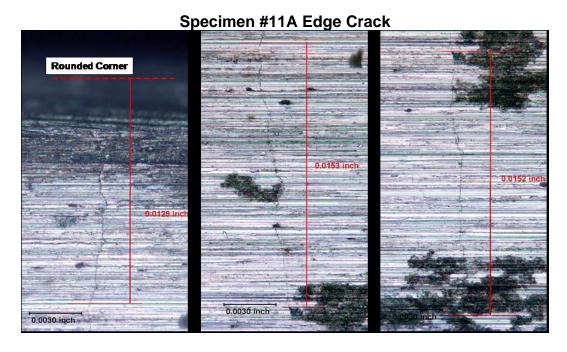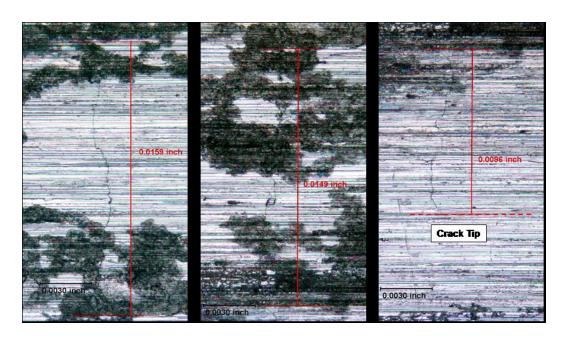**FIGURE 15c.** 200X sequential FOV of Specimen #11A surface crack (length = 0.1128 inches).

Specimen #11A Edge Crack

FIGURE 15d. 200X sequential FOV of Specimen #11A surface crack (length = 0.1128 inches).

FIGURE 15e. 200X sequential FOV of Specimen #11A edge crack (length = 0.0838 inches).
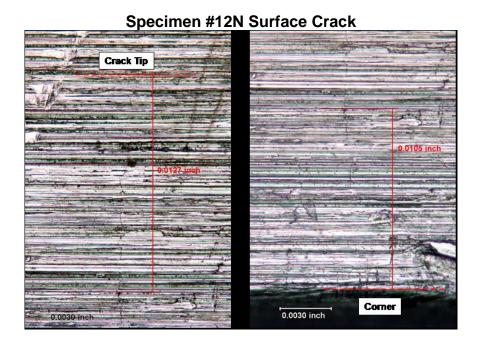
Specimen #12N Surface Crack

FIGURE 16a. 200X sequential FOV of Specimen #12N surface crack (length = 0.0232 inches).
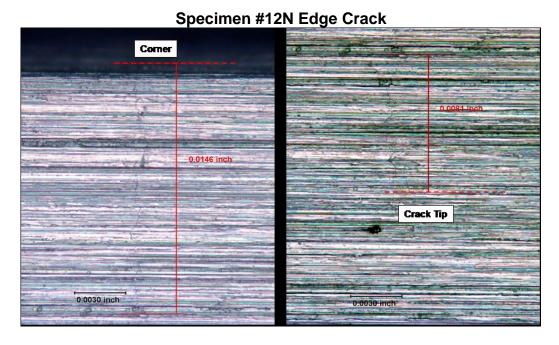
Specimen #12N Edge Crack

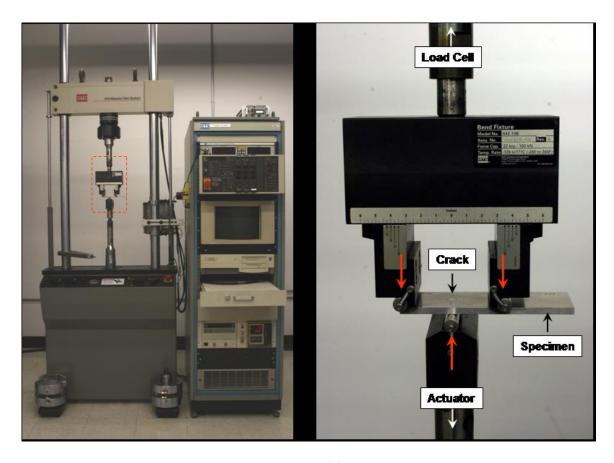**FIGURE 16b.** 200X sequential FOV of Specimen #12N edge crack (length = 0.0227 inches).

FIGURE 17. *LEFT:* Macro photograph of fatigue test machine used to cycle specimens. *RIGHT:* Close-up photograph of three-point-bend fixturing set-up with specimen installed. Note that red arrows depict compressive load.

9.0 Selected Bibliography

- Barden, T.J., D.P. Almond, P. Cawley, and M. Morbidini, "Advances in Thermosonics for Detecting Impact Damage in CFRP Composites," *INSIGHT*, Vol: 48, 2006, pp. 90-93.

- Busse, G., M. Bauer, W. Rippel, and D. Wu, "Lock-in Vibrothermal Inspection of Polymer Composites," *QIRT 92*, Editions Europeenes Thermique et Industrie, Paris, 1992, p.154.

- Dillenz, Alexander; Thomas Zweschper, and Gerd Busse, "Burst Phase Angle Thermography with Elastic Waves," *Thermosense XXIV*, 2002.

- Favro, L.D., Xiaoyan Han, Zhong Ouyang, Gang Sun, and R.L. Thomas, "Sonic IR Imaging of Cracks and Delamination," *Analytical Sciences, Vol. 17*, April 2001, pp. s451-s453.

- Favro, L.D., Xiaoyan Han, Zhong Ouyang, Gang Sun, and R.L.Thomas, "Infrared Imaging of Defects Heated by a Sonic Pulse," *Review of Scientific Instruments*, *Vol. 71, No. 6,* June 2000, pp. 2418-2421.

- Han, Xiaoyan, L.D. Favro, and R.L. Thomas, "Sonic IR Imaging and Vibration Pattern Studies of cracks in an Engine Disk," *Review of Progress in Nondestructive Evaluation Vol. 22*, D.O. Thompson and D.E. Chimenti, eds., 2003, pp. 513-516.

- Han, Xiaoyan; Li, Wei; Zeng, Zhi; Favro, L.D.; Thomas, R.L., "Acoustic Chaos and Sonic Infrared imaging," Applie*d Physics Letters, Vol. 81, No. 17*, October 21, 2002, pp. 3188-3190.

- Henneke, E.G., K.L. Reifsnider, and W.W. Stinchcomb, "Thermography: An NDI Method for Damage Detection," *Journal of Metals*, Sept. 1979, pp. 11-15.

- Henneke, E.G., K.L. Reifsnider, and W.W. Stinchcomb, "Vibrothermography: Investigation, Development, and Application of a New Nondestructive Evaluation Technique," Final Report to U.S. Army Research Office, ARO 1878.5-MS, November 26, 1986.

- Henneke, E.G. and T.S. Jones, "Detection of Damage in Composite Materials by Vibrothermography," *ASTM Special Technical Publication 696*, R.B. Pipes, ed., 1979, pp. 83-95.

- Mignogna, R.B., R.E. Green Jr., J.C. Duke Jr., E.G. Henneke II, and K.L. Reifsnider, "Thermographic Investigation of High-Power Ultrasonic Heating in Materials," *Ultrasonics*, July 1981.

- Miller, Wayne O., "An Evaluation of Sonic IR for NDE at Lawrence Livermore National Laboratory," *Thermosense XXIII*, Andres E. Rozlosnik and Ralph B. Dinwiddie, eds., Proceedings of SPIE Vol. 4360, 2001, pp.534-545.

- Miller, Wayne O., Ian M. Darnell, Michael W. Burke, and Christopher L. Robbins, "Defining the Envelope for Sonic IR: Detection Limits and Damage Limits," *Thermosense XXV*, K. Elliott Cramer and Xavier P. Maldague, eds., Proceedings of SPIE Vol. 5073, 2003, pp.406-416.

- Morbidini, M., P. Cawley, T.J. Barden, D.P. Almond, and P. Duffour, "A New Approach for the Prediction of the Thermosonic Signal from Vibration Records," *Review of Progress in Nondestructive Evaluation Vol. 25*, D.O. Thompson and D.E. Chimenti, eds., 2006, pp. 558-565.

- Ouyang, Zhong, L.D. Favro, R.L. Thomas and Xiaoyan Han, "Theoretical Modeling of Thermosonic Imaging of Cracks," *Review of Progress in Nondestructive Evaluation Vol. 21*, D.O. Thompson and D.E. Chimenti, eds., 2002, pp. 577-581.

- Rantala, J., D. Wu, and G. Busse, "Amplitude Modulated Lock-in Vibrothermography for NDE of Polymers and Composites," *Research in Nondestructive Evaluation*, Vol. 7, 1996, pp. 215-228.

- Simon, Daniel L., "Industrial Uses of a New Hybrid Sonic/Infrared NDT Technique," *Review of Progress in Nondestructive Evaluation Vol. 21*, D.O. Thompson and D.E. Chimenti, eds., 2002, pp. 536-543.

- Thomas, Robert L., Lawrence D. Favro, Xiaoyan Han, Zhong Ouyang, Hua Sui, and Gang Sun, "Infrared Imaging of Ultrasonically Excited Subsurface Defects in Materials," United States Patent # 6,236,049, issued May 22, 2001.